**UNIVERSIDAD AUTÓNOMA DE MADRID**

FACULTAD DE CIENCIAS

DEPARTAMENTO DE BIOLOGÍA MOLECULAR

# Transcription dynamics in TOL plasmid pWW0 of the soil bacterium *Pseudomonas putida* mt-2

TESIS DOCTORAL

Memoria presentada para optar al grado de Doctor en Ciencias

Juhyun Kim

DIRECTOR DE TESIS:

Víctor de Lorenzo Prieto

CONSEJO SUPERIOR DE INVESTIGACIONES CIENTÍFICAS

CENTRO NACIONAL DE BIOTECNOLOGÍA

Madrid, 2014

To my parents and my wife Jiseon

**ACKNOWLEDGEMENTS**

This work would not have been possible without the support of many people. I would like to express my sincere gratitude to my advisor, Víctor de Lorenzo, for the opportunity to join his laboratory, his support, guidance and encouragement throughout my doctorate course. *Muchas gracias, Víctor*.

I am thankful to my tutor, José Berenguer, for his comments and discussion on my study.

I want to acknowledge Woojun Park, my former supervisor at Korea University. Because of a chance to work with him, I could enter the *Pseudomonas world*.

I sincerely appreciate José Manuel Franco and Iria Calvete Silva for helping me design tiling array chips and the assay. I am grateful to Juan Carlos Oliveros for transcriptome analysis and keeping his door open whenever I needed his help.

I am heartily grateful to Natalia E. Broude for introducing me to mRNA visualization techniques in her laboratory with exciting experience in Boston.

Many thanks to my friends, Sangbeom and Juhun. Without their incessant support and encouragement from Korea, I would quit studying.

I would like to give special thanks to Catherine Mark for proofreading this Thesis. I could learn lots of things and it was really nice to talk bout music with you.

My sincere gratitude goes to former and current laboratory members: Inés, Sofía, Belén, Pablo, Danilo, Esteban, Angel, Tomás, Özlem, Ilaria, Alberto, Angeles, Aleyo, Gonzalo, Javier, Rafael, Raul, Aitor, José Ignacio and David. I have received so much help from them for my research. *¡Sin su ayuda, no podría hacer nada!*

## GENERAL INDEX

**Index of Figures……..v**

**Index of Tables……..……....viii**

**Abbreviations……...ix**

**Abstract…….……...xii**

**Resumen…….……xiii**

**I. Introduction ..... 1**

1. IncP-9 pWW0 plasmid ..... 3

2. Transcriptional control of the TOL plasmid pWW0 catabolic pathways... 4

3. Towards high-resolution mapping for the bacterial transcriptome ..... 7

4. Spatial organization of cellular components in bacteria..... 9

5. Analysis of RNA visualization in a bacterial cell..... 14

6. The issue at stake..... 16

**II. Objectives ..... 19**

**III. Materials and Methods..... 23**

1. Culture conditions and media ..... 25

2. Bacterial strains ..... 25

3. Plasmids..... 27

4. Construction of bacterial strains ..... 28

4.1. The *xylS* expression with antisense transcripts..... 29

4.2. *PbenA* transcriptional and translational fusion to *lacZ* reporter ..... 29

4.3. Validation of annotated sequence of the *xylL* gene ..... 29

4.4. *Pmpf* promoter reporter on different backgrounds ..... 30

4.5. Construction of RNAP-labeled cells and dual cell labeling with RNAP and ribosome..... 30

4.6. Replacement of the *Pu* promoter in pWW0 plasmid with the T7 promoter ..... 31

5. High-throughput transcription analysis ..... 33

5.1. RNA preparation..... 33

5.2. High-density tiling array design and analysis..... 33

5.3. cDNA library construction for RNA deep sequencing..... 35
5.4. Sequence read alignment and normalization for RNA deep sequencing ..... 35
6. Preparation of strand-specific RNA and DNA probes ..... 36
7. Northern blot analysis..... 36
8. Measurement of promoter activity ..... 36
8.1. Quantification of GFP fluorescence for the *Pm* promoter..... 37
8.2. *PbenA* promoter activity assay using *lacZ* reporters ..... 37
8.3. Analysis of lux reporter dependent on the *PmpfR* promoter ..... 38
9. Sample preparation for microscopy..... 38
10. Microscopy and image analysis..... 39
11. Fluorescent *in situ* hybridization for TOL catabolic transcripts..... 39
**IV. Results ..... 41**
**Chapter I. High-resolution analysis of the *m*-xylene/toluene biodegradation sub-transcriptome of *Pseudomonas putida* mt-2 ..... 43**
1. Approach for transcription mapping of *xyl* genes responding to *m*-xylene..... 44
2. Definition of operon structure of TOL genes, novel transcription and correction of gene annotation ..... 46
3. Overlapping transcription between *xylS* and *lower* operon gene ..... 49
4. Transcription profiles of TOL *xyl* genes responding to toluene and its derivatives..... 52
5. Effect of *m*-xylene/toluene and derivative aromatic compound assimilation on the b-ketoadipate pathway..... 54
5.1. The *ben* gene expression profile..... 54
5.2. The *cat* gene expression profile..... 56
5.3. The *pca* gene expression profile..... 58
5.4. Phenylpropenoid compounds and p-hydroxybenzoate catabolic gene expression profile ..... 60

**Chapter II A high-resolution transcriptional approach reveals the expression structure of the TOL plasmid pWW0 backbone genes in *Pseudomonas putida* mt-2 ..... 63**

1. pWW0 TOL plasmid whole gene expression profile response to *m*-xylene..... 64
2. Transcriptional characterization of the *orf13* region ..... 66
3. Operon structure of the *mpf* gene cluster and its promoter assay ..... 67
4. Transcriptome of the IncP-9 core region ..... 70

**Chapter III Visualization of ribosomal protein L13 reveals spatial organization separated from the nucleoid in *Pseudomonas putida* ..... 73**

1. Ribosome and nucleoid segregation in *P. putida* cultured in rich medium ..... 74
2. Effect of distinct metabolic networks on ribosome-nucleoid organization ..... 75
3. Ribosome subcellular localization in the TOL plasmid-harboring strain 76
4. Spatial distribution of ribosome and nucleoid in translation inhibition ... 79

**Chapter IV Visualization of mRNA induced from the TOL plasmid reveals its subcellular localization and characterization of transcription in a single cell 81**

1. The mRNAs of catabolic genes expressed from the TOL plasmid are organized spatially ..... 82
2. RNAP spatial distribution coincides with nucleoid organization in *P. putida* ..... 84
3. The *xylUW* mRNAs transcribed from the T7 promoter are found outside the nucleoid with increased copy numbers ..... 87
4. mRNA could be localized by diffusion-capture through affinity with the ribosome ..... 89
5. Transcriptional bursts in TOL catabolic genes ..... 92

**V. Discussion ..... 95**

1. High-throughput transcriptome for the TOL core gene..... 97
2. Transcription analysis of chromosomal *ortho* pathway genes ..... 98
3. Identification of transcriptional structure for TOL backbone genes ..... 100

4. Ribosome-nucleoid segregation in *P. putida* ..... 100
5. Physical force might lead to ribosome-nucleoid segregation ..... 101
6. Spatial distribution of mRNAs induced from the TOL plasmid in *Pseudomonas putida* mt-2 ..... 102
7. Spatial separation between transcription and translation factories in *Pseudomonas putida* ..... 103
8. Diffusion of mRNA toward to ribosome-rich sites ..... 104
9. Characterization of transcriptional bursting in the TOL system ..... 106

**VI. Conclusions ..... 109**

**Conclusioes (Spanish) ..... 113**

**VII. References ..... 115**

**VIII. Annexes ..... 137**

## INDEX OF FIGURES

**Figure 1**. Scheme of the IncP-9 backbone in the pWW0 plasmid…….....3

**Figure 2**. Regulatory networks for TOL catabolic pathway expression and *m*-xylene biodegradation borne by the catabolic enzymes in the TOL plasmid…..5

**Figure 3**. Scheme of the tiling array probe set ..……...……..…8

**Figure. 4**. Discovery of genetic elements by genome-wide transcriptome analysis …….……...……...10

**Figure 5**. Scheme showing of two distinct patterns of spatial distribution of ribosomes and chromosome in bacteria...…….....12

**Figure 6**. The known localization for specific mRNA in bacteria…….....…13

**Figure 7**. Scheme showing RNA visualization methods…….…….....15

**Figure 8**. High-density tiling array-based transcriptome profile of TOL *xyl* genes in *P. putida* mt-2.……...…….…….45

**Figure 9**. RNA deep sequencing-based transcriptome profile of TOL *xyl* genes in *P. putida* mt-2. ……..……...47

**Figure 10**. Transcriptome profiles of TOL plasmid core region responding to aromatic compounds, using a high-density tiling array in *P. putida* mt-2...….48

**Figure 11**. Correction of sequence annotation on the *xylL* gene in the pWW0 plasmid of *P.putida* mt-2……...49

**Figure 12**. Northern blot analysis for the overlapping expression región...…50

**Figure 13**. Assay for artificial *xylS* expression effect on the *Pm* promoter…..52

**Figure 14**. Aromatic compound catabolic pathways in *P. putida* mt-2…....…55

**Figure 15**. Transcription profiles based on tiling array for the *ben* genes that respond to aromatic compounds in *P. putida* mt-2……...……...….56

**Figure 16**. *PbenA* promoter activity analysis and RNA-seq transcriptome for *ben* genes in *P. putida* mt-2……...……....……57

**Figure 17**. Transcription profiles based on tiling array for the *cat* genes that respond to aromatic compounds in *P. putida* mt-2……..…….58

**Figure 18**. Transcription profiles based on tiling array for the *pca* genes that respond to aromatic compounds in *P. putida* mt-2 . …….……...……59

**Figure 19**. Transcriptional intensity based on tiling array for phenylpropenoid and p-hydroxybenzoate catabolic genes in *P. putida* mt-2……..……60

**Figure 20**. RNA deep sequencing-based transcriptome profile of the whole pWW0 plasmid region in *P. putida* mt-2. ……....……65

**Figure 21**. Characterization of the transcriptional unit in the *or*f13 region in the pWW0 plasmid of *P. putida* mt-2……..……...……67

**Figure 22**. Transcriptional structure of the *mpf* genes and analysis of the activity of its putative promoter……..…….……...……69

**Figure 23**. Visualization of the localization of ribosomal protein L13 fusion with GFP in *P. putida* MEG*2*……...……...……..75

**Figure 24**. Substrates and growth phase-dependent ribosome and nucleoid distribution in *P. putida* MEG2……...……77

**Figure 25**. Spatial organization of ribosome and nucleoid in pWW0 TOL plasmid-harboring cells……..……78

**Figure 26**. Translation inhibition effect on ribosome and nucleoid distribution in *P. putida* MEG2. ……..79

**Figure 27**. Scheme showing a fluorescent *in situ* hybridization (FISH) experiment to visualize TOL catabolic transcripts in *P. putida* mt-2……..…...…..…82

**Figure 28**. mRNA FISH with *xylUW* or *xylX* probe sets on *P. putida* mt-2....83

**Figure 29**. Subcellular localization of TOL catabolic transcripts in *P. putida* mt-2 ……..……...……..…84

**Figure 30**. RNAP subunit organization in *P. putida* KT2440……..85

**Figure 31**. Spatial distribution of RNAP and ribosome in *P. putida* KT2440..86

**Figure 32**. Replacement of *Pu* with T7 promoter in the TOL plasmid…….....88

**Figure 33**. Spatial distribution of the specific mRNA expressed from the T7 promoter…….89

**Figure 34**. Visualization of the *xylX* mRNAs expressed from rearrangement of the TOL regulation system……...…….……...90

**Figure 35**. Rifampicin effect on mRNA synthesis by bacterial RNAP or T7 RNAP and its spatial distribution..…….……91

**Figure 36**. Effect of transcriptional inhibition on spatial organization of the

ribosome in *P. putida* KT2440……...92
**Figure 37**. Quantification analysis for mRNA copy number…….93
**Figure 38**. Viability assay for *P. putida* mt-2 in different carbons sources….106

## INDEX OF TABLES

**Table 1.** Description of bacterial strains used in this study……25

**Table 2.** Plasmids used in this work……...27

**Table 3.** Oligonucleotides synthesized in this study for PCR reactions……..31

**Table 4**. The *catR* expression level obtained by tiling array transcription…….58

**Table S1**. Transcriptional activity on pWW0 backbone genes by RNA-seq……139

**Table S2**. Complementary oligonucleotides for mRNA FISH assay……...144

## ABBREVIATIONS

| | |
|---|---|
| AA | Amino acid |
| Amp | Ampicillin |
| AU | Arbitrary units |
| ben | Benzoate |
| bp | Base pair |
| CCM | *cis, cis*-muconate |
| Cm | Chloramphenicol |
| CTP | Cytidine triphosphate |
| DAPI | 4', 6-diamidino-2-phenylindole |
| DEPC | Diethylpyrocarbonate |
| DNA | Deoxyribonucleic acid |
| dUTP | Deoxyuridine triphosphate |
| FISH | Fluorescent *in situ* hybridization |
| GFP | Green fluorescent protein |
| Glc | Glucose |
| Gm | Gentamycin |
| h | Hour |
| HTH | Helix-turn-helix |
| IGB | Integrated Genome Browser |
| IGV | Integrated Genomic Viewer |
| IHF | Integration host factor |
| IPTG | Isopropyl β-D-1-thiogalactopyranoside |
| kb | 1000 base pairs |
| Km | Kanamycin |
| LB | Luria–Bertani |
| m-xyl | *m*-xylene |
| mg | Milligram |

| | |
|---|---|
| min | Minute |
| ml | Milliliter |
| mM | Millimolar |
| mRNA | Messenger RNA |
| MS2 | MS2 coat protein |
| nm | Nanometer |
| nM | Nanomolar |
| nt | Nucleotide |
| o-xyl | *o*-xylene |
| OD | Optical density |
| PBS | Phosphate buffered saline |
| PC | Phase contrast |
| PCR | Polymerase chain reaction |
| Q | Glutamine |
| qCML | Quantile-adjusted conditional maximum likelihood |
| Rif | Rifampicin |
| RNA | Ribonucleic acid |
| RNA-seq | RNA sequencing |
| RNAP | RNA polymerase |
| rRNA | ribosomal RNA |
| RU | Relative units |
| sec | Second |
| Sm | Streptomycin |
| sRNA | Small RNA |
| SSC | Saline-sodium citrate buffer |
| suc | Succinate |
| T7pol | T7 RNA polymerase |
| TC | Tetracycline |
| TCA | Tricarboxylic acid cycle |
| TMM | Trimmed mean of M values |

| | |
|---|---|
| tol | Toluene |
| tRNA | Transfer RNA |
| UAS | Upstream activating sequences |
| UTR | Untranslated region |
| VRC | Vanadyl ribosnucleoside complex |
| wt | Wild-type |
| YFP | Yellow fluorescent protein |
| β' | Beta prime subunit of RNA polymerase |
| μg | Microgram |
| μl | Microliter |
| μm | Micrometer |
| μM | Micromolar |
| σ | Sigma factor of RNA polymerase |
| 3MBA | 3-methylbenzylalcohol |
| 3MBz | 3-methylbenzoate |

## ABSTRACT

*Pseudomonas putida* mt-2 metabolizes *m*-xylene and other aromatics through the convergence of enzymes encoded by the catabolic operons of the TOL plasmid pWW0 with chromosomally derived activities. Using the technique of tiling arrays for the transcriptome of interest in both pWW0 and the genome of this bacterium, we observed that not only all pWW0 *xyl* genes were highly transcribed in response to *m*-xylene/toluene, but a novel transcription unit downstream of *xylN* also became apparent, regardless of culture conditions. The 3'-end of the *lower* operon mRNA penetrated well into the convergent *xylS* transcript. In contrast, *xylR* mRNA for the head regulator of the system was sharply decreased by the aromatic substrates, although the corresponding *upper* operon mRNA was stable throughout its full length. RNA deep sequencing analysis showed a similar expression pattern for *xyl* genes when cells were treated with *m*-xylene, which provided higher resolution at the single nucleotide level, thereby revealing incorrect annotation of the *xylL* sequence. At the same time, the profile showed that the transcription level was apparently increased for several plasmid backbone genes such as *orf13*, *orf31*, *orf124-126, orf188-191* and the *mpf* (mating pili formation) cluster, which led to definition of genetic structure. When we visualized the *xyl* transcripts by mRNA fluorescent *in situ* hybridization in a single cell, the molecules remained within one or two subcellular regions, which were nucleoid-free. Labeling of RNAP or ribosomal protein with fluorescent protein revealed that RNAP colocalizes with chromosomal DNA and the ribosome is spatially separated from those molecules. When the copy number of the target mRNA was increased by the T7 expression system, an increased number of foci was observed and most messages resided in nucleoid-free regions. In addition, the quantification of mRNA copy number with a statistical approach shows that the TOL system is subject to transcriptional bursting.

## RESUMEN

*Pseudomonas putida* mt-2 metaboliza *m*-xileno y otros aromáticos a través de la convergencia de enzimas codificadas por los operones catabólicos del plásmido TOL pWW0 y de actividades enzimáticas de codificación cromosómica. Al emplear la técnica de microchips del tipo *tiling* para estudiar el transcriptoma originado tanto en pWW0 como en el cromosoma bacteriano, observamos que no sólo todos los genes *xyl* del plasmido TOL fueron vigorosamente transcritos en respuesta al *m*-xileno/tolueno; sino que también lo hizo una unidad transcripcional previamente desconocida que se encuentra localizada consecutivamente a *xylN* y que se expresa independientemente de las condiciones de cultivo. Además, el extremo 3' del ARNm del operon inferior se extendió hasta el interior de la región codificante del gen *xylS* ubicado en posición convergente. Por el contrario, el nivel del ARNm de *xylR,* codificante del principal regulador del sistema, fue disminuyendo abruptamente en presencia de substratos aromáticos; no obstante el correspondiente ARNm del operón superior se mantuvo uniformemente estable a través de toda su longitud. Un análisis de secuenciación masiva de ARN muestra un patrón de expresión similar para los genes *xyl* cuando las células fueron tratadas con m-xileno, permitiendo una mayor resolución (hasta el nivel de nucleótido único); y de este modo, revelando una incorrecta anotación para la secuencia del gen *xylL*. Al mismo tiempo, el perfil transcripcional muestra que el nivel de transcritos de varios genes correspondientes a la columna vertebral del plasmido, tales como *orf13, orf31, orf124-126, orf188-191* y el grupo *mpf* (formación del pelo conjugativo) se incrementó; lo cual permite definir su estructura genética. Al visualizar la transcripción de los genes *xyl* mediante hibridación *in situ* fluorescente de ARNm al nivel de célula única, se observa que las moléculas son retenidas únicamente dentro de una o dos regiones subcelulares las cuales se encuentran libres de nucleoides. Mediante marcaje con GFP (proteína fluorescente verde) de la polimerasa de ARN o de proteína ribosomal se observó que la polimerasa se co-localiza con el ADN cromosómico y que el ribosoma se encuentra espacialmente separado de estas moléculas. Al aumentar el número de copias de ARN de TOL

mediante el sistema de expresión T7, se observó un incremento en el número de focos de co-localización y que la mayoría de los mensajeros residían en regiones libres de nucleoides. Además, la cuantificación del número de copias del ARNm con una aproximación estadística muestra que el sistema TOL se encuentra sujeto a *transcriptional bursting*, es decir se expresa en intensas ráfagas de actividad transcripcional intercaladas con periodos silentes.

# I. Introduction

## 1. IncP-9 pWW0 plasmid

As mobile genetic elements, plasmids contribute the ability for bacterial adaptation and evolution, and those extra-chromosomal DNAs are found in various microorganisms (Turner et al., 2002, Ochman et al., 2000). Some plasmids not only enable antibiotic resistance or virulence, but also allow host cells to degrade toxic compounds (Frost et al., 2005, Smets and Barkay, 2005). Such plasmids are categorized into incompatibility (Inc) groups according to their replication and partition system, and there are at least 14 known groups in *Pseudomonas* (Boronin, 1992, Shintani et al., 2010). Among the classified groups, degradation genes for aromatic hydrocarbons such as phenol, carbazole and naphthalene or *m*-xylene/toluene are commonly found on IncP-2, IncP-7 and IncP-9 plasmids, respectively (Shingler et al., 1989, Greated et al., 2002, Takahashi et al., 2009, Dennis and Zylstra, 2004, Sota et al., 2006). In the case of IncP-9 plasmids, large class II transposons carrying degradative genes such as the *nah* and *xyl* genes are inserted into different positions of the IncP-9 backbone and determine the plasmid phenotype observed in NAH7 and pWW0 (Fig. 1), respectively (Tsuda and Genka, 2001, Tsuda and Iino, 1987, Sota et al., 2006, Sevastsyanovich et al., 2008).

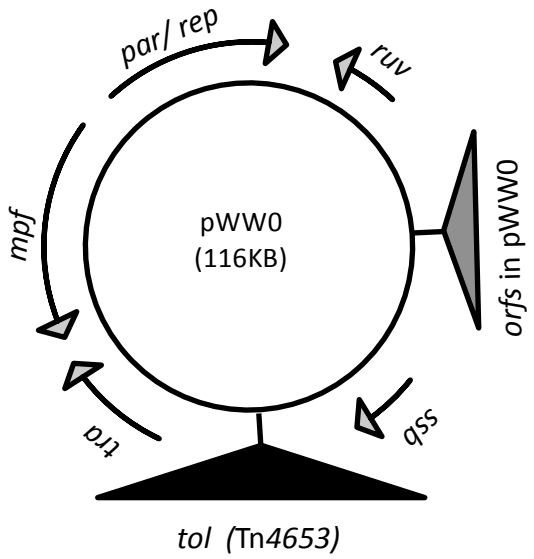


**Figure 1. Scheme of the IncP-9 backbone in the pWW0 plasmid.** The organization of core genes for plasmid replication, maintenance, transfer, specific *orf*s and the tol region, including the *xyl* genes deduced by Tn4653 in pWW0 are depicted.

pWW0 has been extensively studied with respect to biodegradation of *m*-xylene/toluene relative to *xyl* gene expression and regulation mechanisms, as we describe below (Assinder and Williams, 1990, Ramos et al., 1997, Velazquez et al., 2005). In addition to these catabolic genes, DNA sequencing and comparison analysis identified IncP-9 core genes involving replication (*rep*), maintenance (*parA, parB* and *parC*) and transfer functions (*tra* and *mpf* clusters) in the plasmid (Greated et al., 2002). Moreover, a number of genes encoding putative phenotype functions as well as unknown-function genes were also found on the pWW0 backbone (Greated et al., 2002). Nonetheless, little information is available for the transcriptome of the core genes or putative genes in the plasmid, and therefore their functional roles have been overlooked. One of the aims of this Thesis was thus to address covered transcriptional profile on the pWW0 plasmid by comprehensive transcriptome analysis.

## 2. Transcriptional control of the TOL plasmid pWW0 catabolic pathways

The *Pseudomonas putida* mt-2 host of the TOL plasmid pWW0 is able to assimilate *m*-xylene or toluene through a set of enzymes encoded by the TOL plasmid pWW0 (Assinder and Williams, 1990, Marques et al., 1999, Worsey and Williams, 1975). Two plasmid-encoded operons account for the entire metabolic process that leads to biodegradation of the aromatic substrate (Fig. 2). The *upper* operon determines enzymes that convert *m*-xylene or toluene into 3-methylbenzoate (i.e., 3MBz) or benzoate, and the *lower* operon enzymes catalyze the conversion of 3MBz into 3-methylcatechol or benzoate into catechol and its ensuing *meta* ring cleavage, which ultimately leads to intermediates of the TCA cycle (Assinder and Williams, 1990, Ramos et al., 1997). At the same time, benzoate is also degraded *via* the chromosomally encoded *ortho* pathway genes such as *ben, cat* and *pca* (Jimenez et al., 2002, Harwood and Parales, 1996). The TOL plasmid-encoded XylR and XylS regulatory proteins control expression of the corresponding operons. First, in the presence of *m*-xylene or toluene, XylR (expressed from $P_R$) activates both the $\sigma^{54}$-dependent promoters *Pu* (which transcribes the *upper* pathway operon) and *Ps*,

which drives expression of *xylS* (Bertoni et al., 1998, Marqués et al., 1998, Perez-Martin and de Lorenzo, 1995b). Since the $P_r$ promoter overlaps the XylR binding sites of the divergent *Ps* promoter, XylR expression is auto-regulated (Marqués et al., 1998, Bertoni et al., 1998). In turn, the XylS protein activates *Pm,* the promoter of the *meta* cleavage operon (Bertoni et al., 1998, Marques et al., 1999, Dominguez-Cuevas et al., 2008, Dominguez-Cuevas et al., 2010).

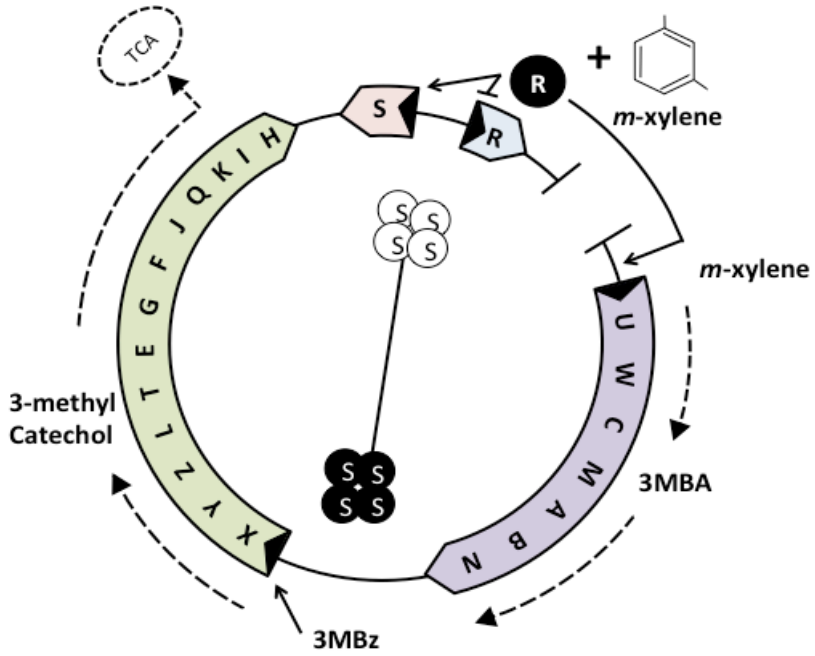


**Figure 2. Regulatory networks for TOL catabolic pathway expression and *m*-xylene biodegradation borne by the catabolic enzymes in the TOL plasmid.** The catabolic and regulatory genes (*xyl*) are described. The promoters *Pr, Ps*, *Pu* and *Pm* are depicted as dark triangles in each gene or operon. Filled circles represent active form regulators. 3MBA, 3-methylbenzylalcohol; 3MBz, 3-methylbenzoate; TCA, tricarboxylic acid cycle.

In addition to these plasmid-encoded regulators and promoters, a number of host factors have also been reported to influence expression of the TOL genes to varying degrees. For instance, the *Pu* promoter includes a target sequence for integration host factor (IHF) protein between the upstream activating sequences (UAS) and the $\sigma^{54}$-RNAP binding region. The IHF contributes structural aid to improve contacts between the RNA polymerase (RNAP) binding positions and the activator protein

attached to the UAS, thereby enhancing promoter activity (Perez-Martin and De Lorenzo, 1995a, Perez-Martin et al., 1994). Histone-like protein HU is also involved in *Ps* stimulation (Perez-Martin and de Lorenzo, 1995b). Moreover, the TurA and PprA proteins, which are known as *Pu* promoter-binding proteins, repress the *upper* pathway activity (Rescalli et al., 2004, Vitale et al., 2008). The system is subject to various catabolite repression and physiological control checks (Aranda-Olmedo et al., 2005, Moreno et al., 2010, Velazquez et al., 2004). In this scenario, pWW0-borne proteins and host native regulators and small molecules interact to shape a complex metabolic and transcriptional circuit that has recently been reviewed (Silva-Rocha et al., 2011b) and (at least partially) modeled (Silva-Rocha et al., 2011a). Specific nodes of such a network have been studied in extraordinary molecular detail (Koutinas et al., 2010, Silva-Rocha et al., 2011b), and even more regulatory devices are likely to appear. The reason for the existence of this complicated genetic circuitry found in the TOL system is still unexplained (Silva-Rocha et al., 2011a).

One approach to addressing this question is to examine the regulatory behavior of the entire system rather than its parts. Velázquez *et al*. (2005) and Domínguez-Cuevas *et al*. (2006) first documented the genome-wide transcriptional response of *P. putida* mt-2 when cells faced various aromatic compounds –whether they are TOL substrates or not (Dominguez-Cuevas et al., 2006, Velazquez et al., 2005). While these studies were instrumental in verifying the layout of the regulatory circuit proposed earlier on the basis of one-at-a-time reporter fusions to the TOL promoters (Marques et al., 1994, Hugouvieux-Cotte-Pattat et al., 1990), the technology of the time was insufficient to examine key aspects of the *m*-xylene sub-transcriptome, e.g., the fine structure of the TOL operons, the regulatory crosstalk of plasmid and host metabolic genes, and the action of post-transcriptional RNA-based regulation devices. To overcome this problem and generate a high-definition expression profile of such catabolic genes, high-throughput transcription approaches are necessary. Since the techniques allow us to study the unbiased transcriptome (Mader et al., 2011, Sorek and Cossart, 2010), it helps to understand

the complexity of bacterial transcription. Further information regarding transcriptional analysis is described in the following section.

### 3. Towards high-resolution mapping for the bacterial transcriptome

Genome-wide transcriptome analyses for bacteria have been studied by two main techniques: RNA sequencing (RNA-seq) and genomic tiling arrays (Guell et al., 2009, Passalacqua et al., 2009, Yoder-Himes et al., 2009, Selinger et al., 2000, Toledo-Arana et al., 2009, McGrath et al., 2007, Kim et al., 2013, Nikel et al., 2014). To follow the sequencing-based approach, an optimal protocol is necessary. First of all, total RNA should be extracted with an acid guanidium thiocyanate-phenol-chloroform mixture to obtain total RNA, including very small size RNA. Column-based systems such as silica-based purification are able to isolate RNAs longer than 200 nucleotides (nt). In addition, the rRNA/tRNA fraction is very high (95%) in the RNA sample, and thus those RNAs are removed before enrichment of mRNA for RNA-seq experiments. While the cDNA is synthesized from the sample, it is also important to avoid artifacts for strand-specific libraries. It was reported that secondary cDNA could be generated during reverse transcription (Perocchi et al., 2007); hence, use of actinomycin D is suggested in this procedure to identify the exact orientation of transcripts (Perocchi et al., 2007). The results of RNA-seq would generate millions of short reads representing RNA expressed in the conditions the researcher is testing. These reads are then matched to the reference genome and further analyzed with the read coverage.

The tiling array is based on hybridization with labeled DNA fixed onto a solid surface such as traditional microarray. The novel array system nonetheless has different probe sets compared to typical arrays, that is, the probes overlapping the adjacent up- and downstream partners respond to target genes as well as non-coding regions (Fig. 3). It can therefore provide unbiased transcription analysis leading to detection of hidden genetic information. The cDNA preparation procedure is very similar to that for RNA-seq, but the removal of rRNA/tRNA is not important,

because the non-specific RNA fraction does not interfere with signal detection in tiling array experiments. However, a gene expression profile such as the one from this analysis could potentially be obtained from non-specific results caused by cross-hybridization (Graf et al., 2007).

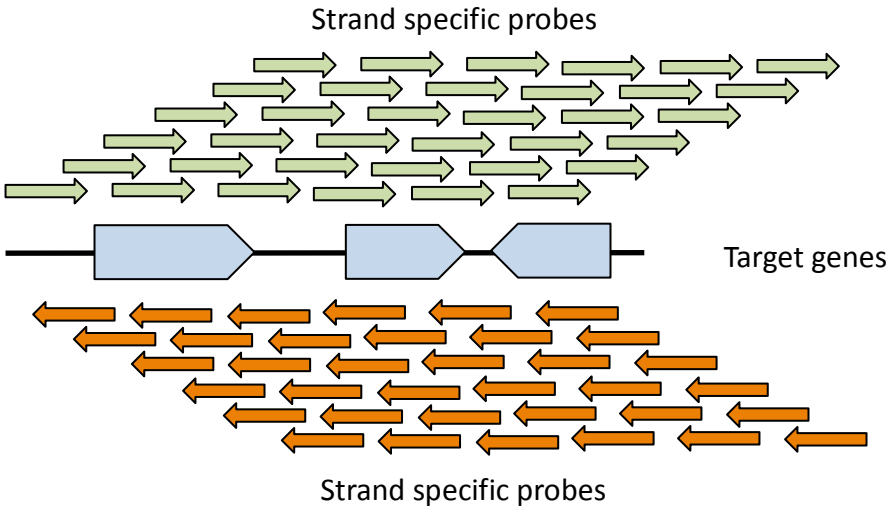


**Figure 3. Scheme of the tiling array probe set.** Blue arrows indicate target genes. Overlapping probes are shown as green or orange arrows responding to sense- and antisense transcripts, respectively.

Tiling approaches are powerful tools to identify genomic elements such as new genes, to define transcription start sites as well as operon structure, which are not possible in classical transcription analysis due to use of a small set of target genes. The studies enable us to detect and characterize transcribed regions that lie outside the known annotation; in this case, it would be mostly new protein-coding genes, *cis*-acting regulatory regions, small (non-coding) RNAs, and antisense transcripts (Fig. 4A). The profile also gives us insight for the gene annotation responding to the actual transcription start site (Fig. 4B) and untranslated region (UTR; Fig. 4C). The non-coding region might contain regulatory elements (e.g., riboswitch), and controls up to 2% of bacterial genes (Mandal et al., 2003). Despite its biological significance, it is not easy to detect using a computational approach without sequence information and structure. High-resolution transcriptome mapping can reveal the regulatory region with respect to the whole genome, as contiguous expression extending into the flanking intergenic region of a protein-coding gene is

indicative of a 5' or 3' UTR. Furthermore, the information can be deployed to determine operon structure (Fig. 4D). Many genes in bacterial cells are arranged in operons, and their prediction by computational analysis is also available, although accuracy is not high (Mao et al., 2009). The continuous expression signals on consecutive genes strongly imply polycistronic mRNA driven by the same regulon.

In this work, we constructed an array that spans 14704 base pairs (bp) of DNA, including the two strands of the corresponding *xyl* genes of the TOL system in its entirety, as well as the chromosomal *ortho* pathway genes involving *ben* and *cat* sequences. Each probe was designed as a 60-mer overlapping 50 nucleotides with the adjacent up- and downstream partners. The use of this type of array is instrumental for visualizing the detailed transcriptional state of cells while they are engaged in degradation of a suite of aromatic compounds. RNA-seq experiments are also considered to validate the array-based analysis, and can give further insight into the genetic elements relative to the TOL catabolic system as well as its backbone structure.

One of the weaknesses of the transcriptome methods is that they show the transcription profile as the *average* level from the cell population. Nonetheless, much evidence has accumulated showing that bacterial gene expression is dynamic from cell to cell, although cells living in the same environment are genetically identical. Single cell transcriptomics will therefore allow us to test the stochasticity in gene expression. Below I discuss the issue in terms of transcriptional bursting induced by the TOL regulatory network.

**4. Spatial organization of cellular components in bacteria**

Although bacteria do not possess an intracellular membrane, this does not mean that cell components are organized irregularly or free to diffuse. Many studies have shown that biomolecules are spatially organized in subcellular regions of bacteria.

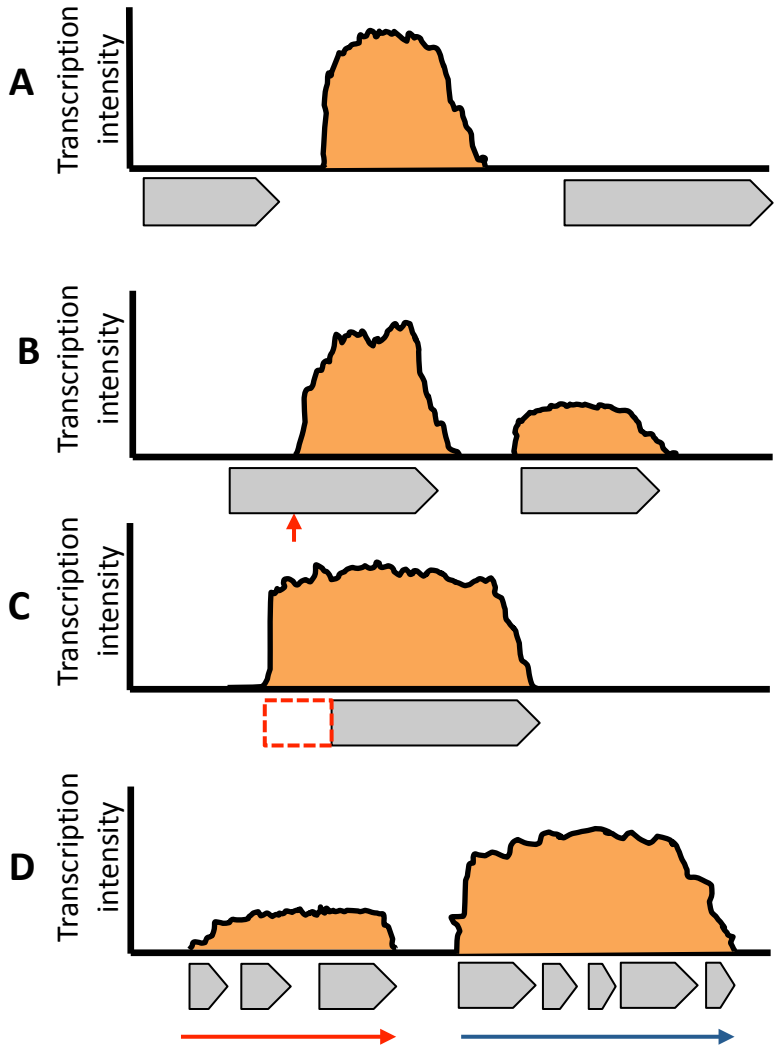


**Figure. 4. Discovery of genetic elements by genome-wide transcriptome analysis.** Based on high-resolution transcription mapping, new genes can be found that imply novel protein-coding genes, *cis*-acting regulatory regions, small (non-coding) RNA, and antisense transcripts (A). The information can also be used to correct gene annotation (B; actual start codon can be predicted in the correct site marked with red arrow). 5' or 3' untranslated regions (dotted square) can be detected in the entire genome (C). The continuous expression profile determines operon structure (D; red and blue arrows indicate each polycistronic mRNA). In all panels, the x axis represents a schematic genomic region and the y axis represents transcriptional intensity as obtained from RNA-seq or tiling array analysis. The gray arrows depict annotated genes.

The best example is chromosome organization in the microbial cell. The DNA that is defined as a nucleoid, with about 1000-fold compaction in bacterial cells, is also concentrated in the central part of the cytoplasm, and bacteria thus have a cellular

positioning mechanism to coordinate chromosome segregation and cell division (Lewis, 2004, Toro and Shapiro, 2010, Lau et al., 2003). In addition to DNA organization, many proteins, especially bacterial cytoskeletal-like proteins such as tubulin (FtsZ, MinCD), actin (MreB, FtsA, ParM) and intermediate filament (Crescentin, FilP), are located in subcellular regions that allow them to maintain cell shape and morphology, subcellular architecture, cell division and differentiation (Esue et al., 2010, Fuchino et al., 2013, Marston et al., 1998, Ausmees et al., 2003, Rico et al., 2004, Chiu et al., 2008, Specht et al., 2013).

In some species, ribosome distribution and concentration is observed in subregions of the cells (Fig. 5A). In *Escherichia coli*, the L7 and L12 subunits of ribosomes were detected indirectly by immunofluorescence microscopy and found to be nucleoid-free (Azam et al., 2000). More recently, Bakshi *et al*., using super-resolution microscopy with S2 subunit-tagged YFP (yellow fluorescent protein), observed that most ribosomes were concentrated in nucleoid-free regions, while only 10-15% of the molecules overlapped with the chromosomal DNA (Bakshi et al., 2012). Similarly, in moderate growth conditions, *Bacillus subtilis* ribosomes appeared toward the cell pole with little overlap with the DNA region (Lewis et al., 2000). A cryoelectron tomographic approach also showed ribosome occupation of the cytoplasmic periphery, which is a nucleoid-free region in the tiny bacterium *Bdellovibrio bacteriovorus* (Borgnia et al., 2008). This ribosome-nucleoid segregation strongly suggests that translation might occur in ribosome-rich sites and protein synthesis seems to be compartmentalized from transcription, since RNA polymerases are distributed within the nucleoid, at least in *E. coli* and *B. subtilis* (Lewis et al., 2000, Bakshi et al., 2012). This biological mechanism is not able to adjust to all species, however, because partitioning of ribosome and DNA is not found in some bacteria such as *Caulobacter crescentus*, *Agrobacterium tumefaciens*, *Sinorhizobium meliloti* and *Mycoplasma pneumoniae* (Briegel et al., 2006, Kahng and Shapiro, 2003, Montero Llopis et al., 2010, Ortiz et al., 2006, Seto et al., 2001, Kuhner et al., 2009). In these cells, ribosomes are evenly distributed in the cytoplasm and DNA is organized throughout the cell (Fig. 5B).

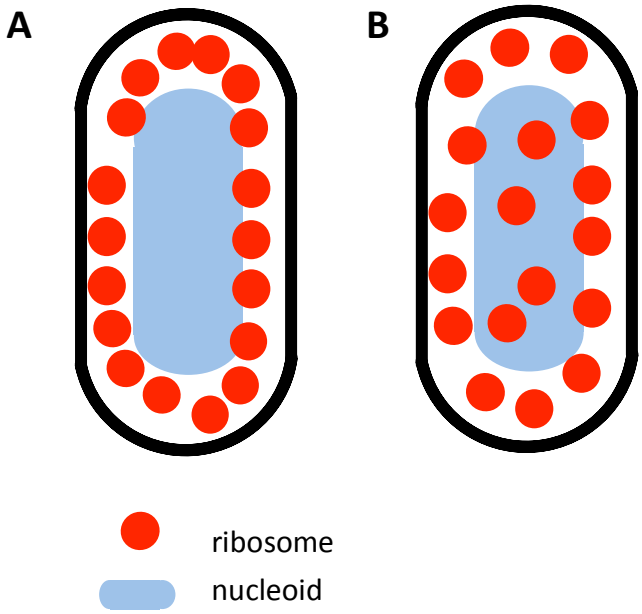


**Figure 5. Scheme showing of two distinct patterns of spatial distribution of ribosomes and chromosome in bacteria.** Nucleoid-ribosome segregation has been observed in *Escherichia coli*, *Bacillus subtilis* and *Bdellovibrio bacteriovoru* (A). In sharp contrast, ribosomes are evenly distributed in cytoplasm in *Caulobacter crescentus*, *Agrobacterium tumefaciens*, *Sinorhizobium meliloti* and *Mycoplasma pneumonia* (B).

Recent studies showed that bacterial transcripts also occupy certain subcellular locations (Fig. 6). The Wagner laboratory used RNA fluorescent *in situ* hybridization (FISH) and detected the *groESL* or *creS* mRNA in *Caulobacter* as fluorescent foci at specific sites; they also found that *lacZ* mRNA in *E. coli* occupied a distinct location (Montero Llopis et al., 2010). Moreover, all the transcripts expressed from chromosomal DNA remained close to their transcription sites, with limited dispersion (Montero Llopis et al., 2010). The *bglGFB* mRNAs for β-glucoside metabolism in *E. coli* were also reported as subcellular localization components; however, each of the messengers is observed in its future protein functional site, which suggests that the mRNAs can migrate to a particular region (Nevo-Dinur et al., 2011). Briefly, the BglG protein (a transcriptional factor) occupies cell poles, the BglF protein (membrane-bound sugar permease) is distributed in the cell membrane and BglB (a phospho-β-glucosidase) is observed in cytoplasm. According to its protein localization, each mRNA for *bglG*, *bglF* or

*bglB* was observed at cell poles, membrane or cytoplasm, respectively (Nevo-Dinur et al., 2011). The localization feature remains unchanged, even though translation is inhibited in the strain (Nevo-Dinur et al., 2011).

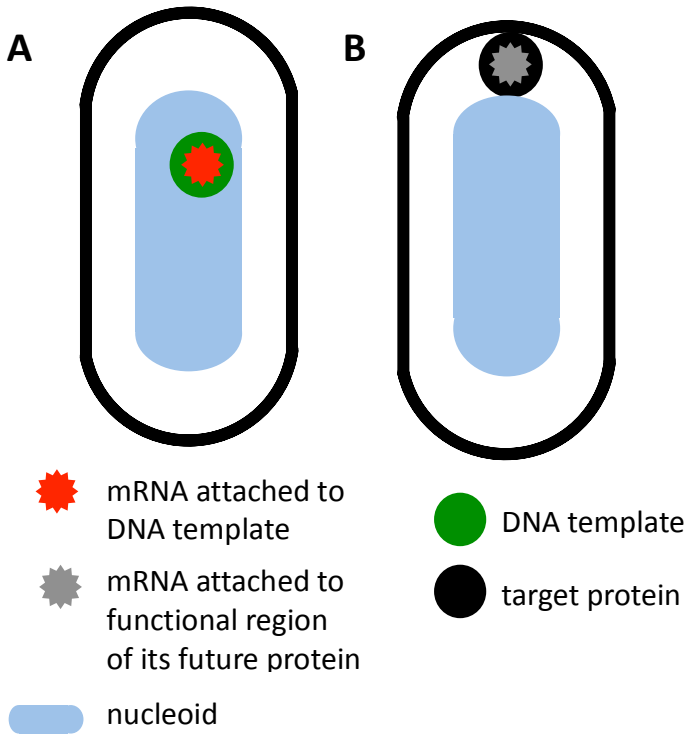


**Figure 6. The known localization for specific mRNA in bacteria.** The molecule resides near its template site (A; e.g., *groESL* or *creS* mRNA in *Caulobacter* and *lacZ* in *E. coli*) or it is likely to migrate to the functional region of the future protein (B; e.g., the *bglGFB* mRNAs in *E. coli*).

In addition to the structural genes, regulatory RNAs are also a characteristic of subcellular localization. tmRNA, a small RNA that interacts with a translating ribosome, is observed as a form of helix-like structure in in G1 phase *C. crescentus* cells (Russell and Keiler, 2009).

*P. putida* KT2440, the pWW0 plasmid-less strain of *P. putida* mt-2, is a metabolically versatile, saprophytic soil bacterium that has been extensively studied for its metabolism and physiology, as it responds to many environmental cues (Jimenez et al., 2002, Reva et al., 2006, Nelson et al., 2002); however, little

information is available regarding the organization of its cellular components. Moreover, there is no report of the localization of transcripts synthesized from plasmid DNA. We therefore examined the distribution of macromolecules such as ribosome protein as translational machinery, RNAP as transcriptional machinery, and mRNA as a genetic message in this soil bacterium. To this end, we traced these machinery proteins using fluorescent protein fusion to ribosomal protein or the RNAP subunit. In addition, we obtained the results of transcript localization using FISH with complementary fluorophore probes corresponding to *xyl* catabolic genes in the TOL plasmid.

**5. Analysis of RNA visualization in a bacterial cell**

Studies of RNA dynamics in bacteria have been conducted using several techniques that enable visualization of RNA molecules (Golding and Cox, 2004, Broude, 2011, Valencia-Burton et al., 2007, Nevo-Dinur et al., 2011, Montero Llopis et al., 2010, Pilhofer et al., 2009). Two types of approaches were used for those studies. RNA can be monitored indirectly with fluorescent fusion to RNA-binding protein (Fig. 7A). For instance, a phage RNA-binding protein can be used; the MS2 coat protein (MS2) is expressed with fluorescent protein by cell manipulation. At the same time, a target mRNA is also required, which is tagged with an array of MS2-binding motifs within the bacterial cell. When these components are expressed simultaneously in a cell, the MS2-fluorescent protein fusion proteins bind the aptamers and the interaction renders the RNA fluorescent. This method allows detection of the molecule in live cells and monitoring in time series. Analysis with this two-component system nonetheless has several drawbacks. First, it can display strong background due to unbound MS2-fluorescent protein fusion protein (Broude, 2011) and second, the fusion proteins tend to aggregate when they are highly expressed; the molecules accumulate in particular regions, which causes artifactual mRNA localization and affects transcript counting (Montero Llopis et al., 2010). In addition, the target mRNA is not endogenous and should be modified to bear the binding motif that affects cell physiology. Moreover, the molecule with the

aptamers becomes stable and hardly degrades regardless of cell growth, since bound MS2-fluorescent protein fusion protects the mRNA from the RNA-degrading enzymes (Golding et al., 2005).

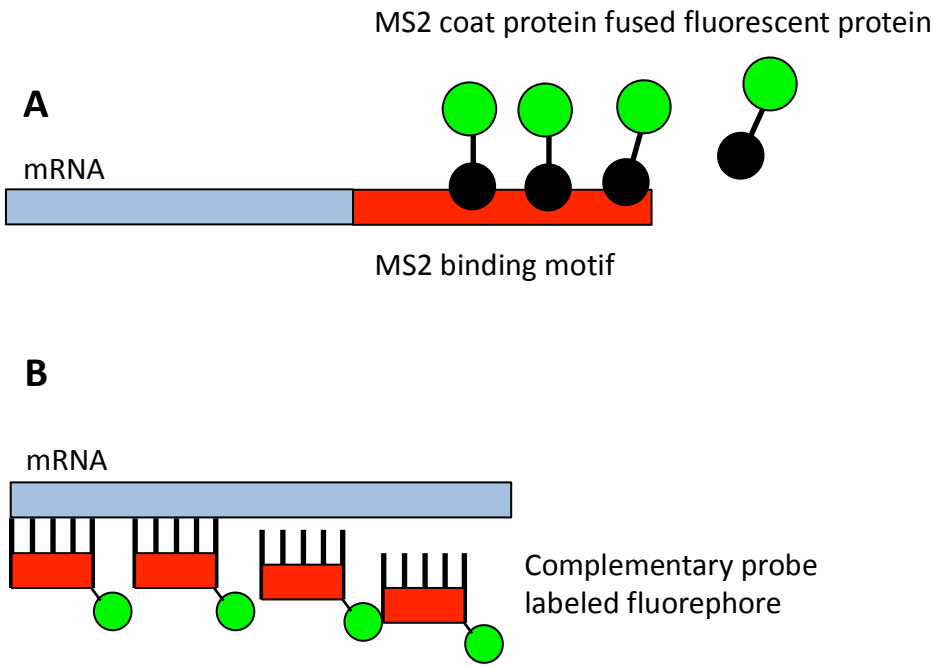


**Figure 7. Scheme showing RNA visualization methods.** (A) In an indirect approach, RNA is tagged with an array of aptamers that bind MS2 coat protein with high affinity. The RNA is then sensed by MS2 coat protein expressed as a fusion with fluorescent protein. (B) In a direct method, the target mRNA can be detected in a cell by fluorescent *in situ* hybridization with its complementary probe that is labeled fluorescently.

Alternatively, the RNA can be sensed directly by fluorescent *in situ* hybridization (FISH; Fig. 7B). Briefly, hybridization of fluorescently labeled oligonucleotide probes enables visualization the RNA of interest. The method does not require modification of the target RNA or any other genetic elements. The signal obtained in the experiment therefore provides information about intact transcripts in a cell. Cell fixation is needed for this approach, however, which can affect cell physiology and makes study of live cells impossible (Russell and Keiler, 2012). Nevertheless, FISH-based RNA visualization analysis shows not only information on the spatial organization of the molecule, but also the transcription profile at the single-cell

level (Fernandez et al., 2012); that is, the fluorescent spots resulting from the experiment imply accumulation of multiple mRNAs. Calibrating the number of the molecules by image analysis, considering negatives false, will provide the expression level in a cell (Skinner et al., 2013). Based on the mRNA copy number statistics, we can better understand the stochastic transcription kinetics (So et al., 2011).

Single cell analysis showed transcriptional bursting, a characteristic of eukaryotes (Yunger et al., 2010, Raj et al., 2006, Zenklusen et al., 2008) as well as prokaryotes (Golding and Cox, 2004, Golding et al., 2005). In other words, induced mRNA levels within a single cell show a pulsating profile that responds to inducer input. This transcriptional behavior leads to a bimodal distribution of the mRNA induction level for genetically identical cells (Gutierrez et al., 2012). Although many results of single cell analysis have accumulated, however, it remains unclear which factors induce this fluctuation and its significance in the cell. To consider this issue, we analyzed *upper* and *lower* pathway gene expression in *P. putida* mt-2 at the single cell level by collecting the data obtained in FISH experiments.

**6. The issue at stake**

Gene expression, synthesis of mRNA from the DNA containing information, is fundamental in living organisms to produce functional products. Transcription is controlled in response to a wide variety of fluctuating conditions, and its regulation also helps organisms to optimize utilization of energy and materials that are limited in their environmental niche. To understand bacterial gene expression and regulation, it is necessary to consider not only biochemical interaction but also the physical effect of the molecules. Recent studies have unraveled the underlying mechanism of transcriptional regulation with respect to *cis* and *trans* genetic elements. At time same time, much evidence is emerging to show that bacterial cell components are organized spatially. This idea strongly suggests that those molecules are functionally associated with the transcriptional network and affect

transcription, influencing bacterial physiology. Such features are little known in *P. putida*, however; although the TOL system has been characterized extensively in this strain, further studies are required to test for hidden aspects such as the existence of another promoter in the operons, *cis* or *trans* regulators, and organization of the transcription and translation factory. To identify such transcription factors and acquire a broader view of the expression profile for aromatic compound metabolism, we employed different techniques to examine the transcriptome of the TOL system in *P. putida* mt-2, as well as the distribution of transcriptional and translational machineries.

# II. Objectives

## Objectives

### General objectives:

To investigate genome wide-transcription with respect to *m*-xylene/toluene assimilation in *Pseudomonas putida* mt-2.

### Specific objectives:

1. To study high-resolution mapping for the TOL catabolic system in the pWW0 plasmid of *P. putida* relative to different aromatic compounds.
2. To identify functional genetic elements of IncP-9 backbone genes in the pWW0 plasmid.
3. To characterize organization of macromolecules such as ribosomes, RNA polymerase and specific mRNAs in *P. putida.*
4. To analyze expression of the *xyl* genes at the single-cell level.

# III. Materials and Methods

## 1. Culture conditions and media

Unless otherwise indicated, *E. coli* and *P. putida* were routinely grown at 37°C and 30°C, respectively, in Luria–Bertani (LB) or M9 minimal medium including 6 g $l^{-1}$ $Na_2HPO_4$, 3 g $l^{-1}$ $KH_2PO_4$, 1.4 g $l^{-1}$ $(NH_4)_2SO_4$, 0.5 g $l^{-1}$ NaCl, 0.2 g $l^{-1}$ $MgSO_4 \cdot 7H_2O$ and 2.5 ml $l^{-1}$ of a trace element solution as noted (Nikel and de Lorenzo, 2013, Abril et al., 1989), with a carbon source as described below. For induction of TOL catabolic genes, the *P. putida* mt-2 strain was cultured in M9 medium with succinate (overnight), and bacterial cultures were then diluted 100-fold in the same medium and grown to the exponential phase ($OD_{600}$ = 0.3-0.5). Samples were then cultured further without additional substrate or exposed to vaporous *m*-xylene, toluene or *o*-xylene (1/2 dilution in dibutylphthalate, which is a non-effector for TOL genes) in a flask (2 h). For soluble substrates, benzoate (5 mM) or 3MBz (5 mM) was added to the culture medium once growth had reached $OD_{600}$ ~0.3. For the reference condition, the cells were cultured for 96 h in succinate-supplemented minimal medium. The antibiotics kanamycin (Km) 50 μg $ml^{-1}$, ampicillin (Amp) 150 μg $ml^{-1}$, streptomycin (Sm) 100 μg $ml^{-1}$, chloramphenicol (Cm) 30 μg $ml^{-1}$ and gentamycin (Gm) 10 μg $ml^{-1}$ were added to bacterial cultures when necessary. Alternatively, to inhibit bacterial transcription and translation, Cm (200 μg ml-1) and rifampicin (Rif; 200 μg ml-1) were used.

## 2. Bacterial strains

The characteristics of the bacteria used are described in Table I.

**Table 1.** Description of bacterial strains used in this study

| Strain | Description | Reference |
|---|---|---|
| *P. putida strains* | | |
| mt-2 | *P. putida* wild type with pWW0 plasmid | Worsey and Williams, 1975 |

| | | |
|---|---|---|
| KT2440 | Wild-type strain derived of *P. putida* mt-2 cured pWW0 plasmid | Nelson et al., 2002 |
| MEG3D | KT2440 derivate harboring *Pm* promoter fused *gfp-lacZ* reporter gene on chromosome | Silva-Rocha and de Lorenzo, 2012 |
| MEG3D (pSEVA224 -XylS [±]) | $Km^R$, MEG3D strain harboring pSEVA224-XylS [±] plasmid | This study |
| mt-2 (pSEVA225-*PbenA→lacZ*) | $Km^R$, mt-2 strain harboring pSEVA225 *PbenA→lacZ* plasmid | This study |
| mt-2 (pSEVA225T-*PbenA→lacZ*) | $Km^R$, mt-2 strain harboring pSEVA225T-*PbenA→lacZ* plasmid | This study |
| KT2440(pSEVA226-*PmpfR→lux*) | $Km^R$, KT2440 strain harboring pSEVA226-*PmpfR→lux* plasmid | This study |
| mt-2 (pSEVA226-*PmpfR*→lux) | $Km^R$, mt-2 strain harboring pSEVA226-*PmpfR→lux* plasmid | This study |
| MEG2 | $Km^R$, KT2440 derivate C-terminal GFP tag of ribosomal protein L13 | Martinez-Garcia et al., 2011 |
| KT2440 β'-msfGFP | KT2440 derivate with RNAP β' subunit labeled by *msf*GFP | This study |
| KT2440 β'-msfGFP/ L13-mChrry | KT2440 β'-*msf*GFP derivate with ribosomal protein L13 labeled by mCherry | This study |
| KT2440L9 | $Km^R$, KT2440 derivate with ribosomal protein L9 labeled by *msf*GFP | Calles et al., In preparation |
| KT2440T7 | $Gm^R$, KT2440 derivate with chromosomal T7 polymerase expression system | Troeschel et al., 2012 |
| mt-2 (TOL-PuxT7) | mt-2 strain carrying manipulated pWW0 plasmid TOL-PuxT7 | This study |
| KT2440T7 (TOL-PuxT7) | KT2440T7 strain carrying manipulated pWW0 plasmid TOL-PuxT7 | This study |

*E. coli* strains

| | | |
|---|---|---|
| HB101 | $Sm^R$, *hsdR⁻M⁺, pro, leu, thi, recA* | Sambrook et al., 1989 |
| CC118 | F-, Δ(*ara-leu*)7697, *araD*139, Δ(*lac*)X74, *pho*AΔ20, *galE*, *galK*, *thi*, *rpsE*, *rpoB* | Manoil and Beckwith, 1985 |
| DH5αλ*pir* | λ*pir* phage lysogen of DH5α | Lab collection |

**3. Plasmids**

The plasmids used in this study are described in Table 2, with brief genotypes. Procedures of specific plasmid construction will be described in following sections.

**Table 2.** Plasmids used in this work

| Plasmid | Description | References |
|---|---|---|
| pRK600 | $Cm^R$, *oriV* ColE1, *tra+mob+* of RK2, helper plasmid for mobilization in tripartite conjugations | Kessler et al., 1992 |
| pSW | $Amp^R$, *ori*RK2, *xylS,* bearing a *Pm→I*-sceI transcriptional fusion | Wong and Mekalanos, 2000 |
| pSEVA224 | $Km^R$, *ori*RK2, Enable expression cloning gene driven Lac$I^q$ *Ptrc* promoter | Silva-Rocha et al., 2013 |
| pSEVA224-XylS [±] | $Km^R$, pSEVA224 carrying both sense and artificial antisense *xylS* transcription by its own promoter *Ps* and Lac$I^q$ *Ptrc* promoter | This study |
| pSEVA225 | $Km^R$, *ori*RK2, promoterless *lac*Z, vector for constructing transcriptional fusions | Silva-Rocha et al., 2013 |
| pSEVA225T | $Km^R$, *ori*RK2, promoterless *lac*Z, vector for cloning *in-frame* translational fusions with *lac*Z | Silva-Rocha et al., 2013 |
| pSEVA225-*PbenA→lacZ* | $Km^R$, lacZ transcriptional fusion to *PbenA* promoter in pSEVA225 | This study |
| pSEVA225T-*PbenA→lacZ* | $Km^R$, LacZ translational fusion to *PbenA* promoter in pSEVA225T | This study |

| | | |
|---|---|---|
| pSEVA431 | $Sm^R$, *ori*pBBR1, Standard broad-host range cloning plasmid | Silva-Rocha et al., 2013 |
| pSEVA431-*xylL* | partial gene of the *xylL* insertion into pSEVA431 | This study |
| pGEM-T | $Amp^R$, bearing T7 and SP6 promoter both ends of the insertion region | Promega |
| pGEM-T-*xylS*nr | $Amp^R$, intergenic region of *xylS* gene cloning into pGEM-T | This study |
| pGEM-T-*xylSH*nr | $Amp^R$, down stream region of *xylS* cloning into pGEM-T | This study |
| pSEVA226 | $Km^R$, *ori*RK2, *luxCDABE* reporter plasmid | Silva-Rocha et al., 2013 |
| pSEVA226-*PmpfR→lux* | $Km^R$, *mpfR* putative promoter cloned in pSEVA226 | This study |
| pEMG | $Km^R$, *ori*R6K, suicide plasmid with two I-SceI sites flanking the *lacZ*α polylinker | Martinez-Garcia and de Lorenzo, 2011 |
| pEMG-PuxT7 | $Km^R$, pEMG carrying T7 promoter with the upstream and downstream flanking regions of *Pu* promoter | This study |
| pEMG-*rpoC*-*msf*GFP | $Km^R$, pEMG carrying *msfGFP* gene with the upstream and downstream flanking regions of *P. putida rpoC* gene | This study |
| pEMG-*rplM*-mCherry | $Km^R$, pEMG carrying *mCherry* gene with the upstream and downstream flanking regions of *P. putida rplM* gene | This study |

**4. Construction of bacterial strains**

General methods for DNA handling were followed according to standard protocols (Sambrook and Russell, 2001). Plasmid DNA was isolated from bacterial cells using commercial Wizard *Plus* SV Minipreps DNA Purification kit (Promega) or the QIAprep Spin Miniprep Kit (Qiagen). To digest PCR products or plasmid DNA,

restriction endonucleases were purchased from New England Biolabs (NEB). For DNA ligation, Quick ligase (NEB) was used. To transfer recombinant DNA into *E. coli* cells, a chemically competent cell was used with heat shock (Sambrook and Russell, 2001). For *P. putida*, the manipulated DNA was incorporated by conjugative triparental mating using the *E. coli* HB101 (pRK600) as helper strain (de Lorenzo and Timmis, 1994) or by electroporation with competent cells as described (Choi et al., 2006). The primers for the PCR reaction in this study are described in Table 3. The procedure of each construction was as follows.

### 4.1. The *xylS* expression with antisense transcripts

For both sense and artificial antisense transcription of the *xylS*, the 1458-bp fragment from the *xylS* region covering its own promoter (*Ps*) and its extended 3' end was amplified using primers *xylS*-F and *xylS*-R. The amplicon was cloned into the XbaI/ SacI cloning site of the pSEVA224 vector including the $LacI^q$ P*trc* cargo to transcribe *xylS* in the antisense direction, to generate pSEVA224-*xylS* [±]. The plasmid construct was then introduced into *E. coli* CC118 by transformation. The pSEVA224-*xylS* [±] plasmid was then introduced by triparental conjugation into *P. putida* MEG3D harboring the *Pm* promoter fused to the *gfp-lacZ* reporter gene on chromosome (Silva-Rocha and de Lorenzo, 2012b), thus generating *P. putida* MEG3D (pSEVA224-*xylS* [±]).

### 4.2. *PbenA* transcriptional and translational fusion to *lacZ* reporter

To generate a transcription or a translation fusion of *PbenA* to *lacZ*, the promoter region was amplified using the Pben-F/Pben-R primer pairs or Pben-F/PbenT-R, and the PCR product was cloned into pSEVA225 or pSEVA225T for the transcription or translation fusion respectively. Each construct was then transferred into the *P. putida* mt-2 strain.

### 4.3. Validation of annotated sequence of the *xylL* gene

To confirm the DNA sequence of the intergenic region of the *xylL* gene, its partial region was amplified using the primers xylL-F/xylL-R based on the TOL plasmid in the mt-2 strain as template. Restricting both the PCR product and the

pSEVA431 plasmid with *Sph*I and *Sac*I enzymes, cloning was performed for the partial *xylL* gene and the construct was used to validate the annotated DNA sequence.

### 4.4. *Pmpf* promoter reporter on different backgrounds

pSEVA226 including *lux* genes was used to construct a reporter plasmid driven by the *mpfR* promoter. A putative promoter region (360 bp) on *mpf*R in the pWW0 plasmid was amplified using primer pairs Pmpf-F and Pmpf-R, and the amplicon was inserted into the *Pac*I and *Sph*I cloning site of the pSEVA226 vector, generating pSEVA226-P*mpf::lux*. The construct was then introduced into the *E. coli* CC118 competent strain by heat shock. The plasmid was subsequently transferred into *P. putida* KT2440 or mt-2 strain by triparental conjugation, thus generating *P. putida* KT2440 (pSEVA226-*PmpfR*→*lux*) or *P. putida* mt-2 (pSEVA226-*PmpfR*→ *lux*).

### 4.5. Construction of RNAP-labeled cells and dual cell labeling with RNAP and ribosome

Using a seamless genomic deletion system and isothermal assembly, we generated the KT2440 derivate strains KT2440 β'-msfGFP and KT2440 β'-msfGFP/ L13-mCherry (Nelson et al., 2002, Martinez-Garcia and de Lorenzo, 2011). To this end, the upstream (TS1, ~0.5 kb) and downstream (TS2, ~0.5 kb) regions of *P. putida rpoC* and *rplM* genes were amplified by PCR with their respective primer pairs (rpoC-TS1F/R and rpoC-TS2F/R; rplM-TS1F/R and rplM-TS2F/R). We used the primer pairs rpoC-msfGFP-F/R and rplM-mCherry-F/R to obtain *msf*GFP or mCherry, which have overlapping regions with TS1 and TS2 fragments derived from *rpoC* and from *rplM*. Thus, TS1 (*rpoC*), msfGFP and TS2 (*rpoC*) were joined by isothermal assembly (Gibson et al., 2009) with the pEMG plasmid digested by *Eco*RI and *Bam*HI, to yield pEMG-*rpoC-msf*GFP, which was introduced into the DH5αλ*pir* strain. In a similar approach, the *E. coli* strain harboring the plasmid pEMG-*rplM*-mCherry was obtained and the plasmid with the *rpoC* fusion was transferred into *P. putida* KT2440 by triparental mating. The

pSW plasmid that expresses I-sceI endonuclease under the *Pm* promoter (Wong and Mekalanos, 2000) was introduced by electroporation into the chromosomally cointegrated strain, and thus has resistance for both Km and Amp. The clones were grown in LB medium with Amp (500 μg $ml^{-1}$) and 3MBz (15 mM) to activate the *Pm* promoter, allowing I-sceI expression. The cells were plated on LB agar and we confirmed precise fusion eliminating the plasmid backbone, including the Km resistance gene, by streak replicates of single colonies on LB and LB-Km plates. The Km-sensitive clones were selected and further confirmed by PCR with rpoC-TS1F/TS2R primer pairs. Finally, pSW was cured from the RpoC labeled strain or remained for another mCherry labeling of ribosomal protein L13 in the cell, using the procedure described above.

### 4.6. Replacement of the *Pu* promoter in pWW0 plasmid with the T7 promoter

Using the scarless deletion system (Martinez-Garcia and de Lorenzo, 2011), the *Pu* promoter was replaced with the T7 promoter in the pWW0 TOL plasmid. The upstream (TS1) and downstream (TS2) flanking regions of the *Pu* promoter, including host and plasmid regulatory sites were amplified by PCR with primer pairs including the T7 promoter sequence (PuxT7 TS1F/-R and PuxT7 TS2F/-R). Each amplicon was then joined by overlap extension (SOE)-PCR, to produce ~1 KB of TS1-$P_{T7}$-TS2. The fragment was digested with *Eco*RI and *Bam*HI and ligated within the same pEMG site to generate pEMG-PuxT7. For further procedures such as cointegration of the plasmid into the pWW0 plasmid, elimination of the antibiotic marker, and clone confirmation, we followed the approach described above for protein labeling by fluorescent protein fusion to replaced the promoter in pWW0. The plasmid was either maintained in the mt-2 strain or transferred into the KT2440T7 strain by conjugation.

**Table 3.** Oligonucleotides synthesized in this study for PCR reactions

| Name (restriction site) | Sequence (5'-3') |
|---|---|
| XylS-F(*Xba*I) | CGCTCTAGACTTAAAAAGAACGTCTTCGTT |
| Xyls-R (*Sac*I) | CGCGAGCTCGGATGCGCCGCTGACCA CGT |

| | |
|---|---|
| Pben-F(*Sac*I) | ATGGAGCTCACCTGGTAGCTGCAAAAGGA |
| Pben-R(*Bam*HI) | GTCGGATCCGCCAGGGTCTCCCTTGTTAT |
| Pben-TR(*Bam*HI) | CGCGGATCCGGGTCGGTGAACATC |
| xylL pt F (*Sph*I) | CGCGCATGCACTTCGAACACCTCGTAGCC |
| xylL pt R (*Sac*I) | CGCGAGCTCGGTCGAGGCAATTCTGTTCC |
| xylSnr-F (*Sph*I) | CGCGCATGCACAATCTCCAGCAACTCGATG |
| xylSnr-R (*Sac*I) | CGCGAGCTCCATCATCGCCAGCTCCGCTAA |
| xylSHnr-F(*Sph*I) | CGCGCATGCGAAGGGATGGGTTGGCATCGC |
| xylSHnr-R (*Sac*I) | CGCGAGCTCTGAAGTGGAGATCCCAAGGGC |
| orf13-F | GCCGTTCCAACTATCGCGAATCAGC |
| orf13-R | AAAGATTCACTTCTGG GACGCGGG |
| Pmpf-F (*Pac*I) | CGCTTAATTAAGGAGCCGGCGACCTAATGCA |
| Pmpf-R (*Sph*I) | CGCGCATGCGGCGACGGCGAAAACCGCCA |
| PuxT7 TS1F (*Eco*RI) | CGCGAATTCGTCGGATACGGCGGGCGACCG |
| PuxT7 TS1R | CCCTATAGTGAGTCGTATTAAGAAGACAGCCTTG ACTTTCA |
| PuxT7 TS2F | TTAATACGACTCACTATAGGGGACTTAAAATAAA AATAGTG |
| PuxT7 TS2R (*Bam*HI) | CGCGGATCCCAAATGTTATAGGTAGCAAGGA |
| rpoC-TS1F | CGGCCAGTATAGGGATAACAGGGTAATCTGAATT CGAGCTCGAAGTTATCTCCGACGGCCCG |
| rpoC-TS1R | CACCTTTACTGCCACCGCCACCGCTATTACCGCTG GAATTCAGCGC |
| rpoC-msfGFP-F | CGAAGCGCTGAATTCCAGCGGTAATAGCGGTGGC GGTGGCAGTAA |
| rpoC-msfGFP-R | GGCTTGCCGGGGCCTTGCCCTGTACTTATTTGTAG AGTTCATCCAT |
| rpoC-TS2F | CGGCATGGATGAACTCTACAAATAAGTACAGGGC AAGGCCCCGGCA |
| rpoC-TS2R | CCCTAGAAGCTTGCATGCCTGCAGGTCGACTCTA GAGGATCCCGGTCTTCAGGTTAGCCCG |
| rplM-TS1F | CGGCCAGTATAGGGATAACAGGGTAATCTGAATT CGAGCTCGAAGTGATGCACCATCACGCAG |
| rplM-TS1R | TGCTCACACTGCCACCGCCACCGCTGATCTTCAG TTCTTGAGGCTG |
| rplM-mCherry-F | TGAAGATCAGCGGTGGCGGTGGCAGTGTGAGCA AGGGCGAGGAGGAT |

| | |
|---|---|
| rplM-mCherry-R | GTCGCCGACATAATGAACTATCCCGTTACTTGTA CAGCTCGTCCAT |
| rplM-TS2F | CGGCATGGACGAGCTGTACAAGTAACGGGATAG TTCATTATGTCGG |
| rplM-TS2R | CCCTAGAAGCTTGCATGCCTGCAGGTCGACTCTA GAGGATCCTCAATGGCACTAAAAATTGGC |

## 5. High-throughput transcription analysis

### 5.1. RNA preparation

Cell cultures were transferred to 1/10 sample volume of ice-cold ethanol/phenol solution (5% water-saturated phenol in ethanol) to protect RNA from degradation and harvested by centrifugation (3,800 rpm, 15 min, 4°C). After supernatant aspiration, pellets were frozen in liquid nitrogen and stored at -80°C until required. Total RNA was extracted by using the miRNeasy kit (Qiagen) with some modifications. The collected pellets were resuspended into 0.3 ml Tris-HCl (pH 7.5) containing 2 mg/ml lysozyme and incubated (10 min, 37°C). Lysate (0.1 ml) was used according to manufacturer's instructions. RNase-free DNase (Qiagen) treatment was performed during the isolation procedure to eliminate residual DNA and quality was evaluated on Model 2100 Bioanalyzer (Agilent).

### 5.2. High-density tiling array design and analysis

A custom tiling microarray was designed to contain probes corresponding to the complete *xyl* operon of the TOL plasmid, as well as chromosome clusters covering all β-ketoadipate and *ortho* pathway genes such as *fcs* cluster, *pca* genes, *ben* genes and *cat* genes. Oligonucleotide probes were 60 nucleotides long and were designed to be spaced every 10 nt and overlapping 50 nt. Both sense and antisense probes were designed to integrate the same regions and to identify natural antisense RNAs. Microarrays were synthesized by Agilent in a 8x15K format using the on-line tool eArray (https://earray.chem.agilent.com/earray/). Four biological replicates were hybridized independently for each transcriptomic comparison. Total RNA (20 μg each) was retrotranscribed and aminoallyl-labeled using the SuperScript Indirect cDNA Labeling System (Invitrogen) and 5-(3-aminoallyl)-2'deoxyuridine-5'-

triphosphate (aa-dUTP, Ambion) following manufacturers' protocols. To avoid antisense artifacts from second-strand cDNA during reverse transcription, actinomycin D was added after the denaturing step at 70°C to a final concentration of 6 μg/ml, as described (Perocchi et al., 2007). For each sample, aminoallyl-labeled cDNA was resuspended in 0.1 M $Na_2CO_3$ (pH 9.0) and conjugated with Cy3 or Hyper 5 Mono NHS Ester (CyTMDye Post-labelling Reactive Dye Pack, Amersham), following a dye-swap strategy. Samples were purified with Megaclear (Ambion) following the manufacturer's instructions. Cy3 and Hyper 5 incorporation was measured in a Nanodrop spectrophotometer (Nanodrop Technologies). Probe preparation and hybridizations were performed as described (Two-Color Microarray-Based Prokaryote Analysis, Agilent Technologies). Samples were placed on ice and rapidly loaded onto arrays, hybridized (65ºC, 17 h), then washed once in GE Wash Buffer 1 (room temperature, 1 min) and once in GE Wash Buffer 2 (37ºC, 1 min). Arrays were drained by centrifugation (2000 rpm, 2 min).

Images from Cy3 and Hyper 5 channels were equilibrated and captured with a GenePix 4000B (Axon) and spots were quantified using GenePix software (Axon) for tiling array data sets (*m*-xylene VS succinate). For other tiling array data sets that are reference condition-based comparisons, we used the Agilent DNA Microarray Scanner and quantified images using Agilent Feature Extraction software. After scanning and quantification, data from both datasets were analyzed using the same methods. Raw intensities were background-corrected by the normexp method with an offset of 50 (Smyth and Speed, 2003). Background-corrected intensities were converted to $\log_2$ scale and normalized by adjusting the quantiles of all replicates as described (Bolstad et al., 2003). After normalization, differential expression for each probe was calculated as $\log_2$Ratios = $\log_2$Intensity (experimental condition) - $\log_2$Intensity (control condition). Differential expression at the gene level was calculated by averaging all $\log_2$Ratios of the probes that overlap with the gene coordinates. All statistical calculations were carried out with R software (TheRDevelopmentCoreTeam, 2011) and the Bioconductor package

*limma* (Smyth, 2004). Integrated Genome Browser (IGB) (Nicol et al., 2009) was used to represent the $\log_2$Ratios of all probes in the genomic regions.

### 5.3. cDNA library construction for RNA deep sequencing

Total RNAs from *m*-xylene-treated cells or reference conditions were prepared. rRNA was depleted using the RiboZero rRNA removal kit (Epicenter Biotechnologies) for gram-negative bacteria with a total RNA input of 4 μg. To confirm rRNA removal, we analyzed the samples with the bioanalyzer as described above. RNA libraries were prepared using the TruSeq RNA sample prep kit (Illumina) following the protocol described in the TruSeq RNA Sample Preparation Guide, starting at the fragmentation step. The library was validated by running a High Sensitivity DNA chip (Agilent Technologies) on the bioanalyzer and quantified by qPCR according to the Illumina Sequencing Library qPCR Quantification Guide, using KAPA SYBR FAST qPCR kit for LC480 (KAPA Biosystems). The libraries were denatured and adjusted to 14 pM prior to generating the clusters as indicated in the Illumina Cluster Generation Guide for a Cluster Station instrument. Clusters were generated in one lane of the flow cell, which was sequenced in a single read 1x75bp run by the Genome Analyzer IIx.

### 5.4. Sequence read alignment and normalization for RNA deep sequencing

Short reads were aligned to the *P. putida* genome and pWW0 plasmid genes with the BWA algorithm with default values (Li and Durbin, 2009). Mapped counts were normalized by trimmed mean of M values (TMM) (Robinson and Oshlack, 2010) using the sample whose 75%-ile (of library-scale-scaled counts) is closest to the mean of 75%-iles as the reference. This is the default normalization method when applyingthe edgeR method (Robinson and Smyth, 2008) for analyzing gene expression differences by RNA-seq. After normalization, differential expression was estimated by the method implemented in edgeR software, based on the negative binomial distribution of the reads. For estimating data dispersion, edgeR uses the quantile-adjusted conditional maximum likelihood (qCML) method. In this case, a common dispersion was considered for all samples.

**6. Preparation of strand-specific RNA and DNA probes**

The *xylS* intergenic region (260 bp) and the non-coding region (170 bp) between *xylS* and *xylH* were amplified by PCR using DNA template from *P. putida* mt-2 with the primer pairs *xylS*nr-F/*xylS*nr-R and *xylSH*nr-F/*xylSH*nr-R. The PCR products were cloned into the pGEM-T-easy vector to generating pGEM-T-*xylS*nr and pGEM-T-*xylSH*nr, respectively. To make sense RNA probes, the recombination vectors were *Sac*I-digested. After the enzyme reaction, klenow (NEB) was used to avoid non-specific transcription. For *in vitro* transcription, we used T7 RNA polymerase with $^{32}$P-radiolabeled CTP (Promega, Riboprobe combination system). To synthesize antisense RNA probes, *Sph*I enzyme and SP6 RNA polymerase were used with the same procedure as sense RNA probe synthesis. Labeled probes were purified using NICK columns (GE Healthcare). To generate the DNA probe for the *orf*13 gene in pWW0, the specific region was amplified by PCR with primer pairs orf13-F and orf13-R. The PCR product was used for labeling with the Random Primed DNA Labeling kit (Roche) following manufacturer's instructions.

**7. Northern blot analysis**

RNA samples (5 μg) were fractionated on 1% agarose-formaldehyde gels and transferred to membranes (Zeta-Probe, Bio-Rad) by capillary methods (Chomczynski, 1992), and fixed by ultraviolet crosslinking. Membranes were hybridized with $^{32}$P-CTP radiolabeled DNA probe (*orf13*) or strand-specific sense- and antisense RNA probes for the *xylS* region and the non-coding region between *xylS* and *xylH* in ULTRAhyb ultrasensitive hybridization buffer (Ambion)(68°C, overnight). Membranes were washed twice with 2X SSC (0.1% SDS)(68ºC, 15 min) and twice with 0.1X SSC (0.1% SDS)(68ºC, 5 min), then exposed to X-ray film.

**8. Measurement of promoter activity**

### 8.1. Quantification of GFP fluorescence for the *Pm* promoter

The GFP reporter strains were cultured in microplates in LB medium. To induce the *xylS* gene, 3MBz (5 mM) was added. Isopropyl β-D-1-thiogalactopyranoside (IPTG, 1 mM) was added for antisense transcription of *xylS*. The $OD_{600}$ and GFP fluorescence intensity were quantified using a microtiter plate reader (Spectramax, M2). The reporter strain expresses a stable GFP variant that absorbs light at 488 nm and GFP activity was normalized as fluorescent unit/$OD_{600}$. For GFP quantification by flow cytometry, cells cultured overnight were diluted 1:100 in fresh medium and allowed to grow to mid-exponential phase, then divided in new medium with 3MBz (5 mM), 3MBz plus IPTG (1 mM) or no inducer (control). Cultures (500 μL) were sampled at each time point (0, 1 and 2 h) and kept on ice for further analysis. For flow cytometry, samples were loaded in a Gallios Flow Cytometer (Beckman Coulter) and analyzed for GFP expression (488/525(40)BP). For each sample, 15000 cells were analyzed. Results were processed using Kaluza software (Beckman Coulter).

### 8.2. *PbenA* promoter activity assay using *lacZ* reporters

To test the activity of transcription or translation fusion for *PbenA* to *lacZ*, reporter strains were cultured in succinate minimal medium until the exponential phase, inducers were added where appropriate (2 h), and cells were prepared to measure β-galactosidase activity. Activity was measured with the Galacton-Light Plus system (Applied Biosystems), which is based on a chemiluminescent substrate of the enzyme (Galacton-Plus, Tropix). A sample of cells (500 μl; $OD_{600}$ = 0.3-0.6) was centrifuged (13,000 rpm, 1 min, room temperature) and the pellet resuspended in 200 μl of lysis buffer (100 mM potassium phosphate pH 7.8, 0.2% Triton X-100). The lysis mixture was subjected to two freeze-thaw cycles and centrifuged to eliminate cell debris. Lysed supernatant (20 μl) was incubated (30 min) with 80 μl of reaction buffer (100 mM sodium phosphate, pH 8.0, 1 mM $MgCl_2$, 1X Galacton-Plus). These reactions were performed in 96-well plates and recorded in a luminometer for 30 sec immediately after addition of 125 μl of a light emission accelerator (Accelerator-II Sapphire-II) following manufacturer's instructions.

### 8.3. Analysis of lux reporter dependent on the *PmpfR* promoter

To measure promoter activity, the *P. putida* derivatives harboring the *PmpfR→lux* transcriptional fusion were inoculated into M9 minimal medium supplemented with succinate (10 mM) as a carbon source and cultured overnight. The cells were then diluted 100-fold in rich medium LB or in fresh minimal medium with glucose (10 mM), succinate (10 mM), succinate plus benzoate (5 mM) or succinate plus 3MBz (5 mM). Diluted cells (200 μL) were then placed in 96-well microplates (Optilux, BD Falcon) and analyzed in a Wallac Victor II 1420 Multilabel Counter (Perkin Elmer). Optical density at 600 nm ($OD_{600}$) and bioluminescence were recorded at intervals of 30 min. Promoter activities were determined as the ratio of bioluminescence to cell density and are given in relative units (RU). The values reported represent the maximal activity after at least 3-4 h incubation.

### 9. Sample preparation for microscopy

To visualize ribosome distribution, the Meg2 strain was cultured overnight with shaking in LB or M9 minimal medium supplemented with glucose (10 mM), fructose (10 mM), glycerol (20 mM), succinate (15 mM) or benzoate (5 mM). The bacterial culture was diluted 100-fold in the respective medium and grown either to exponential phase ($OD_{600}$ = 0.3-0.5) or for a further 96 h to stationary phase. In addition, the reporter strain harboring the pWW0 TOL plasmid was cultured in M9 medium plus either succinate or *m*-xylene as sole carbon source. Alternatively, when the plasmid-harboring reporter strain reached $OD_{600}$ = 0.2-0.3 in succinate-supplemented minimal medium, the cells were exposed to *m*-xylene and cultured for 2 h. To study the effect of translation inhibition, the ribosome-GFP-expressing cells were grown in succinate-amended minimal medium to the exponential phase and the following antibiotics were added to the medium and incubated (1 h): Cm (200 μg $ml^{-1}$), Sm (200 μg $ml^{-1}$) or tetracycline (TC; 50 μg $ml^{-1}$). To fix samples, 1 mL of each culture was removed and immediately mixed with a fix solution, resulting in final concentrations of 1% (w/v) formaldehyde and 30 mM $NaHPO_4$ buffer (pH7.5). The mixture was incubated (15 min, room temperature), transferred onto ice (30 min), after which the fixed cells were washed twice with PBS and finally resuspended in 200 μl PBS. Strains with cells fluorescently labeled to

visualize RNAP or RNA and ribosomes were cultured in minimal medium with succinate as sole carbon source. Before immobilization, cells were fixed as above and resuspended in PBS.

**10. Microscopy and image analysis**

For immobilization, 2 μl of fixed cells were placed onto 0. 01% poly-L-lysine (Sigma-Aldrich)-coated coverslips and dried. For chromosome straining, 4',6-diamidino-2-phenylindole (DAPI; 1 μg $ml^{-1}$) was added to immobilized cells and incubated (2 min, room temperature); after removal of the staining solution, the coverslip was assembled with a slide including Prolong (Life Technologies) to suppress photobleaching and sealed using clear nail polish. Microscopy was performed using an Olympus BX61 microscope equipped with ×100 phase contrast objective and a DP70 camera (Olympus). GFP, DAPI and mCherry were measured using widefield excitation with U-MNIBA2, U-MNU2 and MWIY2 filters, respectively. Relative fluorescence was analyzed by Image J software (National Institutes of Health, Bethesda, MD). To quantify mRNA copy number, we made use of several software packages to obtain spot intensity statistics. First, phase contrast images of our samples were segmented individually to define cell boundaries, for which we used Schnitzcells (http://cell.caltech.edu/schnitzcells/), which outputs a mask that identifies and labels each cell is unequivocally. Second, we used fluorescence images with their corresponding masks to identify spot intensity via Spatzcells (https://code.google.com/p/spatzcells/), which allowed us to extract the relative spot intensity value and the information about its harboring cell label. The latter information was processed using in-house software coded in Python to display the data shown in the figures of this work. Both Schnitzcells and Spatzcells are collections of MATLAB (http://www.mathworks.com) scripts. All software was run on a Linux (Debian squeeze) machine.

**11. Fluorescent *in situ* hybridization for TOL catabolic transcripts**

The cells growing in culture medium were fixed in formaldehyde solution (4% formaldehyde and 30 mM $NaHPO_3$ pH 7.5; 15 min, room temperature and 30 min,

on ice). Samples were washed twice with diethylpyrocarbonate (DEPC)-treated PBS. Cell pellets were resuspended in GTE buffer (50 mM glucose, 20 mM Tris-HCl pH 7.5, 10 mM EDTA pH 8), and lysozyme and vanadyl ribosnucleoside complex (VRC; New England BioLabs) were added to a final concentration of 2.5 μg $ml^{-1}$ and 2 mM, respectively. The mixture was immediately placed onto a poly-L-lysine-coated coverslip and incubated (10 min, room temperature). Excess liquid was aspirated and the coverslip was air-dried (5 min). The sample was then soaked in -20°C methanol (10 min) and -20°C acetone (30 s), dried, and incubated in a 10% formamide solution (10% formamide, 2X saline-sodium citrate buffer (SSC) in DEPC-treated water, 2 mM VRC)(60 min, 37ºC). The solution was removed, and 50 μl of hybridization solution was added (10% formamide, DEPC-treated 2X SSC, 10% dextran sulphate, 2 mM VRC and 250 nM Stellaris FISH probe corresponding to *xylUW* or *xylX*) to the coverslip and incubated in a humidified chamber (overnight, 42°C). The sample was then washed twice in 10% formamide and DEPC-treated 2X SSC solution (15 min, 37°C), and DAPI (2.5 μg $ml^{-1}$) stained in the second washing step. After a brief PBS rinse, the coverslip was assembled with a slide glass including antifade reagent Prolong (Invitrogen) and sealed with clear nail polish. The specimen was visualized in a fluorescent microscope.

# IV. Results

## Chapter I.

## High-resolution analysis of the *m*-xylene/toluene biodegradation sub-transcriptome of *Pseudomonas putida* mt-2

**1. Approach for transcription mapping of *xyl* genes responding to *m*-xylene**

To study the *xyl* gene transcription of the pWW0 core region, tiling array and RNA-seq analyses were carried out. Briefly, the *P. putida* mt-2 strain was cultured to early exponential growth phase ($OD_{600}$ ~0.3) in succinate-supplemented minimal medium, alone or followed by vaporization of a 1:2 dilution of *m*-xylene. Two hours later, total RNAs were isolated and the cDNAs synthesized were used for hybridization to a tiling array chip (see Methods for details). In addition to these conditions, we also prepared a reference condition by culturing the cells in succinate as the sole carbon source for 96 h to derive RNAs used as the alternative control condition (Guell et al., 2009). Expression intensity was normalized by comparing cells grown in succinate and succinate plus *m*-xylene, or to the reference condition. It should be noted that succinate does not interfere with *xyl* gene expression (Cases et al., 1999, Holtel et al., 1994).

Consistent with previous observations using DNA array technology (Velazquez et al., 2005), results from the tiling array showed that all TOL *upper* and *lower* pathway genes and the *xylS* genes were highly expressed, while the *xylR* gene appeared to be downregulated by itself when *P. putida* mt-2 was exposed to *m*-xylene (Fig. 8). To determine the relative gene expression level, the tiling array data was normalized to the RNAs from succinate-cultured cells (Fig. 8A) or the reference condition (Fig. 8B). The tendency of expression did not differ between the two comparisons (Fig. 8). When the profile was taken from *m*-xylene-cultured cells versus succinate-grown cells, however, the expression level was not as high as the reference-based normalization (Fig. 8). This phenomenon is probably caused by a higher basal transcription level for the *xyl* genes in succinate-cultured cells. In addition, transcription intensity was not evenly distributed for continuous genes of the *lower* pathway, whereas constant expression of *upper* pathway genes was observed in the transcription profile when compared with control conditions for succinate-cultured cells (Fig. 8A). By contrast, both *upper* and *lower* operons were evenly transcribed in the profile when the reference condition was used for normalization (Fig. 8B). These results imply that the *lower* pathway genes are

expressed to a notable level in succinate-amended minimal medium in the absence of inducers or substrates-to-be.

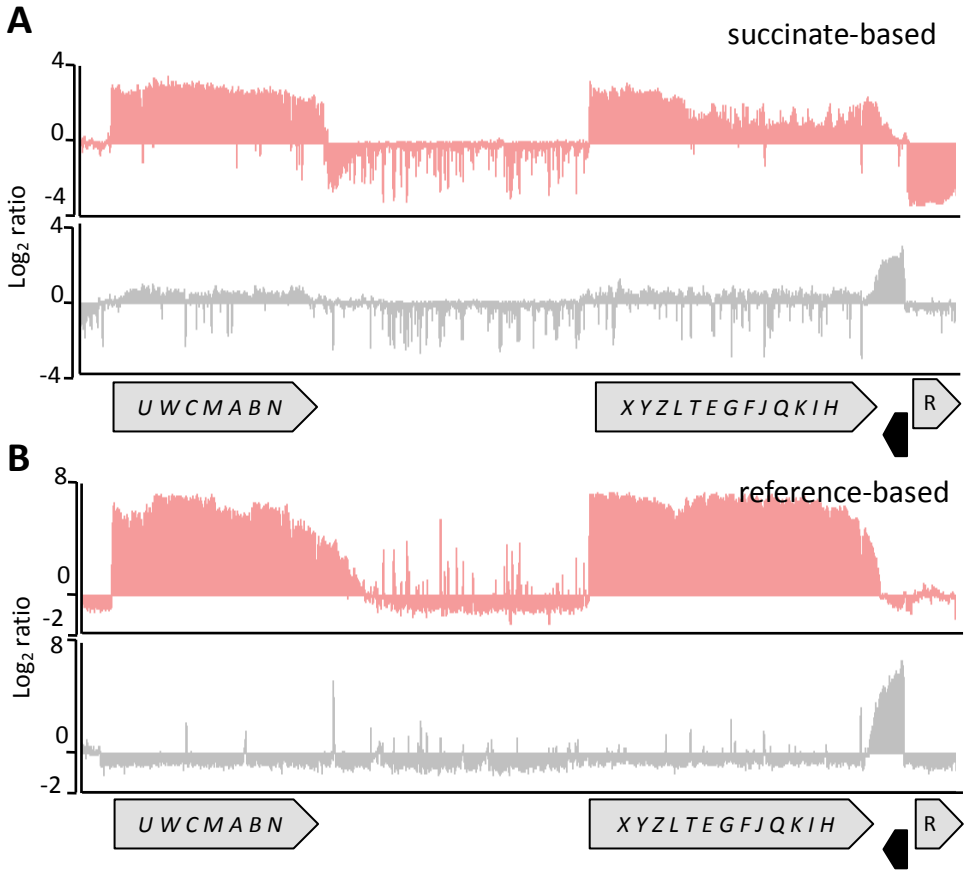


**Figure 8. High-density tiling array-based transcriptome profile of TOL *xyl* genes in *P. putida* mt-2.** (A) Relative gene expression intensity from *m*-xylene-treated versus untreated conditions, or (B) *m*-xylene-treated versus reference conditions. Red signals, forward transcription; gray signals, reverse transcription; *xyl* genes are described as arrows; black arrow indicates the *xylS* gene. IGB software was used for the visualization.

In support of this the scenario, the expression profile showed that the *lower* operon *xyl* genes were induced slightly and unevenly when compared to succinate-grown cells versus reference condition cells (Fig. 10A). Collectively, transcriptional mapping with respect to normalization with the reference condition might reflect actual mRNA expression in the cells. Using the reference condition, we therefore validated the expression profile dependent on the *m*-xylene effect with RNA deep sequencing (Fig. 9). In brief, the cDNA libraries were sequenced using the

Illumina Genome analyzer IIx, and the sequence reads were aligned both to the *P. putida* KT2440 genome and pWW0 plasmid genes. For the *upper* and *lower* pathway genes of the TOL plasmid, the alignment was visualized using the IGV as shown in Fig. 9A (Thorvaldsdottir et al., 2012) and the transcription activity was normalized (Fig. 9B) by trimmed mean of M values (Robinson and Oshlack, 2010). Although the expression intensity level cannot be compared precisely with the tiling array data, the transcription profile from the RNA sequencing result is very similar to the array-based expression pattern (Fig. 8, Fig. 9). The transcription study from the tiling array and RNA sequencing is therefore sufficiently reliable that we could use it to obtain detailed information for transcription mapping.

**2. Definition of operon structure of TOL genes, novel transcription and correction of gene annotation**

Improved resolution by high-density microarray and ultra sequencing can provide insights into genomic elements such as discovery of new genes, definition of untranslated regions, and operon structure (Sorek and Cossart, 2010). Using the high-throughput technologies, we also found these genomic elements in TOL *xyl* genes. The first novelty was the presence of a previously unreported ~1000 bp-long transcription unit downstream of the *xylN* gene (Fig. 8B, Fig.10A). In accordance with the tiling array data, this transcription unit was also observed with the RNA sequencing approach, because many reads accumulated in the same region (Fig. 9A). This transcription unit might be non-coding RNA or a newly identified gene encoding protein (Sorek and Cossart, 2010), since the region is defined as an open reading frame and its function is not known. Further analysis is needed to define its identity for the transcription unit. Although this transcription unit is adjacent to the *upper* operon, the *Pu* promoter does not cause its induction; when the promoter was silent due to absence of its association effectors such as *m*-xylene, toluene or *o*-xylene, the transcript was shown to respond to benzoate, 3MBz and succinate (Fig. 10A). Consequently, the transcription unit might be growth phase dependent, induced by a putative but still unknown promoter.

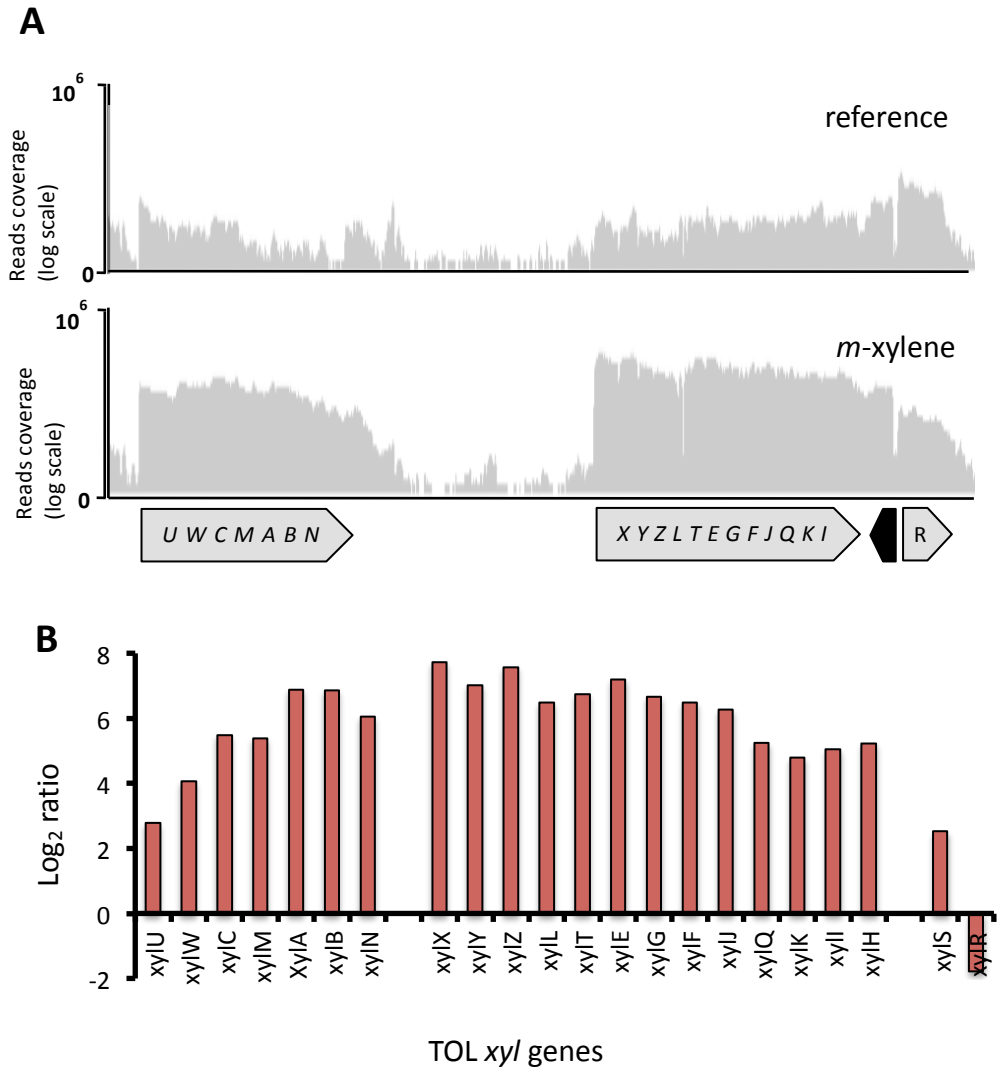


**Figure 9. RNA deep sequencing-based transcriptome profile of TOL *xyl* genes in *P. putida mt-2*.** (A) Total numbers of cDNA reads are annotated responding to the *xyl* genes from RNA isolated from the reference condition (upper panel) or *m*-xylene-exposed cells (lower panel). IGV software was used for visualization. (B) Normalization of transcription intensity for the *xyl* genes, comparing *m*-xylene-cultured and reference conditions.

The transcriptome assay confirmed operon structure in the *xyl* genes. Since this assay showed a continuous expression signal responding to the *upper* as well as the *lower* operons (Fig. 10A), we ruled out the existence of another operon inside the *xyl* structure genes.

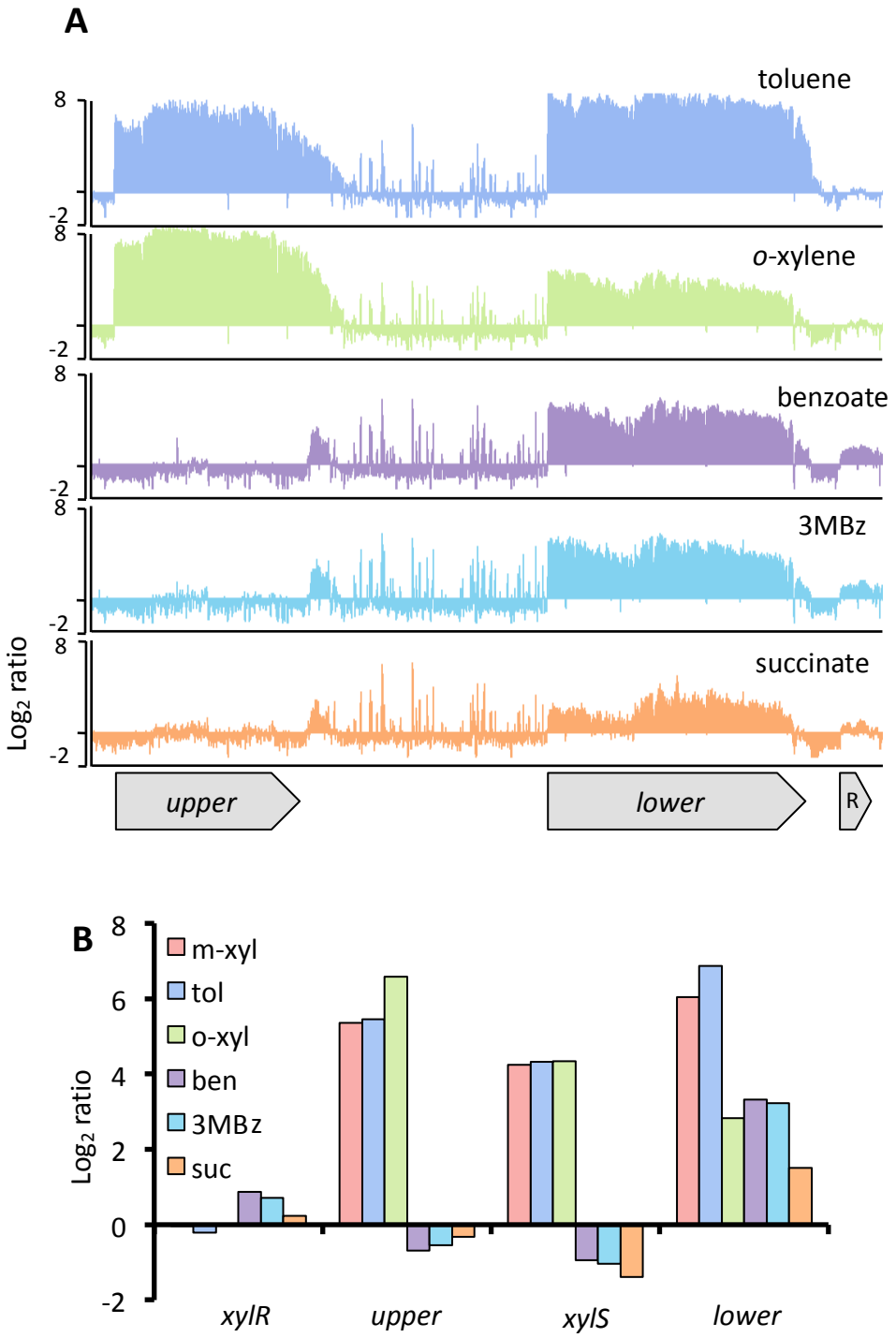


**Figure 10. Transcriptome profiles of TOL plasmid core region responding to aromatic compounds, using a high-density tiling array in *P. putida* mt-2.** (A) Only forward transcriptions are shown. The signal is gene expression relative to the reference condition. Y-axis, $Log_2$ ratio. (B) Average intensity of the probes for *upper* and *lower* operons, the *xylS* and *xylR* genes.

We also found that the reported *xylL* sequence has a noticeable mistake. From the RNA-seq data, no sequencing read was aligned in the 36-bp part of the *xylL* gene annotated in NCBI (GenBank: AJ344068.1; Fig. 11A). To test whether this was caused by a transcription effect or is in the original DNA sequence, we cloned a partial *xylL* gene and analyzed the DNA sequence. Analysis of this sequence revealed that the locus (52320-52355) in the plasmid was not present in the template DNA (Fig. 11B). The strain used for these assays is perfectly able to grow on *m*-xylene as sole carbon source, so the loss of this 36 bp sequence cannot be attributed to mutations in the laboratory.

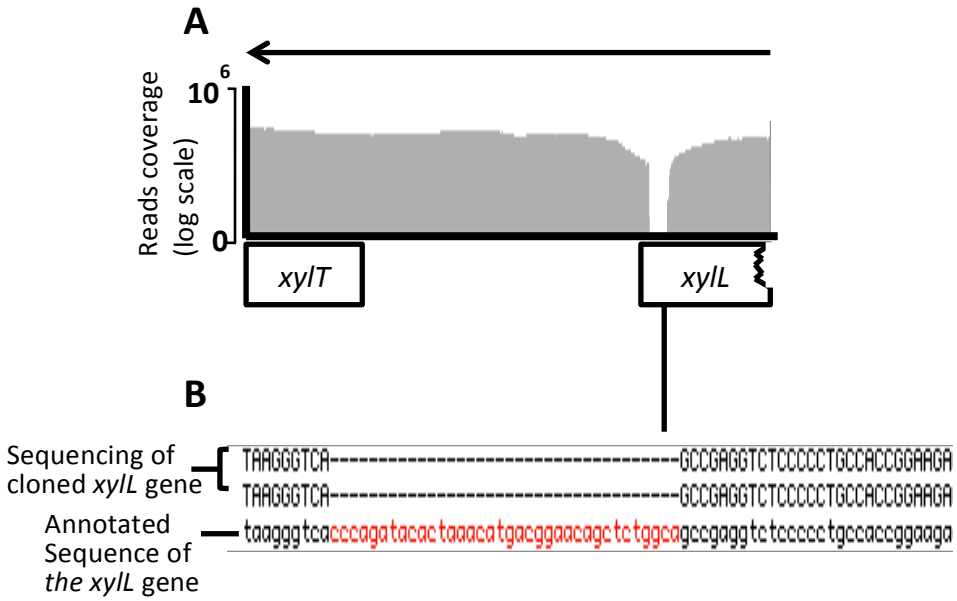


**Figure 11. Correction of sequence annotation on the *xylL* gene in the pWW0 plasmid of *P. putida* mt-2.** (A) Visualization of cDNA reads coverage on *xylL* region from RNA-seq data. (B) Sequencing analysis of the *xylL* gene cloned in pSEVA431. The inserted gene was analyzed using the plasmid-based forward and reverse primers. Arrow indicates transcription direction.

### 3. Overlapping transcription between *xylS* and *lower* operon gene

Strand-specific transcriptome mapping was obtained from tiling array analysis. That is, the *upper* and *lower* pathway genes and the *xylR* gene were transcribed in the same way, whereas the *xylS* gene was expressed in the opposite direction (Fig. 8, Fig. 10). Examination of the transcriptional profile showed signals on both coding strands between the end of the *lower* operon region and the *xylS* gene

(Fig. 12). To validate this overlapping expression, Northern blot analysis was conducted using strand-specific RNA probes. Specific probes were designed for both strands of the to non-coding region between the *xylS* and the end of the *lower* operon region (Fig. 12, red line) and both strand-specific probes were hybridized with each mRNA strand in the case of *m*-xylene-exposed cells (Fig. 12). Several signals were detected by the antisense probe of the non-coding region, whereas a single band was observed for the sense probe (Fig. 12). A plausible explanation is that the *lower* operon mRNA is not present in full-length size (~11 Kb) due to its rapid decay in bacteria (Marques et al., 1993, Rauhut and Klug, 1999). With regard to the internal probe for *xylS* (Fig. 12, blue line), a marked signal appeared when only the sense probe was used for the hybridization (Fig. 12).

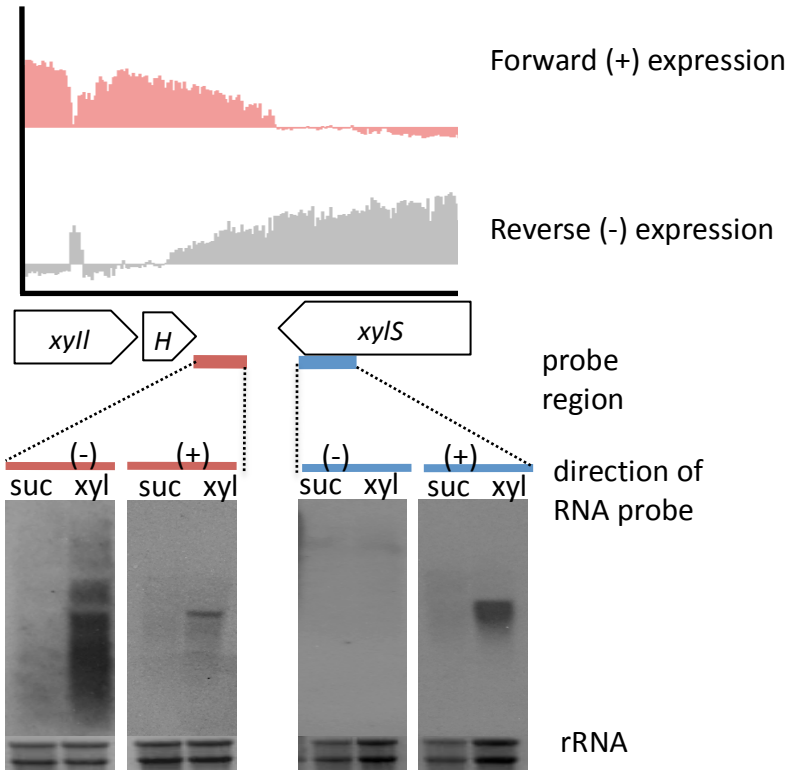


**Figure 12. Northern blot analysis for the overlapping expression region.** Two different regions (non-coding, red; intergenic region of *xylS*, blue) were studied using the forward (+) or reverse (-) RNA probes corresponding these regions of the pWW0 plasmid of *P. putida* mt-2. suc, succinate ; xyl, *m*-xylene.

The Northern blot analysis result thus strongly indicates that both strands are transcribed by converging transcription at the 3' end, which might thereby produce

a base pairing structure. The formation of a pairing complex by sense and antisense transcripts is able to alter mRNA structure and affect translation indirectly (Thomason and Storz, 2010). Within this scenario, we recently observed that, when induced with *m*-xylene, the TOL promoters are subject to a stochastic process; we considered that the interference between the *meta* pathway and the *xylS* gene might be involved in this process. Nonetheless, the *Pm* promoter does not present the bimodal regime when expressed from a strain devoid of the TOL plasmid (Silva-Rocha and de Lorenzo, 2012c), and this process could indeed be related to some type of interference with XylS production in the *P. putida* mt-2 strain.

To examine the effect of the overlapping expression on XylS stability and its function for *Pm* promoter activation, we used an artificial antisense *xylS* expression system. Briefly, the region including the *Ps* promoter, *xylS*, and its extended 3' end was cloned under the *Ptrc* promoter by constructing the pSVEA224-xylS [±] plasmid to obtain sense and antisense transcription by 3MBz and IPTG, respectively (Fig. 13A). The plasmid was introduced into the *P. putida* strain harboring the *Pm* promoter fused to a bi-cistronic reporter system based on *gfp-lacZ* genes (Silva-Rocha and de Lorenzo, 2012b). First, we focused on GFP as a reporter to monitor *Pm* promoter activity in a microplate reader. Only the antisense *xylS* expression system under the *Ptrc* promoter did not interact with the *Pm* promoter. We thus cultured the reporter strain with the *xylS* sense and antisense expression vector in LB and LB plus 3MBz, with or without IPTG (1 mM). As anticipated, the promoter activity was greatly increased in the presence of 3MBz (Fig. 13B, gray circle), but showed no further change when IPTG was added in these conditions (Fig. 13B, white circle). In further analysis, we studied the stochastic effect of the overlapping *xylS* expression by measuring the GFP activity by flow cytometry (Fig. 13C). By assaying the *Pm* promoter activity in different *P. putida* KT2440 strains with sense and anti-sense expression of *xylS*, we found that this promoter showed graded expression behavior (Fig. 13C). These results therefore indicate that the overlapping transcription in the *xylS* region does not appear to produce any impact on XylS synthesis and *Pm* promoter activation.

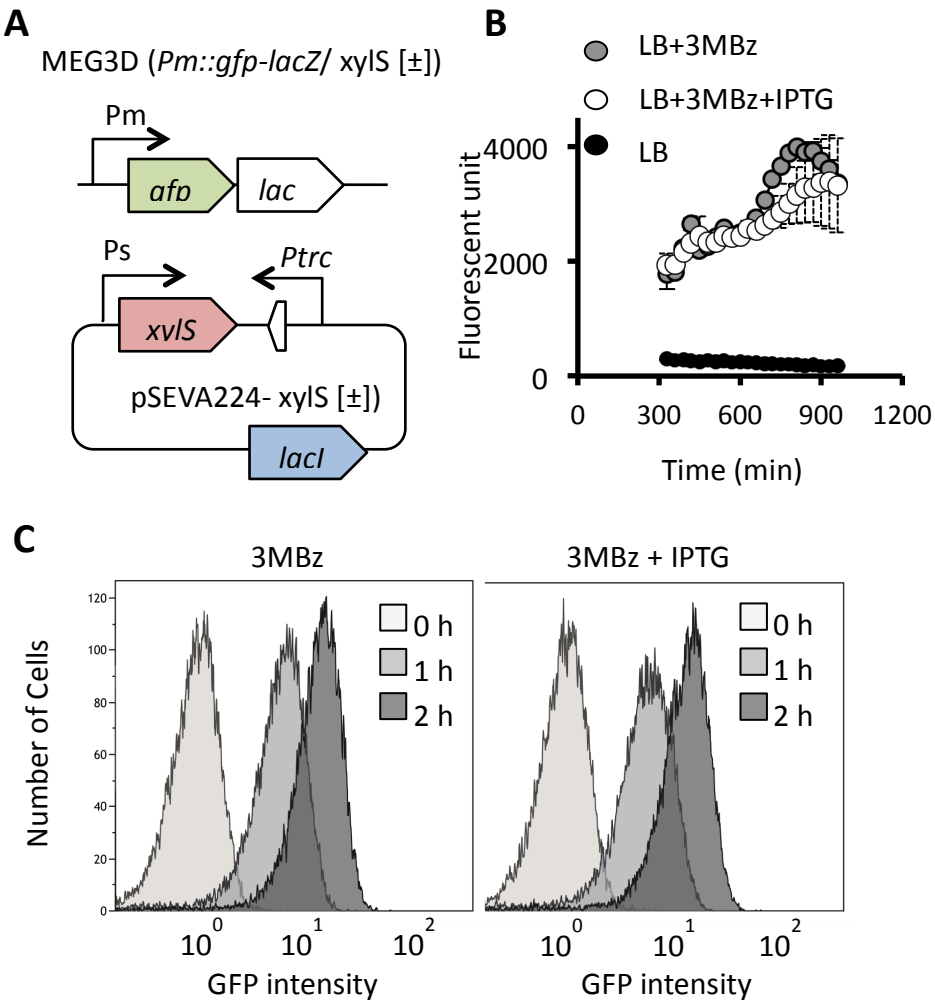


**Figure 13. Assay for artificial *xylS* expression effect on the *Pm* promoter.** (A) The scheme of the reporter strain MEG3D (*Pm::gfp-lacZ*/ XylS [±]). (B) Time-dependent GFP quantification using the reporter strain by culture on LB (black circles) or LB plus 3MBz and IPTG (gray circles) or without IPTG (white circles). (C) Flow cytometry analysis for GFP activity. The reporter strain was cultured in succinate-amended M9 minimal medium overnight. Cells (diluted 100-fold) were inoculated on the same medium and cultured until early exponential growth phase ($OD_{600}$ ~0.2). At this time, cultures were divided into three conditions for control, 3MBz (5 mM) and 3MBz plus IPTG (1 mM). After adding these substrates, the cells were cultured and harvested after 1 or 2 h. For each sample, 1.5 x $10^4$ cells were analyzed.

## 4. Transcription profiles of TOL *xyl* genes responding to toluene and its derivatives

As for the *m*-xylene transcriptome, we tested other substrates such as toluene, *o*-xylene, benzoate and 3MBz through the high-density tiling array approach;

Fig. 10A shows the expression profile of each substrate for TOL core genes. When the cells were cultured in succinate-supplemented minimal medium with toluene as effector, the expression pattern was the same as for the *m*-xylene condition (Fig. 8B, Fig. 10A). In other words, *upper* and *lower* operons and the *xylS* genes are highly expressed, whereas the *xylR* gene was likely to be downregulated (Fig. 10A). In cells exposed to *o*-xylene, however, the induction level of *upper* operon genes was much higher than in *m*-xylene- or toluene-exposed conditions, while the activity of the *meta* cleavage pathway was much lower, although the *xylS* gene was apparently expressed (Fig. 10). Previous work showed that this is not caused by translational inhibition of *xylS* (Velazquez et al., 2005). Hence, a plausible explanation for the transcription pattern is that non-metabolizable effectors such as *o*-xylene can stimulate *xylR*, whose product enhances both *Pu* and *Ps* promoters. Following the cascade reaction, both the *upper* pathway genes and the *xylS* gene are highly induced. Despite elevated accumulation of the XylS protein, it does not appear to enhance the *Pm* promoter strongly, since XylS-associated effectors such as benzoate or 3MBz are not generated in *o*-xylene-cultured cells.

Benzoate and 3MBz, known as *meta* pathway inducers (Gonzalez-Perez et al., 2004), induced only *lower* operon genes, but the intensity level of the genes of the whole *lower* pathway was conspicuously decreased compared to the effect of *m*-xylene/toluene conditions (Fig. 10). The transcription profiles were perfectly consistent with a previous study which suggested a regulation model for the *Ps* promoters; in this model, the *xylS* gene is expressed from two tandem promoters (Gallegos et al., 1996) and the protein is induced at low levels from the *Ps2* promoter in the absence of the *upper* operon inducers. In contrast, the *xylS* gene would be highly transcribed from the *Ps1* promoter in association with XylR when *upper* operon effectors are present and the large amount of XylS can stimulate the *Pm* promoter (Gonzalez-Perez et al., 2004). As for constitutive *xylS* induction from *Ps2, meta* pathway genes are slightly transcribed in cells cultured in succinate minimal medium without any substrate (Fig. 10).

## 5. Effect of *m*-xylene/toluene and derivative aromatic compound assimilation on the β-ketoadipate pathway

The β-ketoadipate pathway is a convergent pathway for diverse aromatic compounds in *P. putida* (Harwood and Parales, 1996, Jimenez et al., 2002). There are two branches concerned in this pathway. One is the catechol pathway, derived from benzoate, and the other is the protocatechuate branch, derived from catabolism of many aromatic compounds such as vanillate, caffeate, *p*-coumarate, hydroxybenzoate, and so on (Harwood and Parales, 1996, Jimenez et al., 2002). In *P. putida*, the two branches converge at β-ketoadipate enol-lactone (Fig. 14). The enzymes encoded by the *fcs* cluster and the *pob*, *ben*, *cat* and *pca* genes are required for the β-ketoadipate pathway, and *FerR*, PobR, BenR, CatR and PcaR are known regulators for the structure genes (Cowles et al., 2000a, Jimenez et al., 2002, Rothmel et al., 1991). There is nonetheless little information available for the β-ketoadipate pathway transcriptome relative to *m*-xylene/toluene degradation, which generates 3MBz/benzoate connected to the catechol pathway in *P. putida* m-2 (Fig. 14). We therefore examined expression of β-ketoadipate pathway genes using a tiling array chip set with the mt-2 stain was assimilating aromatic compounds.

### 5.1. The *ben* gene expression profile

The core genes *benABCD* are expressed from the *PbenA* promoter, controlled by BenR, which needs benzoate as effector (Cowles et al., 2000a, Moreno and Rojo, 2008, Silva-Rocha and de Lorenzo, 2012a). In our transcriptome approach for *ben* genes by tiling array, all the genes were highly induced when benzoate was supplied in the culture medium (Fig. 15). As we described above, the *meta* cleavage pathway was also expressed in this condition (Fig. 10), which showed that benzoate could be channeled by both *meta* and *ortho* cleavage pathways in *P. putida* mt-2. Nontheless, no marked transcription level was detected in the presence of *o*-xylene, 3MBz and succinate (Fig. 15). Based on that result, we determined that the effect of XylS, a known homologue of BenR, is not associated to the *PbenA* promoter because XylS accumulation in the presence of *o*-xylene or 3MBz has little influence on *ben* gene expression (Fig. 15). When we further

investigated regulation of the *Pm* and *PbenA* promoters by these two regulators (XylS and BenR) using different techniques, we found that XylS was unable to trigger *PbenA* activation in any conditions tested (Pérez-Pantoja et al., unpublished), contrary to previous observations for *P. putida* PRS2000 (Cowles et al., 2000b). The mechanism by which XylS is *Pm*-specific while BenR can promiscuously recognize both *Pm* and *PbenA* is currently under study.

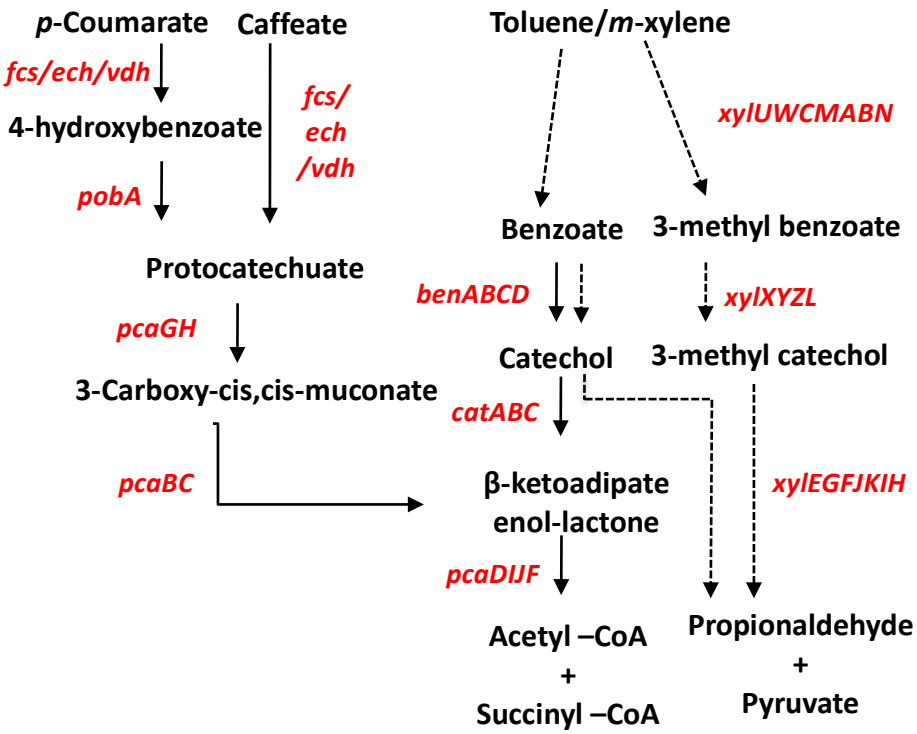


**Figure 14. Aromatic compound catabolic pathways in *P. putida* mt-2.** Chromosomal catabolic pathway genes are shown by solid lines and TOL plasmid-encoded genes are shown as dotted lines. The catabolic genes responsible for the metabolites are in red.

When *P. putida* mt-2 strains were exposed to *m*-xylene or toluene, an elevated, uneven signal appeared on *benABCD* genes (Fig. 15). To validate its transcription and functional level, *PbenA* promoter activity was measured using both transcriptional and translational fusion with the *lacZ* reporter.

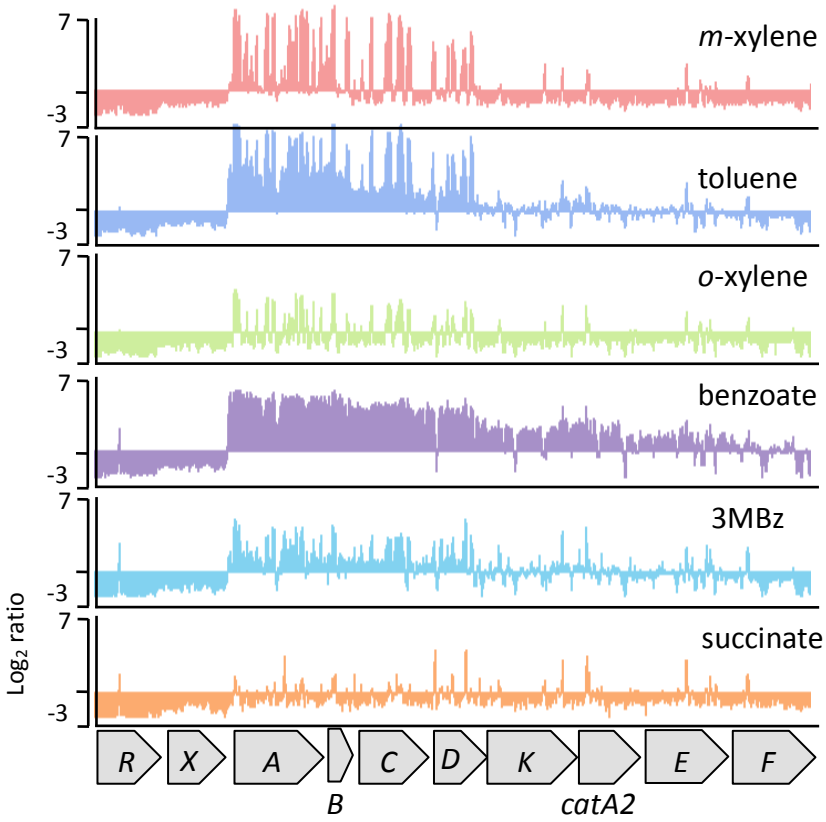


**Figure 15. Transcription profiles based on tiling array for the *ben* genes that respond to aromatic compounds in *P. putida* mt-2.** Expression profiles are visualized for benzoate catabolic genes as different substrates. Profile signal intensities are normalized based on the reference conditions. Arrows indicate transcriptional direction. Y-axis, $Log_2$ ratio.

The promoter activity was only increased when cells were cultured benzoate-supplemented minimal medium (Fig. 16A). This result suggests that the *m*-xylene or toluene signals in the tiling array transcriptome are not caused by *PbenA* stimulation, but could be an artifact caused by cross-hybridization due to the high similarity of *benABCD* and *xylXYZL* genes (Harayama and Rekik, 1993). We observed few transcriptional reads for *ben* genes in RNA-seq analysis, which does not produce cross-hybridization (Fig. 16B).

### 5.2. The *cat* gene expression profile

Like the *ben* gene transcriptional profiles, little variation was seen for *cat* genes when *P. putida* mt-2 was treated with *m*-xylene/toluene and derivative aromatic

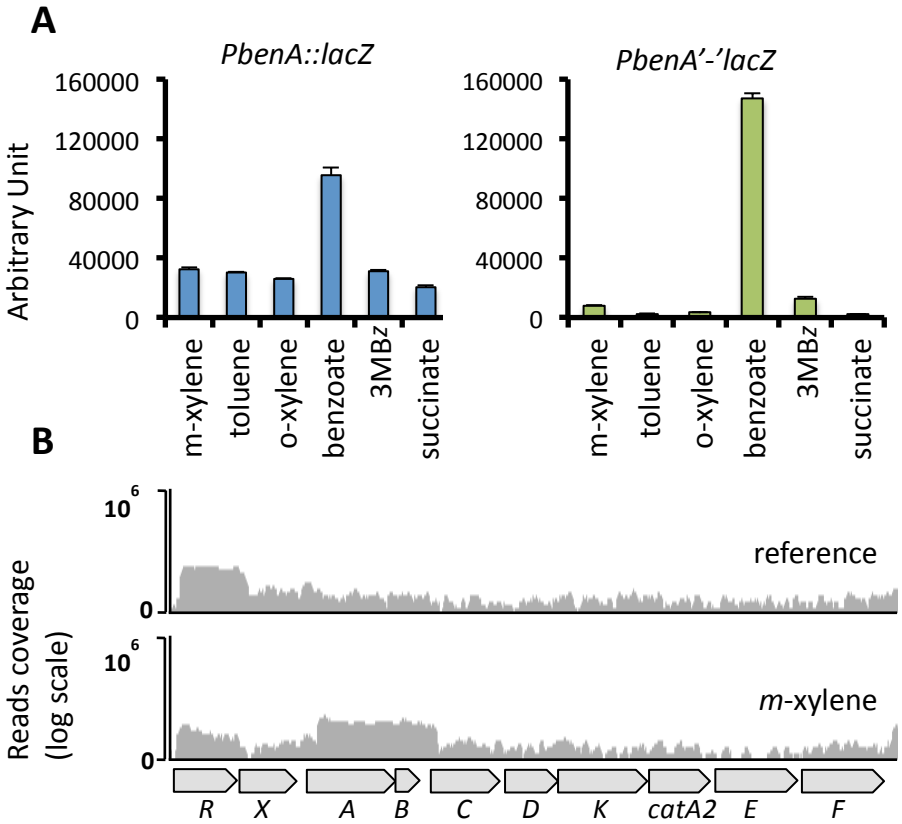


**Figure 16. *PbenA* promoter activity analysis and RNA-seq transcriptome for *ben* genes in *P. putida* mt-2.** (A) The promoter was transcriptionally (left panel) or translationally (right panel) fused to *lacZ* to analyze substrate-dependent activity. The reporter strains were cultured in succinate minimal medium to the exponential phase ($OD_{600}$ ~0.3), then effectors were either added where appropriate. After 2 h, the cells were harvested for measurement of β-galactosidase activity. (B) Visualization of transcription read coverage on the *ben* genes relative to reference and *m*-xylene exposure conditions. The arrows indicate the set of *ben* genes in the mt-2 strain.

compounds except benzoate (Fig. 17). This was predicted, because CatR, which regulates *catBCA* genes, needs *cis, cis*-muconate (CCM) as an effector (Chugani et al., 1998, Rothmel et al., 1991, Schell, 1993); the inducer does not accumulate in the cell, as mt-2 uses mainly the *meta* cleavage pathway for biodegradation of the substrates. We did not observe a clear induction level of the *catR* gene in any culture condition (Table 4). Despite this caveat, *cat* gene expression in benzoate-cultured cells is not caused by other regulators, because a *catR*-deficient mutant strain derived from *P. putida* KT2440 cannot utilize benzoate as an energy source,

even if CCM is highly accumulated in the cell (van Duuren et al., 2011). Thus, only CatR is likely to activate the *catBCA* operon at low levels when the cells use the *ortho* cleavage pathway.

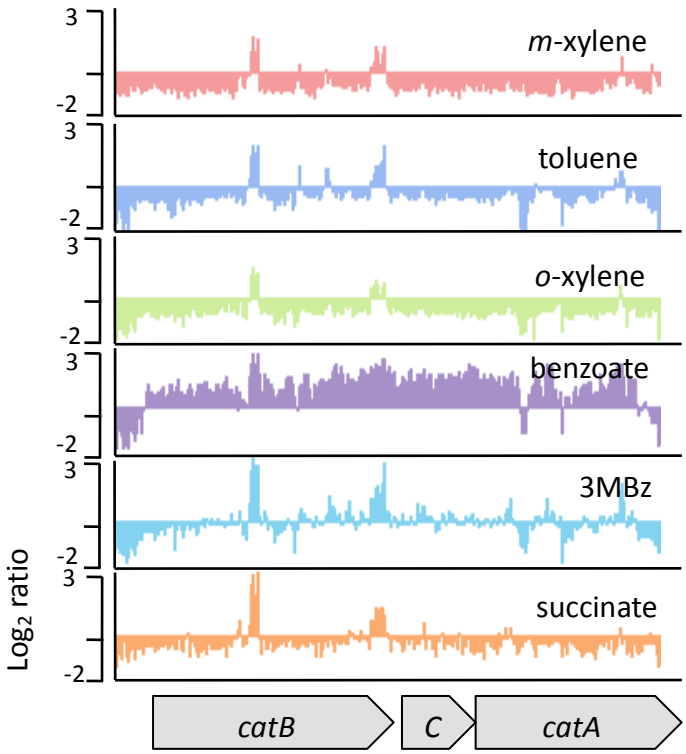


**Figure 17. Transcription profiles based on tiling array for the *cat* genes that respond to aromatic compounds in *P. putida* mt-2.** Expression profiles are visualized for the *cat* genes as different substrates. Prolife signal intensities are normalized to the reference conditions. Arrows indicate transcription direction. Y-axis, $Log_2$ ratio.

**Table 4**. The *catR* expression level obtained by tiling array transcription

| Effector | *m*-xyl | tol | *o*-xyl | ben | 3MBz | suc |
|---|---|---|---|---|---|---|
| Expression level[a] | 0.09 | 0.12 | 0.09 | 0.18 | 0.36 | 0.5 |

[a]The expression intensity for the *catR* gene was considered as average level from corresponding total probes

### 5.3. The *pca* gene expression profile

In *P. putida*, the *pca* genes are scattered over several portions of the chromosome and are organized in three different clusters, *pcaRKFTBDCP*, *pcaIJ* and *pcaGH*

(Jimenez et al., 2002). All of the *pca* genes are controlled by the PcaR in *P. putida* PRS2000, except the *pcaT* and *pcaGH* genes (Guo and Houghton, 1999, Hughes et al., 1988, Parales and Harwood, 1993, Romero-Steiner et al., 1994). As described above, the *pca* genes are responsible for the two branches of the β-ketoadipate pathway, the protocatechuate branch and the catechol branch, and leads to β-ketoadipate enol-lactone degradation (Fig. 14).

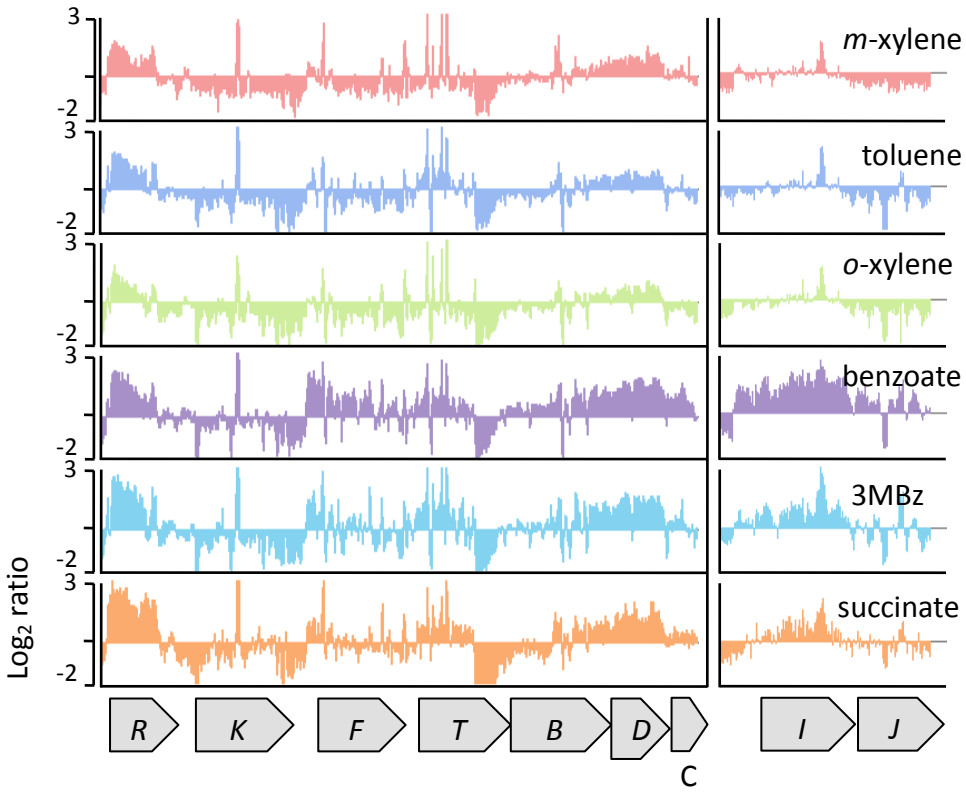


**Figure 18. Transcription profiles based on tiling array for the *pca* genes that respond to aromatic compounds in *P. putida* mt-2.** Expression profiles are visualized for *pca* genes as different substrates. Profile signal intensities are normalized based on reference conditions. Arrows indicate transcriptiol direction. Y-axis, $Log_2$ ratio. Note that *pcaI* and *pcaJ* genes are not continuously clustered with other *pca* genes in this strain.

In this study, we found that *pca* genes, especially *pcaF, pcaBDC* and *pcaIJ*, were induced only when cells were cultured in benzoate minimal medium (Fig. 18). Although *pcaK* also belongs to the *pcaR* regulon, it might be repressed by benzoate as reported (Nichols and Harwood, 1995). In addition, the *pcaR* gene signal was

detected above the basal level in all conditions, although the intensity decreased slightly in response to *m*-xylene, toluene and *o*-xylene compared to other substrates for reasons we cannot define (Fig. 18). As the *pcaR* signal increased, the *pcaBDC* gene also increased, even if its effector (β-ketoadipate) was not present, while *pcaIJ* levels remained low (Fig. 18).

### 5.4. Phenylpropenoid compounds and p-hydroxybenzoate catabolic gene expression profile

Some bacteria are able to utilize phenylpropenoid compounds such as coumaric acid, caffeic acid, ferulic acid and so on (Jimenez et al., 2002). To this end, they use enzyme sets, Fcs (feruloyl-CoA synthetase) and Ech (enoyl-CoA hydratase/aldolase), leading to vanillin production (Overhage et al., 1999, Priefert et al., 2001). Vanillin is further degraded through the Vdh protein (aldehyde dehydrogenase). These similar genes were identified in *P. putida* KT2440; in particular, *p*-coumaric acid and caffeic acid are channeled with *p*-hydroxybenzoate, which is further converted to protocatechuate by the *pobA* gene product and the protocatechuate pathway *via* those enzyme sets (Jimenez et al., 2002).

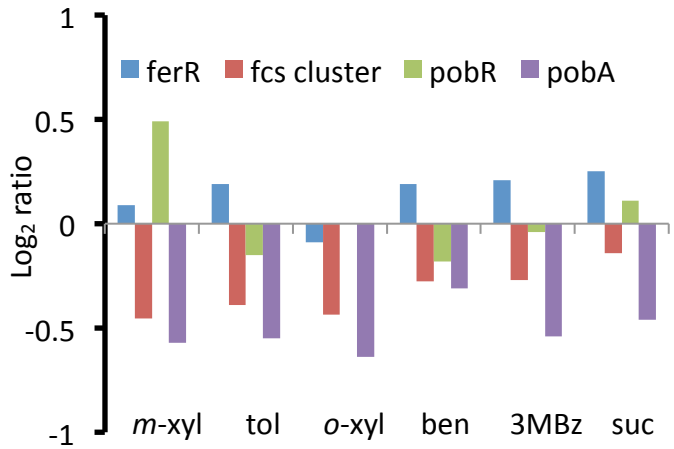


**Figure 19. Transcriptional intensity based on tiling array for phenylpropenoid and p-hydroxybenzoate catabolic genes in *P. putida* mt-2.** The intensity for each gene was considered as average level from corresponding total probes. The difference in expression level is normalized based on reference conditions. Y-axis, $Log_2$ ratio. *m*-xyl, *m*-xylene; tol, toluene; *o*-xyl, *o*-xylene; ben, benzoate; suc, succinate.

We examined whether these genes are induced in the presence of *meta* or *ortho* cleavage intermediates using tiling array. The result showed that expression of the genes for *ferR* (the putative regulator for the *fcs-vdh-ech* operon) and *pobR* remained low; accordingly, the intensity of their structure genes was little changed (Fig. 19). These peripheral genes of the β-ketoadipate pathway and their regulators thus do not seem to be associated with intermediates of the *meta* or *ortho* pathways.

## Chapter II

## A high-resolution transcriptional approach reveals the expression structure of the TOL plasmid pWW0 backbone genes in *Pseudomonas putida* mt-2

## 1. pWW0 TOL plasmid whole gene expression profile response to *m*-xylene

Based on our RNA-seq data for the transcriptome as described above, in this chapter, the transcriptional profile was addressed by focusing on the plasmid genes. Briefly, we observed a high level of read coverage in both *upper* and *lower* pathway genes, due to the stimulation of each promoter, *Pu* and *Pm* respectively, by interaction with the activator proteins XylR and XylS in response to *m*-xylene (Fig. 20B). In contrast, few reads coverage appeared in the same region in the reference sample (Fig. 20A). We also observed relatively higher transcription of the backbone genes *orf13*, *orf31*, *orf124-126, orf188-191* and the *mpf* cluster in cells growing in succinate-amended minimal medium with the aromatic compound (Fig. 20B, Table S1). This result strongly suggests that those mRNA either convert to enzyme products or remain as small RNAs (sRNA), although their functions are not be defined here. Except for *orf*188-191, such transcriptionally increased genes do not belong to the IncP-9 common backbone genes, but exist only in the pWW0 plasmid (Sevastsyanovich et al., 2008). It is not certain whether the transcripts in those backbone genes are dependent on an effector such as *m*-xylene, and thus the inducer of the expression is not clear. Despite the inability to designate the inducer for these transcripts, the expression profile can provide hints to define gene annotation and operon structure (Sorek and Cossart, 2010, Mader et al., 2011). We thereby sought to use the profile regarding transcriptional structure for specific genes, which will be described in the following sections.

---

**Figure 20. RNA deep sequencing-based transcriptome profile of the whole pWW0 plasmid region in *P. putida* mt-2.** Total numbers of cDNA reads are annotated responding to the whole genes from the reference condition, for which cells were cultured in succinate-amended minimal medium for 96 h (A) or *m*-xylene assimilated cells in their exponential phase (B). IGV software is used for visualization. Y-axis, value of cDNA reads coverage corresponding to the region.

---

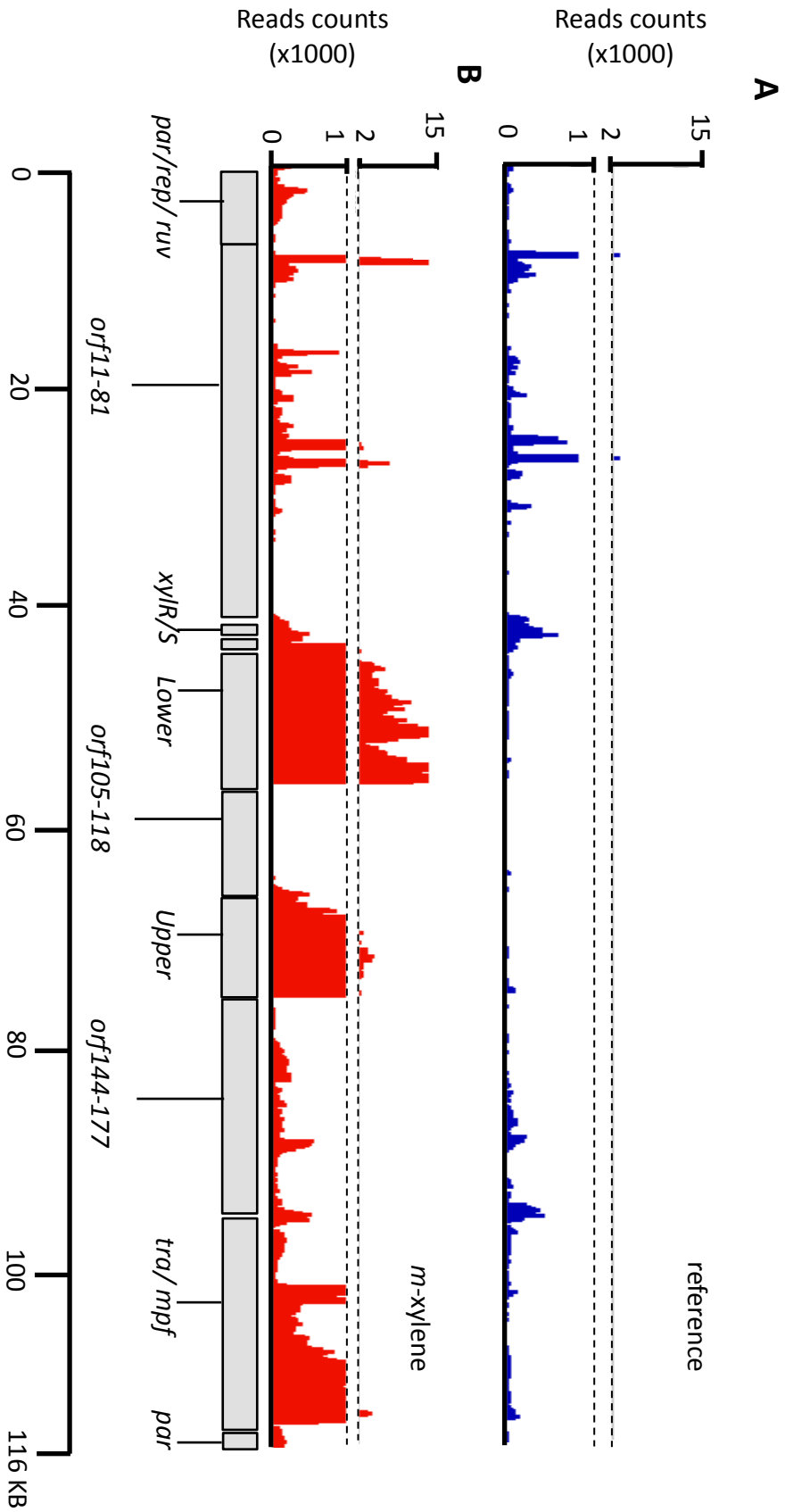
A
Reads counts
(x1000)
15
2
1
0
reference
B
Reads counts
(x1000)
15
2
1
0
m-xylene
par/rep/ ruv
xylR/S
Lower
Upper
tra/ mpf
par
orf11-81
orf105-118
orf144-177
0
20
40
60
80
100
116 KB

**2. Transcriptional characterization of the *orf13* region**

Greated *et al.* reported 148 open reading frames (*orf*) based on sequence analysis of pWW0; some *orf* are very specific to the plasmid, making it difficult to anticipate their function (Greated et al., 2002). For example, the *orf12-14* clusters are not found other IncP-9 plasmids such as pDTG1 and NAH7 (Sevastsyanovich et al., 2008, Dennis and Zylstra, 2004), and we found no homologous regions of this cluster in the NCBI gene bank database. In spite of limited functional information about these genes, a notably high throughput sequencing result showed that many reads were covered, particularly in the *orf13* region (Fig. 21A). The read coverage does not match the defined coding structure of *orf13*, but the expressed mRNA appears to come precisely from between *orf12* and *orf14* (locus 8451-8780; Fig. 21A). This implies that the transcriptional unit can be a small RNA or coding region for a short peptide against incorrect annotation. To validate expression relative to culture conditions, we conducted Northern blot analysis. The DNA probe was designed based on the read coverage region (locus, 8491-8740) as 250 bp. To extract total RNA, the mt-2 strain was cultured in LB, or in minimal medium with different carbon sources such as succinate, citrate and glucose. In parallel, cells growing in succinate-amended minimal medium were treated with the effectors benzoate, 3MBz or *m*-xylene. As a negative control, we also tested total RNA from the KT2440 strain in which the plasmid is absent. We examined induction of the *orf13* transcriptional region (for procedures, see Methods). mRNA from this region was expressed highly with similar activity, regardless of culture conditions, whereas the messenger was barely detected in the RNA sample from strain KT2440 (Fig. 21B). This result indicates that the undefined region between *orf12* and *orf14* might be transcribed constitutively, although the strain that harbors the TOL plasmid uses a different metabolic system (Fig. 21B); hence, it is not an effect of *m*-xylene, but a result of more stable mRNA accumulation in growing cells, whose *orf13* transcription level was 8-fold higher than that of stationary cells in the transcriptional comparison (Table S1). The question remains how the unique region is incorporated into the pWW0 plasmid and that it is highly expressed. The reason for the existence of this novel transcription unit requires further study.

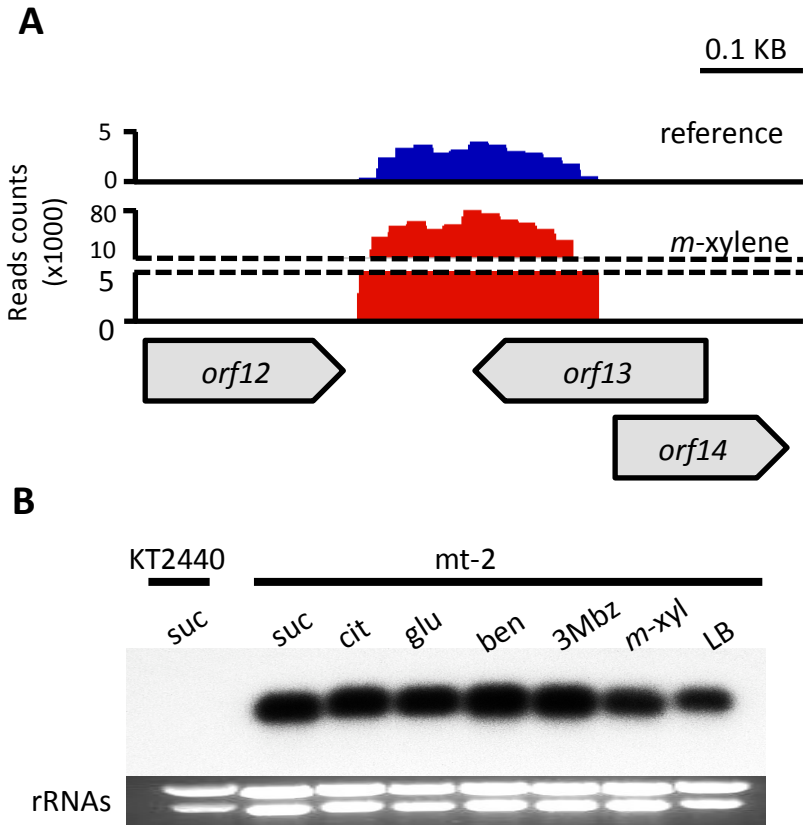


**Figure 21. Characterization of the transcriptional unit in the *orf*13 region in the pWW0 plasmid of *P. putida* mt-2.** (A) The cDNA reads are plotted by the RNA-seq approach, responding to the *orf12-orf14* cluster from the reference (blue for coverage) or *m*-xylene exposure conditions (red for coverage). (B) Northern blot analysis with the probe relative to the *orf13* transcription unit appeared on the transcriptional profile. Total RNAs were prepared from the mid-log growth phase of the mt-2 strain cultured in succinate (suc), glucose (glu) or citrate (cit) as sole carbon source, or in LB. Cells growing in succinate minimal medium were treated with the aromatic compounds benzoate (ben), 3-methylbenzoate (3MBz) or *m*-xylene (m-xyl) (2 h) and RNAs were extracted from the samples. The plasmid-less strain KT2440 grown in succinate culture was examined with the same probe (control).

### 3. Operon structure of the *mpf* gene cluster and its promoter assay

The *mpf* genes are subject to plasmid transfer and these 16 genes are proposed to comprise a single operon structure in the pWW0 plasmid (Greated et al., 2002). In the cluster, five putative genes are included, with two (*orf199* and *orf200*) positioned between *mpfD* and *mpfE*, and three (*orf188, orf189* and *orf191*) adjacent to the *mpfJ* gene (Greated et al., 2002). At difference from the predicted

transcriptional unit, however, the cluster appears to be organized as two operons because of the discontinuous expression profile of the *mpf* region (Fig. 22A); that is, the level of read coverage increased sharply for the *orf188-189-191* cluster region relative to the end of the *mpf* cluster (Fig. 22A). This result strongly suggests that those three genes are not involved in the same operon of the *mpf* cluster, and putative promoter is present to activate expression of the *orf188-189-191* genes. In contrast, read coverage of the *orf199-200* region differed less from its adjacent *mpfD* and *mpfE* genes (Fig. 22A); the hypothetical genes thus belong to the *mpf* operon, although it is not certain whether the proteins have a transfer function. In other words, the polycistronic genes of the *mpf* cluster could be activated independently of *orf188-189-191*.

The question arises as to how the *mpf* genes are regulated. The promoter for these genes might be present in the intergenic region between *mpfR* and *parA*, and it controls entire *mpf* genes as a repressor (Lambertsen et al., 2004). Briefly, when promoter activity is measured on the mt-2 background, it is reduced to basal levels whereas the activity is increased in the KT2440 strain. Moreover, when the promoter region is included in the *mpfR* gene, the activity is not increased on any genotype background. The *PmpfR* promoter is therefore negatively autoregulated by the MpfR protein itself (Lambertsen et al., 2004). In our transcription analysis, expression of all *mpf* genes was about 8-fold higher (Table S1). The different activity was based on the reference condition, and this higher expression might be due to mRNA stability in the growing cell. To further study the *mpf* gene transcription, we generated a reporter plasmid including the *PmpfR* promoter fusion with *lux* genes (Fig. 22B). The reporter plasmid was then introduced into either KT2440 or the mt-2 strain and *lux* activity measured by growth in minimal medium with various carbon sources or in LB medium. The promoter activity in the mt-2 strain was lower compared to KT2440 background, regardless of culture conditions (Fig. 22B). The negative regulator is therefore present in the pWW0 plasmid, as reported (Lambertsen et al., 2004).The difference in activity between strains was higher in LB culture than in any other growth conditions (Fig. 22B). This implies

that the repressor is likely to accumulate more in LB than in minimal medium. Aromatic compounds such as benzoate and 3MBz did not seem to stimulate the promoter (Fig. 22B). The activity of the P*mpfR* promoter was therefore decreased when the TOL plasmid-derived repressor was present and its suppression was attenuated when the strain was grown in minimal compared to rich (LB) medium.

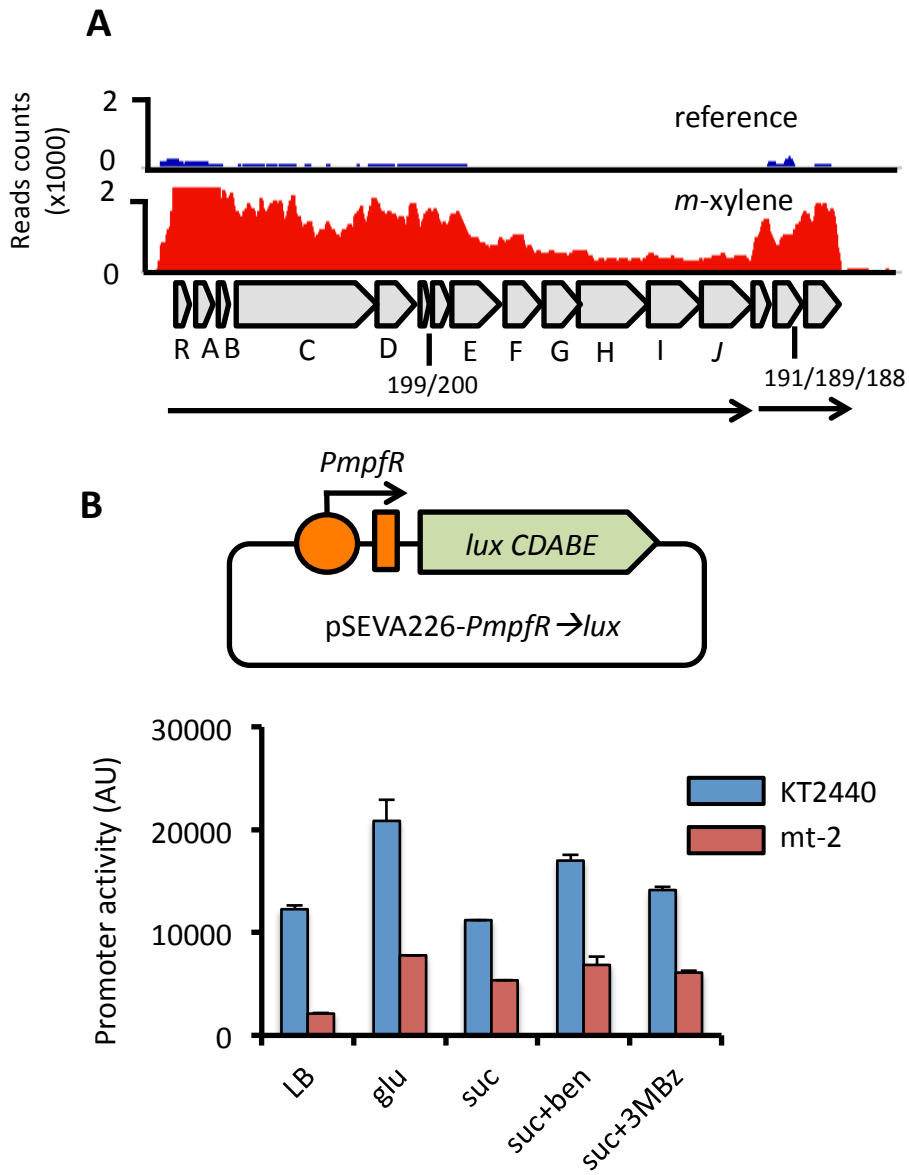


**Figure 22. Transcriptional structure of the *mpf* genes in the pWW0 plasmid of *P. putida* mt-2 and analysis of the activity of its putative promoter.** (A) Transcriptional profile by RNA-seq of the region of the mpf, *orf199-200* and *orf188/orf189/orf191* gene clusters. Plausible operon structures are shown as black arrows. (B) *PmpfR* promoter activity as luminescence intensity measured in KT2440 (blue) or mt-2 strains (red). Maximal promoter activities for each condition were calculated. Data shown as mean ± SD, n = 3. AU, arbitrary units are calculated as luminescence/$OD_{600}$.

**4. Transcriptome of the IncP-9 core region**

There are many putative backbone genes in pWW0 and their functions are not known; most of those genes were transcriptionally inactive in the conditions used in this study (Table S1). Apart from the hypothetical genes, pWW0 replication- and maintenance-encoding genes are highly similar to those of pMT2, which belongs to the IncP-9 group. For instance, the pWW0 *rep* gene, involved in replication, shows 96.2% identity compared to that of pMT2 (Greated et al., 2002, Greated et al., 2000). The protein has a known helix-turn-helix (HTH) motif, and might bind to the plasmid origin site to initiate replication (Greated et al., 2002). Since there are no other potential *rep* genes in pWW0, the protein is only a single replicon in the plasmid. Based on the transcriptome approach, *rep* expression was slightly increased in the normalized comparison result (Table S1). As the number of normalized reads for the gene was in a small range (normalized reads: reference, 751; experimental, 1473) in both conditions tested, however, a small amount of the Rep protein might be responsible for plasmid replication.

The genes for plasmid stability, such as the *par* and *KorA* genes in pWW0, are also highly similar to the same functional genes in pMT2 (Greated et al., 2002, Greated et al., 2000). Based on sequence similarity, the putative ParA and ParB proteins might play a role as an ATPase and a DNA-binding protein, respectively; when the plasmid is partitioned, ParC in the membrane might be linked to the plasmid during segregation, although detailed function is not known (Greated et al., 2002). The pWW0 KorA protein could be a *par* gene regulator, due to similarity with the global IncP-1 regulator protein KorA (Pansegrau et al., 1994). According to our transcription assay, the genes responsible for plasmid stability and its regulator were transcribed at a low level under the conditions examined (Table S1). Such plasmid replication and partition functions are essential to maintain the plasmid in the host. Hence, although gene expression is relatively much lower compared to highly activated genes (e.g., the *xyl* genes), the low enzyme activities might be sufficient for plasmid segregation in the host cell.

It is thought that Tra and two hypothetical proteins (Orf176 and Orf177) might associate to plasmid transfer during *oriT* recognition and processing by these proteins (Greated et al., 2002). Sequence comparison showed that TraA, TraB and TraC are very similar to TrwA, TrwB and TrwC, respectively, from the IncW plasmid R388 (Cabezon et al., 1994). Briefly, the TrwA protein has a regulatory role on *trwABC* operon as a repressor, and the *trwB* gene product enhances DNA cleavage (Cabezon et al., 1994). TrwC is not only able to nick the plasmid at *oriT*, but also has helicase activity (Llosa et al., 1996). TraD from the pWW0 plasmid shows about 30% similarity to IncP-1 TraK, which is related to *oriT* topology alteration and facilitation of the relaxsome (Ziegelin et al., 1992). The four *tra* genes, as well as two hypothetical proteins adjacent to *traD* (*orf 176* and *orf 177*) were downregulated in our experiments (Table S1), strongly suggesting that unknown signals might control these genes simultaneously, although each of the *traABC* and *traD-orf177-orf176* cluster promoters is transcribed divergently (Lambertsen et al., 2004). Nonetheless, we could not establish why these transfer functional genes were transcriptionally attenuated, while *mpf* gene expression, which correlates to the same function, was elevated in the condition as described above. Further experimental investigation is needed, for which determination of the regulator for the *tra* genes would be the key.

## Chapter III

## Visualization of ribosomal protein L13 reveals spatial organization separated from the nucleoid in *Pseudomonas putida*

**1. Ribosome and nucleoid segregation in *P. putida* cultured in rich medium**

To visualize the ribosomal protein in *Pseudomonas,* we used the MEG2 strain, which has a C-terminal fluorophore tag of ribosomal protein L13 (PP_1315; *rplM*) derived from the pBAM1-GFP transposon system (Martinez-Garcia et al., 2011). Although the insertion region is Q136 of the 142 amino acid length of the protein, the fusion protein is functional, as the MEG2 strain growth rate is indistinguishable from that of the mother strain. We traced the protein distribution with a fluorescent microscope after growing the cells in rich (LB) medium. Briefly, the MEG2 strain was cultured in LB (overnight); samples were then diluted 100-fold in the same medium and cultured to the exponential phase. Cells were fixed in a 1% formaldehyde fix solution, then dropped onto a poly-L-lysine-coated coverslip to immobilize the cells and DAPI-stained to define chromosome organization; the fluorescence microscope was used to measure GFP and DAPI signals.

In these conditions, we detected both the ribosome-GFP and DNA-DAPI signals in the cells (Fig. 23A). Green fluorescent signals were spatially organized within the cell, rather than uniformly diffused (Fig. 23A). Furthermore, the ribosome was more concentrated on the outside of chromosomal DNA, based on DAPI-stained nucleoid distribution (Fig. 23A). The relative intensity profile for each fluorophore from the selected cell (marked) suggested correlation of the ribosome peaks with DNA valleys (Fig. 23B). When the cells reached stationary phase, ribosome occupation became less spatially organized, due to bacterial shrinkage and nucleoid compaction, with irregular forms compared to the mid-exponential phase (Fig. 23C). Strong GFP intensity appeared in the nucleoid-free region of the cytoplasm, however, although the cell might have reduced translation activity because of lower mRNA synthesis in such a dormant state (Fig. 23C). Weaker ribosome-GFP signals were also observed throughout whole cells regardless of growth phase, although the protein predominantly occupied the subcellular nucleoid-free region. It remained to be tested whether the small amount of ribosomal protein colocalized with the nucleoid. Our data strongly indicate that most of ribosomal protein is spatially distributed throughout the bacterial cell and

localized in the nucleoid-free region. This observation raises the question as to how ribosome-nucleoid segregation occurs in *Pseudomonas putida*. To respond to this question, we tested the spatial organization pattern in other culture conditions.

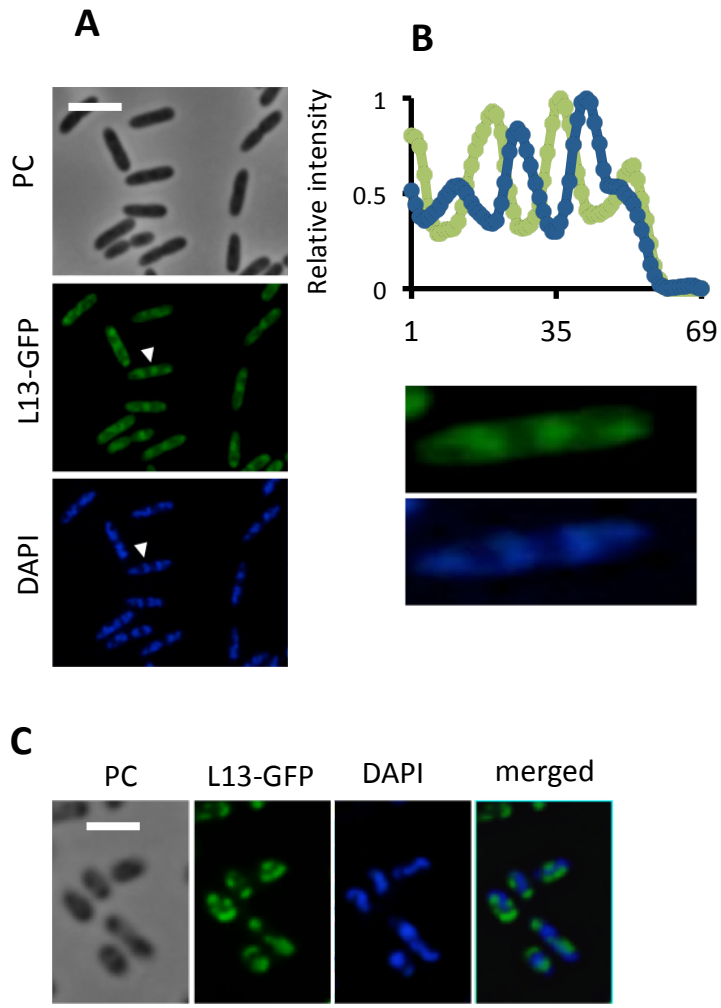


**Figure 23. Visualization of the localization of ribosomal protein L13 fusion with GFP in *P. putida* MEG2.** (A) Microscope image of the MEG2 strain grown in LB medium to the exponential phase to test for distribution of ribosome-GFP (green) and DAPI-stained nucleoid (blue) corresponding to the cells in the phase contrast (PC) image (grey). (B) Relative intensity of each green and blue channel for cells marked (arrowheads) in A). (C) Ribosome-GFP and nucleoid distribution in cells grown 96 h in LB medium. Green and blue channels were merged. Bars = 2.5 μm.

### 2. Effect of distinct metabolic networks on ribosome-nucleoid organization

The ribosome-GFP-expressing strain was cultured in M9 minimal medium with succinate, glucose, benzoate, fructose or glycerol. The samples were then fixed in

exponential or stationary phase conditions and microscopy used to define ribosome-nucleoid organization (see Methods). When tested in growing cells, we found one or two nucleoid lobes depending on cell size and ribosome-GFP was detected outside the DAPI-stained region; there was this little overlap in moderate growth conditions such as glucose, succinate and benzoate addition (Fig. 24A). In contrast, we observed shorter cell length and a spread-out nucleoid in both glycerol and fructose culture medium, and ribosome-nucleoid segregation was not apparent compared to moderate growth conditions (Fig. 24A). This might be caused by a low growth rate in such conditions, so that the copy number of fused ribosomal protein is not sufficiently high to yield distinct fluorescent signals. A small amount of ribosome-GFP intensity was found in specific regions without dense DNA, and in the cell periphery (Fig. 24A).

We also examined the ribosome and chromosome partition pattern in dormant state cells grown in minimal medium plus each carbon source for 96 h. In these conditions, the nucleoid was compacted, since cell length was greatly shortened, and it localized to the central part of the cell irrespective of carbon source (Fig. 24B). In contrast to DNA occupation, a stronger GFP signal was observed in the peripheral cytoplasm than at the central part of the cell (Fig. 24B). Since cells were very small in stationary phase, it was difficult to measure apparent segregation. Despite this limited resolution, our observations indicate a tendency to partition between ribosomal protein and chromosomal DNA in these cells, even in weak biological interaction conditions such as stationary growth phase.

**3. Ribosome subcellular localization in the TOL plasmid-harboring strain**

A discrete bacterial chromosome, for instance a plasmid, is not randomly distributed but lies in specific cell regions. Plasmids such as F, P1 and R27, which have low copy number in *E. coli*, are localized at the quarter or middle of the cell, and the R1 plasmid is positioned at the cell pole (Gordon et al., 1997, Niki and Hiraga, 1997, Lawley and Taylor, 2003, Jensen and Gerdes, 1999). Reyes-Lamothe *et al*. also very recently described that the ColE1-type plasmid is localizes

predominantly at the cell poles, which leads to efficient random partition into daughter cells (Reyes-Lamothe et al., 2013). It is nevertheless unknown whether the plasmid molecule affects organization of other cytoplasmic components.

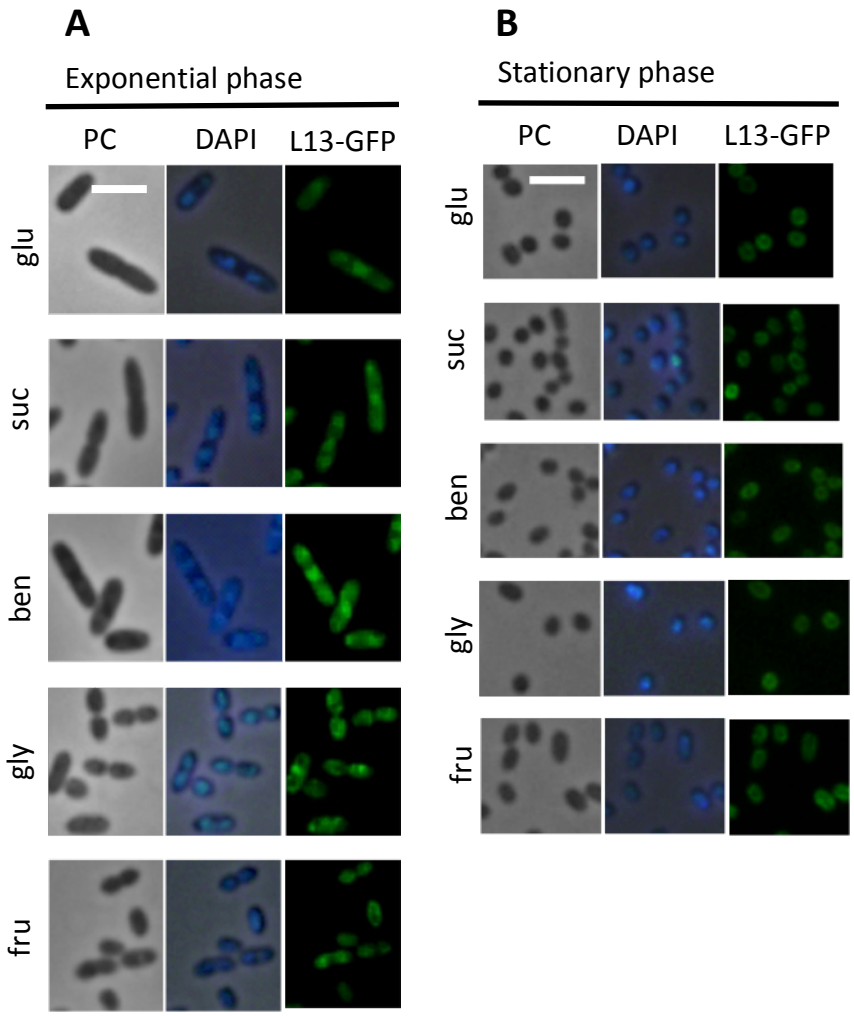


**Figure 24. Substrates and growth phase-dependent ribosome and nucleoid distribution in *P. putida* MEG2**. (A) Cells were cultured in minimal medium with various carbon sources until exponential phase. (B) Each sample was further cultured for 96 h, to reach to stationary growth. glu, glucose; suc, succinate; ben, benzoate; gly, glycerol; fru, fructose. Image for DNA overlaid on phase contrast. Bar = 2.5 μm.

To examine this idea, we introduced the IncP-9 TOL plasmid pWW0 (116 kB) into the MEG2 strain. This plasmid from *P. putida* mt-2 has been characterized with transcriptional activity for *m*-xylene/toluene degradation (Ramos et al., 1997, Dominguez-Cuevas et al., 2006, Velazquez et al., 2005); however, there is no study

of the plasmid localization and segregation. The results from FISH to detect mRNA signals in a single cell indicated that the pWW0 plasmid transcription products remained within one or two subcellular regions that are nucleoid-free sites (Chapter IV).

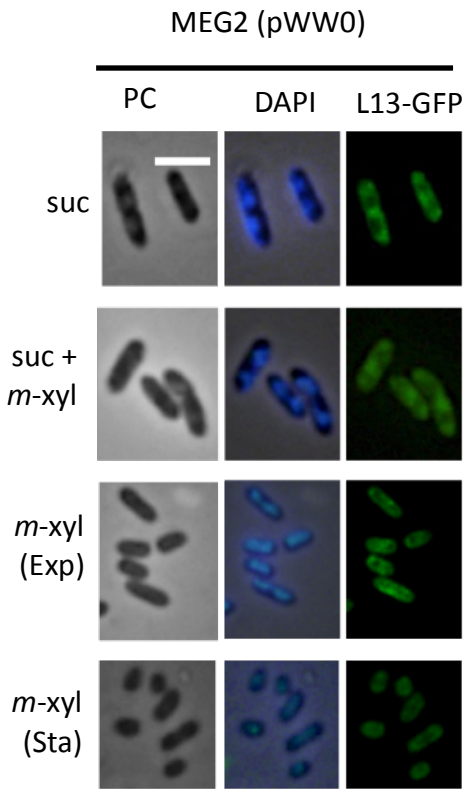


**Figure 25. Spatial organization of ribosome and nucleoid in pWW0 TOL plasmid-harboring cells.** The cell bearing the TOL plasmid was cultured in succinate-amended minimal medium to early exponential phase ($OD_{600}$ ~03), then exposed to *m*-xylene (2 h). Other cells were cultured in M9 plus *m*-xylene (*m*-xyl) as sole carbon source to exponential or stationary phase. Scale bar, 2.5 μm.

Although the plasmid and its transcripts might be confined inside the cell, the segregation was unaffected (Fig. 25). Cells harboring the pWW0 plasmid and cultured in succinate-amended M9 medium showed the same ribosome-nucleoid segregation as the plasmid-less strain (Fig. 25). Moreover, when the strain growing in the same medium was exposed to *m*-xylene, segregation between the two molecules was not affected (Fig. 25). When the cells were grown with *m*-xylene as sole carbon source, the segregation pattern was not apparent due to low ribosome copy number in poor growth conditions such as glycerol or fructose. In addition,

the GFP fusion proteins accumulated in stationary phase; fluorescence signals were found at the border whereas nucleoid signals were in central region of the cell (Fig. 25). Increasing cell density caused by presence of the plasmid, its transcriptional and translational products thus might not affect ribosome-nucleoid segregation.

**4. Spatial distribution of ribosome and nucleoid in translation inhibition**

Chloramphenicol halts translation by binding to the 50S subunit and the drug also affects nucleoid morphology, which contracts both radially and axially in *E. coli* (Bakshi et al., 2012, Dworsky and Schaechter, 1973). We measured the drug effect on distribution of ribosome and nucleoid in *Pseudomonas*.

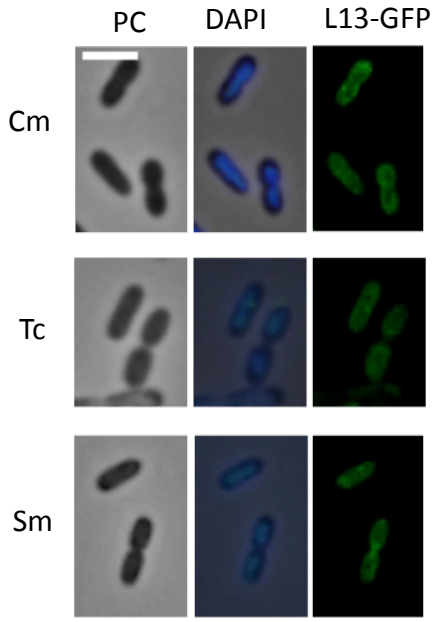


**Figure 26. Translation inhibition effect on ribosome and nucleoid distribution in *P. putida* MEG2.** Cells were cultured in M9 plus succinate to exponential phase, followed by addition of chloramphenicol (Cm; 200 μg $ml^{-1}$), tetracycline (Tc; 50 μg $ml^{-1}$) or streptomycin (Sm; 200 μg $ml^{-1}$)(1 h); cells were then harvested and prepared for microscopy. Scale bar, 2.5 μm

*P. putida* shows resistance to chloramphenicol (Fernandez et al., 2012), but high concentrations of the drug (200 μg $ml^{-1}$) inhibit cell growth completely. We therefore added this antibiotic concentration to cells growing in succinate-supplemented minimal medium (1 h) and monitored cells for a ribosome-GFP

signal. Nucleoid distribution was expanded throughout in *Pseudomonas* (Fig. 26), which is different of features found in *E. coli*, although the reason is unknown. In addition to nucleoid organization in these conditions, we found that the ribosome-GFP signal localized to the peripheral space of the cell (Fig. 26). We tested he effect of other antibiotics such as tetracycline (50 μg $ml^{-1}$) or streptomycin (200 μg $ml^{-1}$), also known to inhibit bacterial translation. The nucleoid was spread out within the cell, and the ribosome occupied the cell border (Fig. 26). These data suggest that ribosome distribution might be reorganized as nucleoid occupation is changed.

## Chapter IV

## Visualization of mRNA induced from the TOL plasmid reveals its subcellular localization and characterization of transcription in a single cell

**1. The mRNAs of catabolic genes expressed from the TOL plasmid are organized spatially**

To visualize specific mRNA, we used the RNA FISH approach as reported by the Wagner group (Montero Llopis et al., 2010) with some modifications (Fig. 27). To this end, the *P. putida* mt-2 strain was cultured in succinate-amended M9 minimal medium to the exponential phase, then the culture was treated with vaporized *m*-xylene to induce the catabolic genes (*xyl* genes) or the cells were further cultured. After 2 h, the cells were formaldehyde-fixed, followed by hybridization with specific probes (see Methods). Each fluorescent probe set (Sterllis) was designed to include 48 complementary oligonucleotides (20 nt; Table S2) with different sequences, each with a fluorescent label, responding to *xylU*/*xylW* (*xylUW*) for the *upper* pathway and *xylX* for the *lower* pathway. Since the gene length of *xylU* is too short to be covered by a probe set, its adjacent gene *xylW* was considered in a probe set. After hybridization, the samples were washed and observed under a fluorescence microscope. Images with distinct fluorescent signals at 5 sec and 0.5 sec exposure time were acquired for *xylUW* and *xylX* hybridizations, respectively.

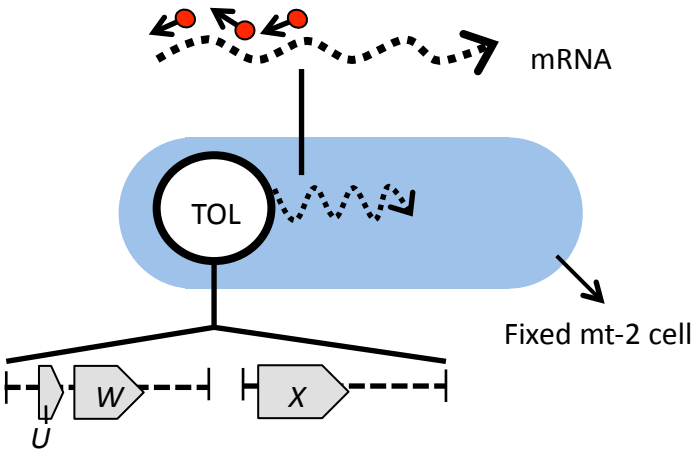


**Figure 27. Scheme showing a fluorescent *in situ* hybridization (FISH) experiment to visualize TOL catabolic transcripts in *P. putida* mt-2.** To sense the *xylUW* and *xylX* mRNAs representing *upper* and *lower* pathway transcription, respectively, their complementary fluorescent probe sets (48 oligonucleotide probes) were used for hybridization.

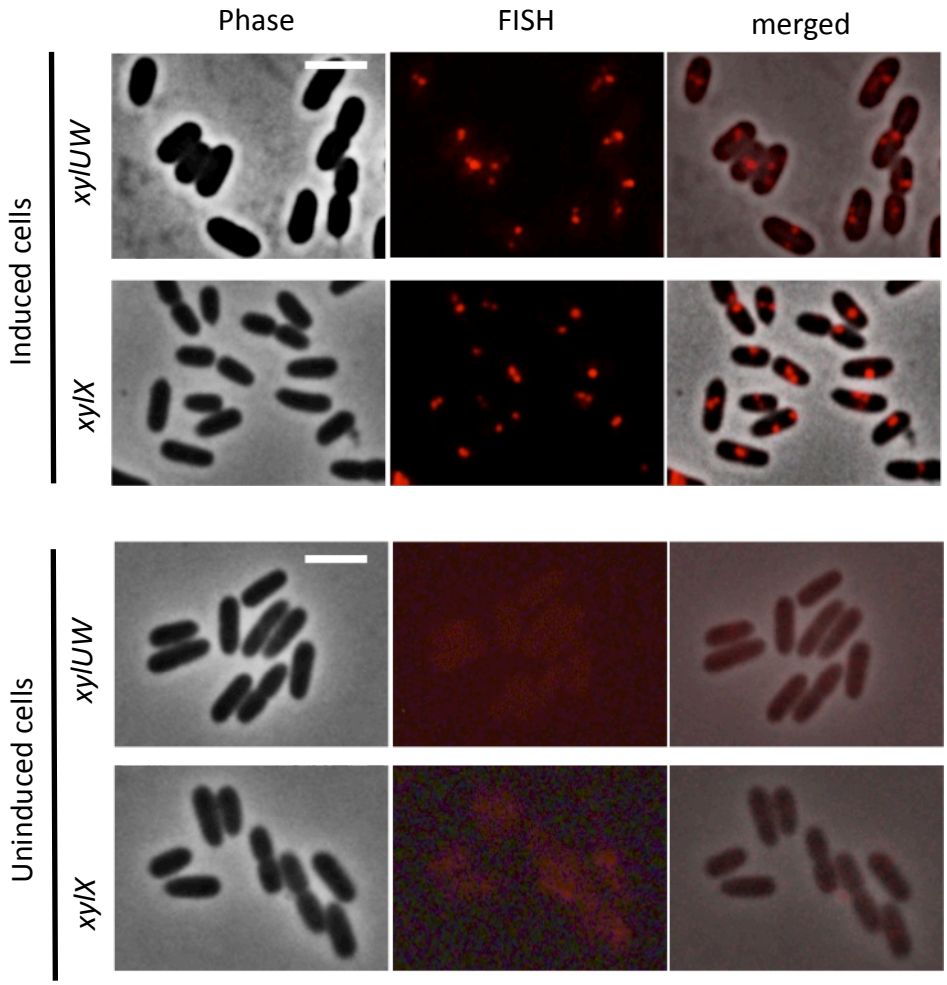


**Figure 28. mRNA FISH with *xylUW* or *xylX* probe sets on *P. putida* mt-2.** The strain was grown in succinate-supplemented minimal medium to the exponential phase, then further cultured for 2 h without inducer or exposed to *m*-xylene to induce the *xyl* genes. After fixation, the FISH experiment was performed (see Methods). Scale bar, 2.5 μm.

Fluorescence microscopy showed signals as one or two foci, responding to both mRNAs in specific regions within most *m*-xylene-treated cells, whereas no signals were detected in succinate growth conditions (Fig. 28). These results implied that the probes were unable to sense the DNA and only detected the mRNAs. The fluorescent signals in Fig. 28 are thus a result of hybridization with the specific mRNAs from *xylUW* or *xylX*, and the molecules accumulated at restricted sites rather than evenly dispersed throughout the cell (Fig. 28). Moreover, the position

of fluorescent spots within a cell was irregular; for example, located near the cell center, boundary or septum (especially *xylX* mRNA during cell division; Fig. 28).

To identify the relative localization of the transcripts, the bacterial chromosome was stained with 4', 6-diamidino-2-phenylindole (DAPI) after hybridization with the fluorescent probe sets. We observed both chromosomal DNA and the specific plasmid transcripts simultaneously in a cell. Most spots representing *xylUW* or *xylX* mRNAs obtained by FISH analysis were found in nucleoid-free regions (Fig. 29). To characterize the spatial organization of the transcripts, we examined cellular localization of transcriptional and translational machineries.

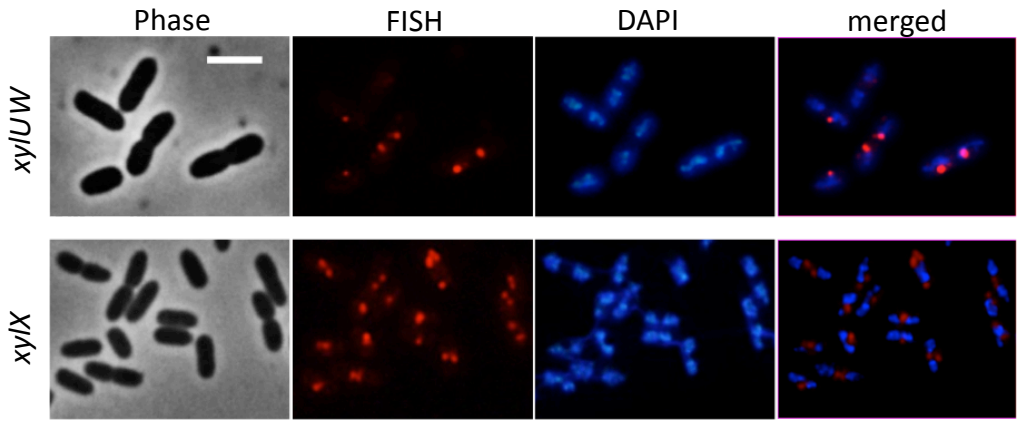


**Figure 29. Subcellular localization of TOL catabolic transcripts in *P. putida* mt-2.** The mRNA signals obtained by FISH assay were spatially organized in a cell; most foci accumulated in nucleoid-free regions. DAPI staining was performed to identify the DNA-dense region. FISH and DAPI signals were merged. Scale bar, 2.5 μm**.**

**2. RNAP spatial distribution coincides with nucleoid organization in *P. putida***

To visualize the transcriptional machineries in *P. putida* KT2440*,* the *rpoC* gene that encodes the β′ subunit of the core enzyme was tagged with monomeric super fold GFP (*msf*GFP) in the chromosome (Fig. 30A). The fusion protein is functional, as the growth rate of the reporter strain is indistinguishable from that of the mother strain. Accordingly, we used fluorescence microscopy to trace protein distribution by growing cells in M9 minimal medium supplemented with succinate as sole carbon source.

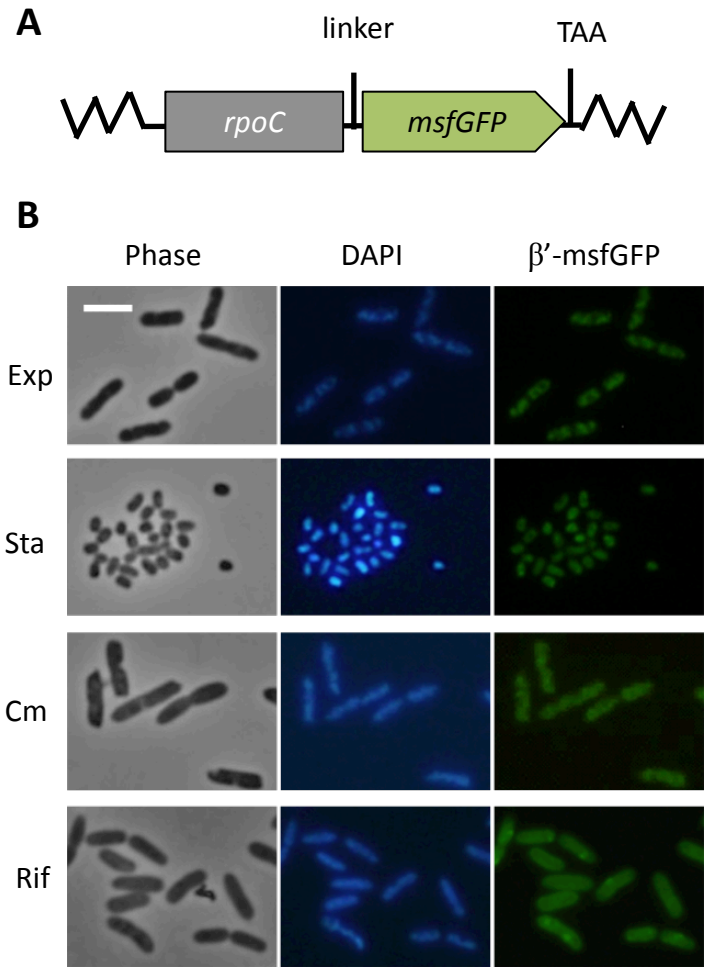


**Figure 30. RNAP subunit organization in *P. putida* KT2440.** (A) Scheme depicting chromosomally expressed *rpoC-msfGFP* to monitor the β′ subunit in the cell. (B) Microscopy of RNAP labeled strain in different conditions. The cells were grown in M9 medium with succinate as sole carbon source to the exponential phase (exp) or to stationary phase (96 h; sta). The translational and transcriptional inhibition drugs chloramphenicol (Cm; 200 μg $ml^{-1}$) and rifampicin (Rif; 200 μg $ml^{-1}$), respectively, were added to growing cells in M9 plus succinate medium. After 2 h treatment, samples were fixed and visualized. Scale bar, 2.5 μm.

The RNAP-msfGFP signals coincided precisely with DAPI staining in exponential phase cells, and the same co-localization pattern appeared in stationary phase cells, although both signals were contracted as cell size had shrunk (Fig. 30B). The results indicate that RNAP molecules are located predominantly within or surrounding the nucleoid. We also tested the drug effect on molecule distribution in terms of translation or transcription inhibition using chloramphenicol (200 μg $ml^{-1}$) or rifampicin (200 μg $ml^{-1}$). After 2 h drug treatment in growing

cells, we hardly observed distinct nucleoid-free regions and the nucleoid appeared to be expanded in the cytoplasm (Fig. 30B). In addition, the RNAP signals appeared to overlap the DAPI-stained region, despite chloramphenicol accumulation in the cell (Fig. 30B). In contrast, when bacterial transcription was halted by rifampicin action, the fluorescent signals expanded uniformly in the cell (Fig. 30B). The RNAP molecule might thus interact with DNA and when the interaction is blocked by rifampicin, it could be dispersed.

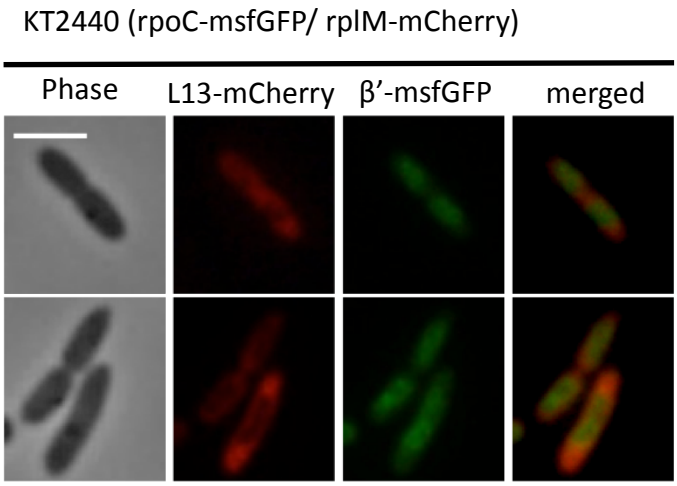


**Figure 31. Spatial distribution of RNAP and ribosome in *P. putida* KT2440.** Microscopy of the dual-labeled cell KT2440 (rpoC-msfGFP/rplM-mCherry). Cells were grown in succinate-amended minimal medium to the exponential phase and labeled molecules were analyzed by microscopy. Representative cells show different molecule segregation patterns. Scale bar, 2.5 μm.

We also identified RNAP localization compared to the ribosomal protein counterpart in cells. We obtained cells dual-labeled for RNAP and ribosome by introducing the fusion of m-cherry to *rplM* encoding the L13 subunit of the 50S ribosomal protein into the RNAP-labeled strain. Fluorescence microscopy showed that in dual-labeled cells, L13-mCherry did not coincide with RNAP-msfGFP signals (Fig. 31). That is, mCherry fluorescence was observed around the cell periphery or cell poles, depending on the RNAP distribution (Fig. 31), and ribosome localization coincided with data for ribosome-nucleoid segregation described in Chapter III. Our approach does not permit quantitative measurement of fluorescence; thus we cannot rule out a small amount of molecular overlap in

subcellular regions. Most of the RNAP and ribosome are likely to be separated in this bacterium, and the data thus strongly suggest that transcription and translation are compartmented.

**3. The *xylUW* mRNAs transcribed from the T7 promoter are found outside the nucleoid with increased copy numbers**

The *Pu* promoter in the pWW0 TOL plasmid was replaced with the T7 promoter and TOL-PuxT7 was generated in *P. putida* mt-2 (Fig. 32). The construct was also introduced into KT2440T7, which is able to express T7 polymerase (T7pol) driven by the *Plauv5* promoter (Troeschel et al., 2012). In this soil bacterium, IPTG is not significant for T7pol levels because of leaky expression under the promoter. In accordance with this concept, intensity with and without IPTG treatment (1 mM) was indistinguishable for the T7pol-dependent transcripts and hence, the inducer was not used in subsequent T7pol expression experiments. The KT2440T7 host bearing the plasmid with the viral promoter for the *upper* pathway was able to degrade *m*-xylene, leading to growth on this compound as sole carbon source, whereas the mt-2 strain with the TOL-PuxT7 plasmid could not use *m*-xylene as an energy source, although 3MBz was metabolized by the *lower* pathway genes (Fig. 32).

The FISH approach detected no transcript for *xylUW* with its specific probes in mt-2 (TOL-PuxT7; Fig. 33), consistent with the growth profile. In sharp contrast, strong *xylUW* mRNA signals were sensed by hybridization when T7pol was present in the host cell, regardless of culture conditions (Fig. 33). In cells with the T7 expression system, fluorescent spots were detected in more than two different subcellular regions compared to the mt-2 strain (Fig. 28, 29 and 33). In the images for FISH results at 5 sec exposure, we reduced brightness uniformly to allow determination of the transcript sites and to compare with DNA-dense region in a cell. Most, if not all fluorescent spots were localized outside the nucleoid, as shown in the merged picture in Fig. 33.

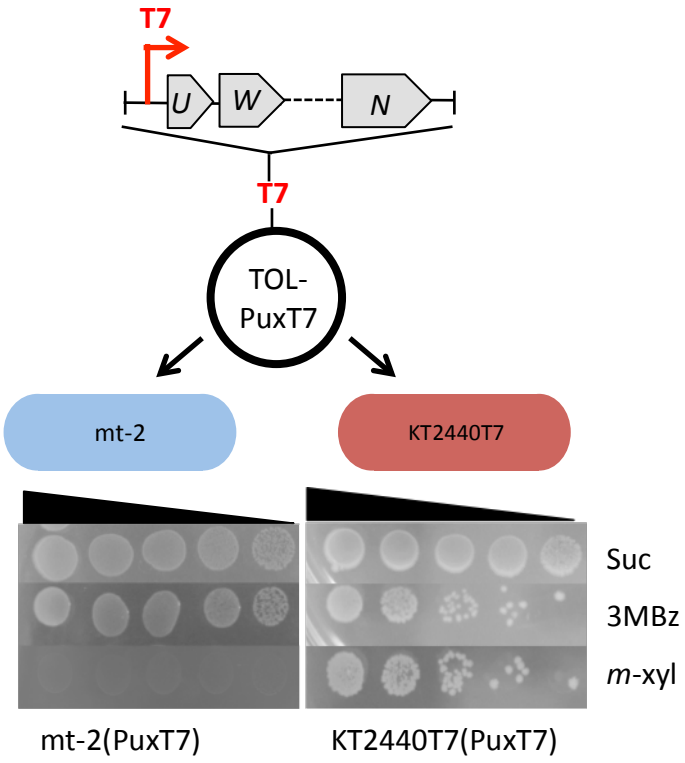


**Figure 32. Replacement of *Pu* with T7 promoter in the TOL plasmid.** Scheme showing the modified pWW0 plasmid and its effect on aromatic compound use in the mt-2 strain and the KT2440T7 strain, which expresses T7 polymerase.

We also analyzed distribution of the *xylX* mRNA induced from the manipulated TOL plasmid. There was no hybridization when we tested it without an inducer in the T7pol-lacking strain, as predicted; however, many fluorescent spots were observed in a cell exposed to *m*-xylene (Fig. 34). The expression of *xylX* despite the absence of T7pol is probably due to transcription networks in the TOL plasmid. That is, *m*-xylene is able to activate XylR, which stimulates *Pu* and *Ps* promoters by binding to the promoter regions. In the TOL-PuxT7 plasmid, the *upper* pathway promoter is not present, and surplus XylR might lead to more XylS production. Finally, the overexpressed XylS could be responsible for *lower* pathway transcription. Most transcripts were distributed to several nucleoid-free subcellular regions (Fig. 34). The *xylX* foci, produced from the TOL-PuxT7 plasmid in T7pol-harboring host cells, were similarly likely to occupy several subcellular nucleoid-free regions (Fig. 34). Based on these data, we consider that polymerase type and

transcriptional factors such as activators, sigma factors and DNA-binding proteins are not critical for mRNA localization in specific regions.

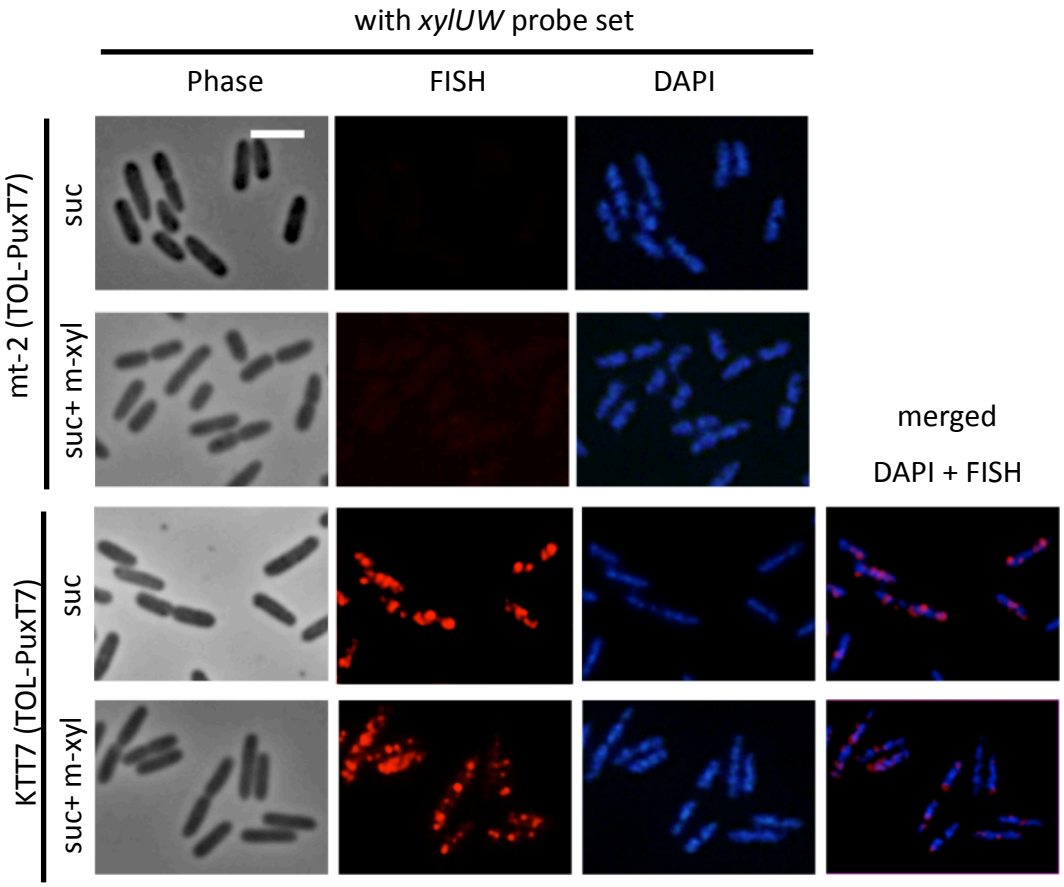


**Figure 33. Spatial distribution of the specific mRNA expressed from the T7 promoter.** mRNA FISH was performed with the *xylUW* probe set in mt-2 (TOL-PuxT7) and KT2440T7 (TOL-PuxT7). Cells were grown in succinate or succinate plus *m*-xylene exposure. Note that the contrast of the *xylUW* signal in the merged image was adjusted uniformly to a different scale as the mRNA signal in FISH was too bright to identify its foci. Scale bar, 2.5 μm.

## 4. mRNA could be localized by diffusion-capture through affinity with the ribosome

We attempted to visualize mRNAs from the T7 expression system in the presence of rifampicin, which blocks only bacterial RNA polymerase. After 2 h treatment with the drug and the inducer for *xyl* gene transcription in growing cells without T7pol, the mRNA signals were scarcely visible by FISH analysis (Fig. 35A).

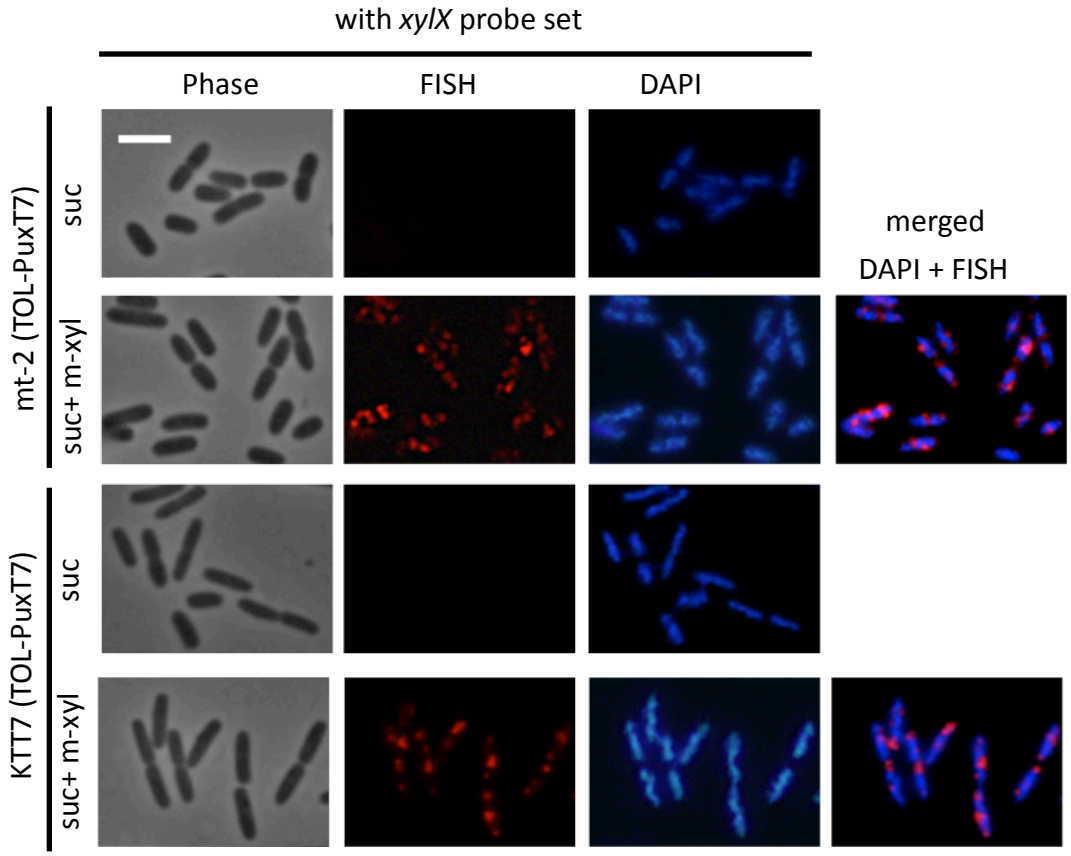


**Figure 34. Visualization of the *xylX* mRNAs expressed from rearrangement of the TOL regulation system.** mRNA FISH was performed with the *xylX* probe set in mt-2 (TOL-PuxT7) and KT2440T7 (TOL-PuxT7). Cells were grown with succinate or succinate plus *m*-xylene exposure. Scale bar, 2.5 μm.

When the fluorescent signal was tested for the *xylUW* transcripts in a viral expression system, the fluorescence intensity was extremely high, covering the whole cell region in <5 sec exposure time (Fig. 35B). This increased expression in rifampicin-treated cells might coincide with a previous study of improved enzyme yield by the T7 expression system using rifampicin, although the exact mechanism is still unknown (Kuderova et al., 1999).

Although confined signals were not detected in these microscopy conditions, several foci were identified in a cell by reducing exposure time to avoid light

diffraction (Fig. 35B). Most fluorescent signals remained outside the nucleoid, especially in peripheral regions or cell poles (Fig. 35B).

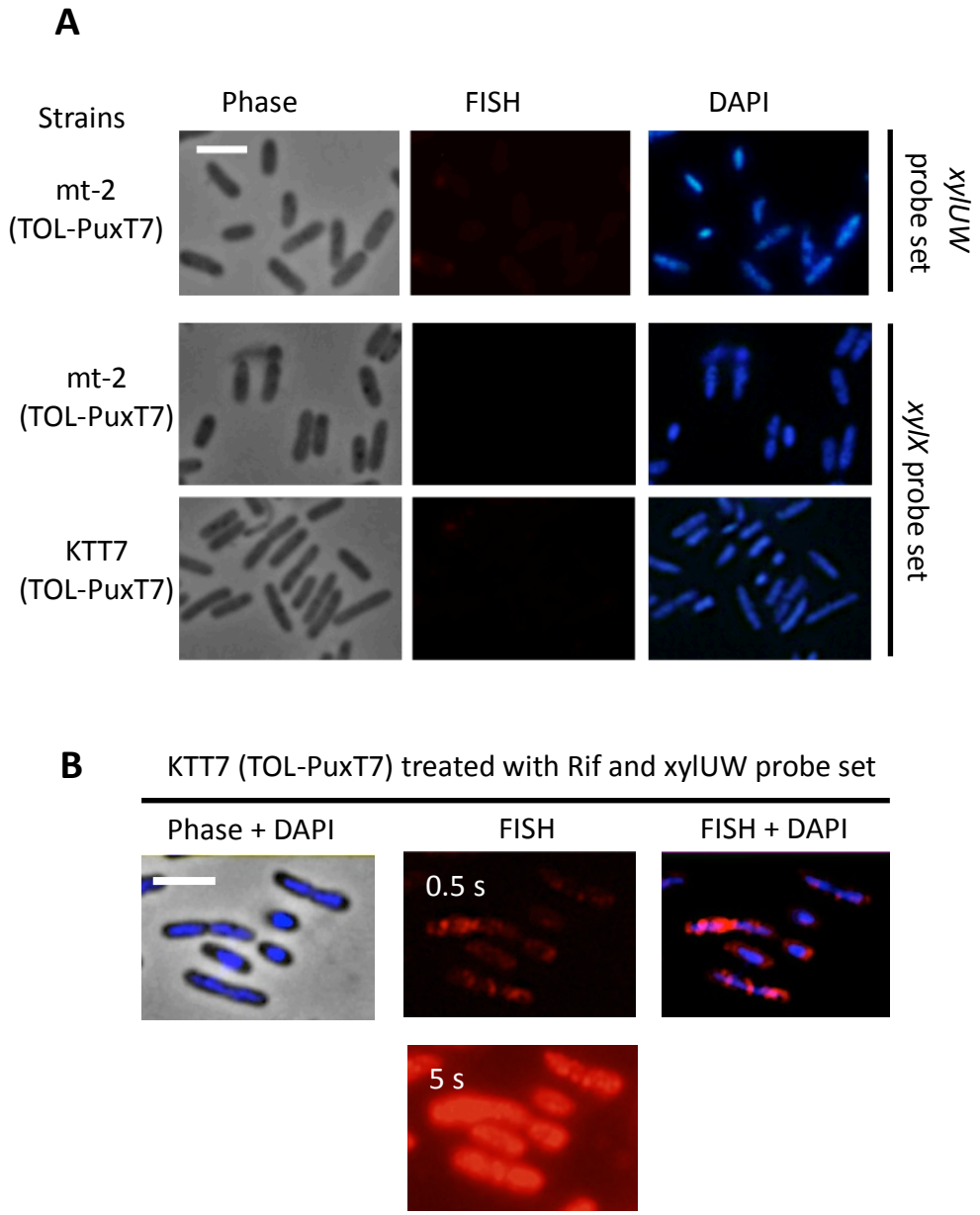


**Figure 35. Rifampicin effect on mRNA synthesis by bacterial RNAP or T7 RNAP and its spatial distribution.** The effector *m*-xylene and transcriptional inhibition drug rifampicin (200 μg $ml^{-1}$) were added to different strains growing in M9 medium plus succinate; 2 h later, the cells immediately fixed. No transcript signal was detected in the strains responding to the probes described in (A) and high transcript signal in the T7 expression system for the *xylUW* mRNAs (B). To identify the region in which mRNAs accumulated, the FISH image was taken at different exposure times. Scale bar, 2.5 μm.

Coincidently, using the msfGFP-tagged L9 in KT2440 obtained by the transposon insertion system (Calles et al., in preparation), we found that the ribosomal protein was also distributed at the cell boundary or cell poles after rifampicin treatment of KT2440 strain cultures (Fig. 36). The mRNA molecule, which is able to diffuse in a cell, might have affinity with the ribosome and its localization would thus be determined as the organization of the translational machinery

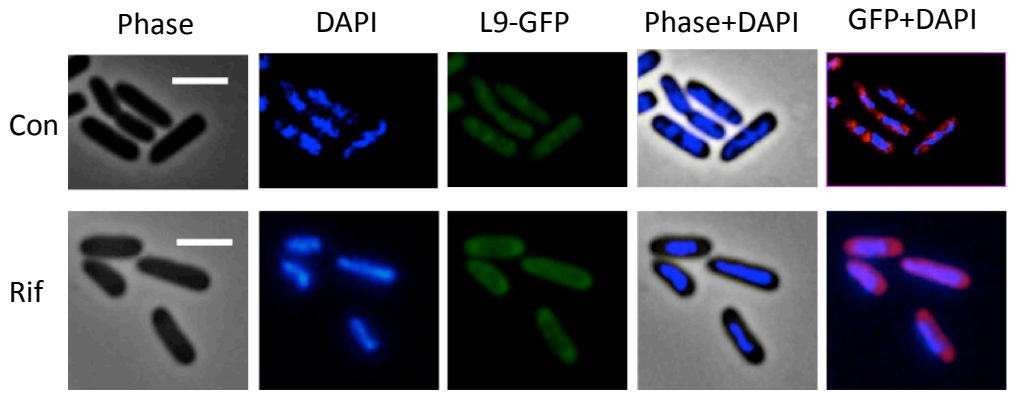


**Figure 36. Effect of transcriptional inhibition on spatial organization of the ribosome in *P. putida* KT2440.** msfGFP-labeled strain L9, obtained by the transposon insertion system, was used to examine the rifampicin effect. Note that the GFP in merged images is depicted in false color to distinguish it from DAPI staining. Scale bar, 2.5 μm.

**5. Transcriptional bursts in TOL catabolic genes**

Apart from the study of molecule organization, we also characterized transcription in a single cell from the FISH experiment, and quantified mRNA copy number statistics of a cell population using an image analysis technqiue designed by the Ido Golding lab (Skinner et al., 2013). To induce the *xyl* genes in *P. putida* mt-2, aromatic compounds such as *m*-xylene, *o*-xylene and 3MBz were used to treat cells in culture medium as described above.

Quantification analysis indicated that 79% of the cell population showed the *xylUW* transcriptional signal, with narrow cell-to-cell variation after *m*-xylene exposure (Fig. 37A). The remainder of the population showed hardly any fluorescent signal.

Whether transcriptionally inactive cells show any signal remains to be tested. Alternatively, lack of signal detection could be due to low sensitivity of the FISH experiment.

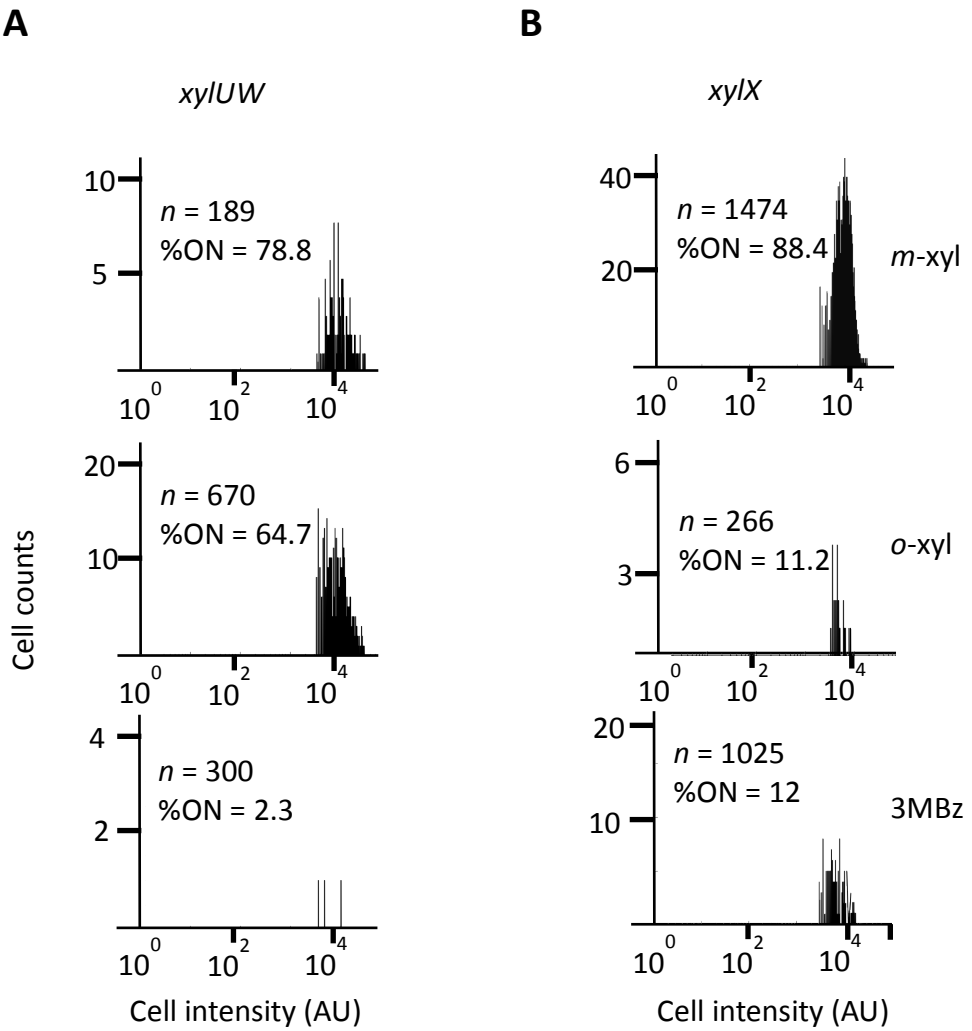


**Figure 37. Quantification analysis for mRNA copy number.** Signals as fluorescent spots obtained from FISH experiments were used to measure mRNA copy number with a statistical approach. Each *xylUW* (A) and *xylX* (B) transcript was induced by effectors such as *m*-xylene (*m*-xyl), *o*-xylene (*o*-xyl) or 3MBz. x-axes indicate expression level per cell and y-axes indicate cell counts (note different scales for each condition). Cells without signals were not counted for this experiment.

This cell-to-cell variation in genetically identical cells is the result of periodical mRNA synthesis over time (So et al., 2011). In other words, the *Pu* promoter is not always in the *on* state, despite the existence of the inducer, but can be switched

between *on* and *off*. This phenomenon leads to transcriptional bursting. We also observed such pulsating expression for *upper* pathway genes in the presence of *o*-xylene (65% of the cell population showed expression; Fig. 37A), while there was little mRNA production when 3MBz was introduced (Fig. 37A).

Measuring *xylX* copy number statistics, most cells (not all, ~88%) had messages that responded to *m*-xylene (Fig. 37B). Only 12% of the cells showed transcriptional signals after either *o*-xylene or 3MBz treatment (Fig. 37B). As a plausible explanation for the result, the burst frequency was decreased in the presence of poor inducers compared to a superior inducer like *m*-xylene. Furthermore, considering the *on* state population, we observed that transcriptional intensity in single cells was unchanged, although the type of inducer differed (Fig. 37B). Cells not treated with effectors gave no detectable signals, as shown in Fig. 28.

# V. Discussion

**1. High-throughput transcriptome for the TOL *xyl* gene**

Transcriptomics is a useful means to understand gene expression and regulation mechanisms. Nonetheless, custom DNA microarray technology using annotated gene probes permit only a narrow view of all genes. To overcome this weakness and explore the whole transcriptome in the cell, high-throughput technologies such as RNA deep sequencing and high-density tiling arrays have been used for eukaryotic and prokaryotic cells (Cheng et al., 2012, Juneau et al., 2007, David et al., 2006, Passalacqua et al., 2009, Toledo-Arana et al., 2009, Yoder-Himes et al., 2009). These unbiased transcriptome technologies make it possible to define novel genes or sRNA detection, untranslated regions and operon structures (Sorek and Cossart, 2010).

In this study, we concentrated on *m*-xylene/toluene-dependent transcription with these high-throughput technologies in the TOL plasmid and its associated chromosomal genes in *Pseudomonas putida* mt-2. The tiling array data showed that both *upper* and *lower* operon genes are highly induced, in accordance with previous results (Velazquez et al., 2005, Dominguez-Cuevas et al., 2006). This mode of normalization might nonetheless overlook constitutively expressed genes in both conditions. We therefore exploited the reference condition for normalization to obtain actual gene expression (Guell et al., 2009). We observed non-specific expression of *lower* pathway genes in the succinate cultured cells and found a novel transcript unit contiguous to the *xylN* gene (Fig. 8).

Based on this result, normalization considering the reference condition could be more informative means to investigate gene transcription analysis. We therefore studied the transcriptome with the reference condition in further assays, including RNA deep sequencing. The tiling array allowed us to discover overlapping transcription between the 3' end of the *xylS* gene and the *lower* operon by converging transcription (Fig. 12), which was validated using the Northern blot assay with strand-specific RNA probes (Fig. 12). We nonetheless observed that the overlapping structure does not appear to influence XylS function, since *Pm* promoter activity is almost the same, despite the overlap of anti-sense *xylS* transcription and sense *xylS* transcription (Fig 13). Høvik *et al*. also frequently observed a similar RNA expression pattern for RNA signals on both

strands caused by extended transcription forward to the 3' end where the untranslated region is found in *Porphyromonas gingivalis* W83 (Hovik et al., 2012). The expression pattern might thus be common in bacterial cells, and its secondary structure probably does not allow a base pairing structure in the overlapping region.

The transcription profile resulting from our tiling array and RNA deep sequencing ruled out the existence of a putative promoter on the intergenic *xyl* genes, because continuous transcription was shown to respond to *upper* and *lower* operons enhanced from the *Pu* and *Pm* promoters respectively (Fig. 8, 9A and 10A). As demonstrated above, the tiling array and RNA deep sequencing are powerful tools, not only for understanding gene expression, but also for defining transcriptional elements. Array-based studies can sometimes be limited, however, because of cross-hybridization and noise expression (Sorek and Cossart, 2010). We also faced this problem when the mRNA responding to *m*-xylene and toluene was examined for the tiling array. That is, not all but partial signals of the probes on the *benABCD* region appeared, especially in *m*-xylene- or toluene-exposed culture conditions (Fig. 15); this was certainly cross-hybridization expression, given the great similarity between the *benABCD* and the *xylXYZL* genes. In support of this scenario, the *PbenA* promoter was not stimulated in any condition except in benzoate-treated cells (Fig. 16A). In addiiton, there were few reads on the *benABCD* genes when total RNAs extracted from *m*-xylene-treated cells were used for the RNA deep sequencing assay (Fig. 16B). RNA deep sequencing can thus give as accurate transcriptome mapping as single nucleotide resolution. Due to the merits of the technology as a high resolution approach, we identified incorrectly annotated sequencing in the *xylL* gene (Fig. 11).

**2. Transcription analysis of chromosomal *ortho* pathway genes**

Based on the high-throughput technologies, we were able to make a genome-wide transcriptome map while *P. putida* mt-2 assimilated *m*-xylene/toluene and its derivatives. The aromatic compounds can be degraded *via* the plasmid *meta* pathway or the chromosomal *ortho* pathway (Fig. 14). While the strain is treated with *m*-xylene or toluene, it is likely to use only the *meta* cleavage pathway to degrade the aromatic

compounds, because the transcriptome profile showed no signals related to *ortho* cleavage pathway genes such as *ben*, *cat* or *pca* (Fig. 10A, 15, 17 and 18). Surprisingly, benzoate generated from toluene catabolism by the *upper* pathway does not appear to enhance *ortho* cleavage pathway genes (Fig. 10A, 15, 17 and 18), probably due to the regulator titration. That is, if high XylS accumulation resulting from XylR-*Ps1* promoter interaction (Fig. 10A) strongly enhances the *meta* cleavage pathway enzymes, then intracellular benzoate could be rapidly degraded *via* this pathway, silencing the *benR* gene. By contrast, when benzoate was added directly to culture medium, both *meta* and *ortho* pathway genes were expressed (Fig. 10A, 15, 17 and 18). Regarding the *ortho* pathway genes, we did not observe a signal for *benR* or *catR* induction, although their target genes are transcribed (Table 4, Fig. 15 and 17). Our unpublished data (Pérez-Pantoja et al., unpublished) clearly show that the XylS homologue of BenR is not responsible for the *PbenA* promoter, and a recent study indicated that the *catR*-deficient mutant strain could not grow on benzoate, although it produces CCM (van Duuren et al., 2011). BenR and CatR are the only positive regulators that control expression of the *ben* and *cat* genes, respectively, even though transcription of their regulator genes are below detectable levels in the tiling array approach (Fig. 15 and 17).

As anticipated, the *pca* genes were also expressed in response to benzoate (Fig. 18). The *pcaR* gene, which encodes the positive regulator, is induced constitutively regardless of conditions, although its intensity is slightly lower in the presence of *m*-xylene, toluene or *o*-xylene (Fig. 18). Since *o*-xylene cannot be metabolized, this finding indicates that the reduction in the regulator gene is not caused by metabolites of the aromatic compounds. Considering the peripheral genes of the β-ketoadipate pathway, this result shows no connection with the *meta* or *ortho* pathways in the mt-2 strain (Fig. 19). This first transcriptome study combining results from tiling array and deep sequencing techniques gives a broad, high resolution view of TOL catabolic gene expression, and the results provide fundamental information that can be helpful for further biological application.

**3. Identification of transcriptional structure for TOL backbone genes**

DNA sequencing and its comparative analysis revealed the genetic structure of the IncP-9 plasmid pWW0, and common backbone genes in the group were identified in the plasmid (Greated et al., 2002). Nonetheless, the function of many genes in the pWW0 plasmid remains unknown and expression information is limited. In chapter II of this Thesis, we addressed the transcription of several backbone genes using an RNA deep sequencing approach and characterized their genetic structure. The *orf13* region in the plasmid had unexpectedly strong transcriptional activity (Fig. 21), although we were not able to define its function here; however, it would be interesting to identify this, because of its potential ability as a sRNA to regulate gene expression in the plasmid or the host cell. The study also showed the transcriptional profile of IncP-9 core genes such as *par*, *mpf* and *tra*; and it would be useful to determine expression and operon structure for the same functional genes of other plasmids in the same group.

**4. Ribosome-nucleoid segregation in *P. putida***

In this Thesis, we examined the organization of ribosome and chromosomal DNA in *P. putida* by monitoring ribosomal protein fused with GFP, using microscopy. Strong ribosome-GFP signals were observed in nucleoid-free regions in growing cells (Fig. 23A). Nucleoid organization became more irregular in stationary phase cells compared to those in exponential phase. Regardless of the growth phase, the spatial distribution of the ribosome was likely to be rearranged relative to the position of the nucleoid, with strong ribosome-nucleoid segregation (Fig. 23C). A question then arises: what makes the ribosome segregate from the nucleoid?

To consider biological mechanisms, we monitored distribution of the ribosomal protein while the reporter strain was cultured with different carbon sources; however, the segregation pattern appeared in all conditions we examined (Fig. 24). This finding implies that the spatial organization of this protein is not dependent on substrates such as glucose, succinate and benzoate, even if the cells use different metabolic networks (Harwood and Parales, 1996, Kim et al., 2013). When cells

reached stationary phase, cell size shrunk to a striking degree; the nucleoid occupied central regions of the cell, whereas ribosome-GFP signals were peripheral (Fig. 24B). RNA sequencing approaches show that there are few total mRNAs in stationary compared to exponential phase cells (Guell et al., 2009, Kim et al., 2013). There would thus be less ribosome-mRNA interaction in the growth phase, but the reduced activity does not seem to affect segregation between chromosomal DNA and the ribosome. These data indicate that the bacterial metabolic network might not the key factor in deciding segregation between the molecules.

We also analyzed the effect of macromolecule crowding in a cell on molecule organization. Cellular density increased since harboring the pWW0 plasmid led to accumulation of transcriptional and translational products inside cell, but the segregation pattern was unchanged (Fig. 25). This finding indicates that the physical density does not affect ribosome-DNA segregation. After chloramphenicol treatment of *E. coli*, very strong ribosome-nucleoid segregation was observed, while the nucleoid was compacted (Bakshi et al., 2012). In contrast to *E. coli*, chromosomal DNA spread out in *P. putida* when this drug was introduced into the growing culture (Fig. 26). Similarly, both tetracycline and streptomycin treatment also dispersed the nucleoid throughout the cell (Fig. 26). In these translational inhibition conditions, apparent segregation was not detected, but the major GFP signal accumulated at the cell borders; this implies that the ribosome is spatially distributed despite low biological activity due to translation inhibition.

**5. Physical force might lead to ribosome-nucleoid segregation**

Since our collected analyses did not identify a biological cue for DNA-ribosome organization, we might consider the effects of physical forces for the elucidation of this process. It is reported that cellular components can be mixed and demixed to maximize conformational entropy (Jun and Wright, 2010). Based on this argument, Mondal *et al*. derived a model of the separation between nucleoid and ribosome using simulation, with excluded volume and polymer conformational entropy for an *E. coli* case study (Mondal *et al*., 2011). Briefly, considering DNA as a

hyperbranched polymer, monomeric ribosomes as hard spheres, and chains of ribosomes as freely jointed chains of hard-sphere ribosomes, they showed that when a mixture of the polymer and small spheres is confined, the polymer occupies the interior section of the container, while the small spheres occupy the periphery (Mondal et al., 2011). This simulation coincides exactly with our observations in *P. putida*, although they studied only one nucleoid lobe. It is therefore probable that the spatial distribution of the ribosome is determined by a nucleoid exclusion effect in this soil bacterium.

### 6. Spatial distribution of mRNAs induced from the TOL plasmid in *Pseudomonas putida* mt-2

The subcellular localization of RNA and its diffusion are well characterized in eukaryotes (Holt and Bullock, 2009, St Johnston, 2005), but until recently, mRNA distribution was studied in only a few microorganisms such as *Caulobacter crescentus* and *Escherichia coli*, as discussed in the Introduction. In Chapter IV, we addressed the spatial organization of mRNAs transcribed from the TOL pWW0 plasmid in *P. putida* mt-2 using FISH with specific fluorescent complementary probes. We observed that the catabolic transcripts *xylUW* and *xylX* activated from the *Pu* and *Pm* promoters, respectively, were localized in subcellular regions with restricted dispersion (Fig. 28). The limited fluorescent signals indicate that the molecule is not free-floating inside the cell, but it is likely to accumulate in specific regions devoid of nucleoids (Fig. 29). As we described above, the translation factory is enriched in nucleoid-free regions in *Pseudomonas*, and the mRNA loci observed in this species might therefore be associated with translation. Since the functional regions of XylU/XylW (unknown/benzyl alcohol dehydrogenase II) and XylX (toluate 1,2-dioxygenase alpha subunit) are not defined, it is not clear whether the transcripts are located in the sites where the gene product acts. Nevertheless, based upon the characteristic dynamics of RNA molecules, we envisioned two scenarios for TOL catabolic mRNAs constrained in nucleoid-free regions as protein synthesis sites in the host cell. First, while RNA is being transcribed, it could be tethered to the TOL plasmid DNA, where it might be

positioned at nucleoid-free regions; the complete mRNAs might also remain near the transcription site for subsequent translation. In the second alternative, the transcripts released from the template could diffuse to ribosome-rich regions. These two possibilities are not mutually exclusive, and might be found in a cell at the same time.

### 7. Spatial separation between transcription and translation factories in *Pseudomonas putida*

Visualization of the RNAP subunit and ribosomal protein in *E. coli* and *B. subtilis* showed that these molecules are spatially separated, which suggests that bacterial transcription is not coupled with translation (Bakshi et al., 2012, Lewis et al., 2000). We also followed the RNAP location in *P. putida* KT2440 using msfGFP tagged to the β′ subunit. We found that the molecule colocalized with a dense DNA region and it appeared to interact strongly with DNA, because the chromosomal DNA and RNAP signals overlapped even though the cells were in stationary phase or translation was halted (Fig. 30B). This observation implies that the region where mRNA signals accumulate is not a transcriptionally active site. Nonetheless, we cannot rule out the possibility that the mRNA remains near its template site, because the TOL plasmid location has not been identified. If the plasmid is found outside the chromosomal DNA, the transcripts synthesized by the small amount of RNAP would be detectable and remain close to the template site. Further study of the plasmid localization is therefore required to determine the organization of the specific TOL transcript.

In addition to coincident occupation of RNAP and DNA, by tracking both molecules in a cell, we also found that RNAP localized almost exclusively outside the ribosome in *P. putida* (Fig. 31). Although we could not measure the amount of RNAP in the cell, the data implied that transcription and translation occur predominantly in separate subcellular regions. The same pattern has been observed in other species such as *E. coli* and *B. subtilis* (Bakshi et al., 2012, Lewis et al., 2000). In sharp contrast, other laboratories found a physical link between

transcription and translation in *E. coli* (Proshkin et al., 2010, Burmann et al., 2010). Briefly, these latter reports offered the following evidence: 1) the transcription rate is dependent on translation rate, 2) codon usage also affects the rate of transcription, and 3) the transcription factor NusG can bind to both ribosomes and RNAP. This paradox was reconciled by Campos and Jacobs-Wagner, who suggested three models. In the first, assuming co-transcription and translation is a marginal mechanism, only small subset genes would be involved in the coupling; RNA and protein synthesis would therefore occur independently, leading free mRNA to move toward to ribosome-rich sites. In the second model, by means of gene relocation (although the mechanism unclear), actively transcribed genes would migrate to the interface between the nucleoid and the ribosome-rich regions. Finally, a small amount of ribosome in dense DNA regions would be responsible for ribosome-mRNA complex migration by entropic force (Campos and Jacobs-Wagner, 2013). Defining a detailed mechanism of bacterial transcription and translation thus also requires further experimental studies. Other microorganisms such as *P. putida* and *B. subtilis*, with known compartmental organization of the two molecules, are therefore necessary for research on the physical interactions between RNAP and ribosomes.

**8. Diffusion of mRNA toward to ribosome-rich sites**

In *Pseudomona*s, functional coupling of transcription and translation has not been defined as in *E. coli.* Despite this caveat, we sought to examine the possibility of mRNA diffusion, because most of the transcription factory is separate from the active translation site. The copy number of specific mRNA expressed from the TOL plasmid is tightly regulated and maintained constant by the plasmid and host cell transcription factors. To increase the transcription level, we used viral T7 promoter to replace the *Pu* promoter (Fig. 32). The T7 expression system is functional for the expression of *upper* pathway genes when the viral RNA polymerase is present, since the strain harboring the modified TOL plasmid with T7pol metabolized *m*-xylene as a sole carbon source, whereas the strain lacking T7pol did not grow on this compound (Fig. 32). Compared to FISH data obtained

from wild type (shown in Fig. 28), it was intriguing to see that signal intensity in response to *xylUW* mRNA expressed by the T7 promoter was not only increased, but many distinct foci were restricted to a few subcellular regions, regardless of culture conditions (Fig. 33). This observation strongly implies that the molecule is able to diffuse, because the mRNA signals are observed in many different cell regions; the foci would otherwise appear as larger fluorescent spots in one or two subcellular sites. When culture medium of the strain harboring the modified TOL plasmid was supplemented with *m*-xylene, we detected similar organization of *xylX* transcripts in several regions, rather than one or two foci, regardless of the presence of T7pol (Fig. 34). In this case, XylS accumulation due to interaction of surplus XylR with the *Ps* promoter seems to increase copy number of *lower* pathway genes.

By and large, most bacterial plasmids are located at specific position(s), and the partition system encoded by the *par* genes plays a critical role in maintaining their stability (Lawley and Taylor, 2003, Erdmann et al., 1999, Niki and Hiraga, 1997). A well-conserved Par system is also found in the IncP-9 plasmid (Greated et al., 2002, Greated et al., 2000), so the TOL plasmid, which belongs to the same group, would be localized at a specific site. Accordingly, a number of foci in different subcellular regions, as seen by FISH experiments in the T7 system, might not be caused by random plasmid distribution, but could be a result of mRNA diffusion and capture. A plausible mechanism for this diffusion is cytoplasmic mobilization by thermal energy in the form of infrared radiation (Trevors, 2012); the bacterial cytoplasm was recently characterized as a glass-forming liquid, leading cytoplasm components to move (Parry et al., 2013). It is not enough to understand specific mRNA movement to the region of its protein function (Nevo-Dinur et al., 2011), however, and other mechanisms or forces should thus be considered.

This leads us to ask, where is the molecule going? We can answer that the mRNA is likely to move toward ribosome-rich regions, because most signals were detected in nucleoid-free regions, where the translation factories are abundant in *Pseudomonas putida* (Fig. 33, 34). In support of this concept, 2 hours of rifampicin

treatment in growing cells showed that both ribosomal protein and mRNA occupied the peripheral regions (Fig. 35, 36). It is still unclear how the mRNA can migrate to the ribosome, even though both molecules are negatively charged. The Trevors lab proposed that the high $Mg^{2+}$ concentration in ribosomes might provide a force that attracts the bacterial transcripts (Yamamoto et al., 2010, Trevors, 2012).

**9. Characterization of transcriptional bursting in the TOL system**

Visualization of mRNA in a cell also allows study of the single cell transcriptome, which is not possible using other approaches such as Northern blotting, RT-PCR, microarray and deep RNA sequencing. Through the mRNA copy number statistics, we could obtain characteristics of TOL gene expression at a fixed time. The *xyl* genes are likely to be expressed periodically, rather than being transcribed constantly in the presence of effectors. Since some cells had no detectable signals in hybridization with probe sets representing *upper* and *lower* operons, those genes might be in the *off* state of transcription (Fig. 37). This observation is not due to loss of the TOL plasmid or cell death, because the number of cells when grown on *m*-xylene or 3MBz as sole carbon source was very similar to that of cells grown on succinate (Fig. 38).

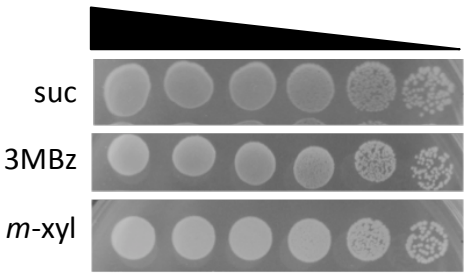


**Figure 38. Viability assay for *P. putida* mt-2 with different carbon sources.** Serial dilutions of the mt-2 strain were cultured on M9 agar minimal medium supplemented with succinate (suc), 3MBz or *m*-xylene as sole carbon source, shown at 48 h post-inoculation.

As mentioned in the Introduction, this fluctuation is observed in many organisms and is defined as transcriptional bursting. In the case of *upper* pathway genes, a similar ratio of cells was transcriptionally active in the presence of the XylR-

associated effector (*m*-xylene or *o*-xylene), whereas most cells remained inactive in 3MBz and succinate (Fig. 37A). In parallel, we found little variance for active cells (Fig. 37A). This suggests that burst size and frequency for *xylUW* expression depend on intracellular cues such as XylR-*Pu* promoter interaction. In the case of the *lower* pathway gene, 88% of the cell population was in an active state, but only 12% of cells had detectable signals in response to *o*-xylene or 3MBz (Fig. 37B). These results indicate that transcription frequency was changed, since intracellular cues can be different (e.g., highly concentrated XylS and *Pm* interaction, low level of XylS and *Pm* interaction) for the *lower* operon, and the frequency could be very low with such poor inducers compared to *m*-xylene. Nonetheless, the expression intensity for a single cell was not so different, irrespective of effector type (Fig. 37B). This is somewhat surprising because typical transcription analysis, including the tiling array data in this Thesis, have shown that *lower* operon activity is reduced in the presence of 3MBz or *o*-xylene. As these approaches are unable to consider transcriptional bursting, the *average* intensity produced a distorted transcriptional profile.

It remains to be determined how the transcriptional bursting for the TOL system occurs in a cell. Hence further molecular studies are needed, as understanding stochastic gene expression and bimodal distribution of fluorescent cells by the TOL promoters (Silva-Rocha and de Lorenzo, 2012c) would be a key factor. Our findings show that transcription burstiness appears in this soil bacterium and this feature of gene expression would confer a fitness advantage to the overall population.

# VI. Conclusions

The studies performed in this Thesis have allowed us to reach the following conclusions:

1. **The high-throughput transcriptome reveals a novel transcription unit contiguous to the *xylN* gene, as well as an incorrectly annotated sequenceg in the *xylL* gene, and it defines the structure of *upper* and *lower* operons in the TOL plasmid pWW0.**

2. ***Pseudomonas putida* mt-2 preferably uses the *meta* cleavage pathway for biodegradation of *m*-xylene/toluene.** Although the bacterium is able to express *ortho* cleavage enzymes, these aromatic compounds do not activate *ben* genes in the chromosome.

3. **Ribosomal protein predominantly occupies a nucleoid-free region in *Pseudomonas putida.*** The ribosome-nucleoid segregation is caused by the chromosomal DNA exclusion effect.

4. **Ribosome and RNA polymerase are spatially separated in *Pseudomonas putida*.** The spatial distribution of the molecules suggests that transcription and translation are not coupled in the bacterium.

5. **Specific mRNAs induced from the TOL plasmid reside in ribosome-rich sites.** The transcripts are also spatially organized rather than free-floating, and diffuse toward ribosome-rich regions.

6. **TOL gene expression is subject to transcriptional bursting.** The *xyl* genes are not always transcriptionally active, but show pulsating expression. This characteristic mRNA production leads to stochastic gene expression.

Los experimentos descriptos en esta Tesis nos han permitido elaborar las siguientes conclusiones:

1. **El análisis transcripcional de alta definición reveló una nueva unidad transcripcional contigua al gen *xylN*, e identificó un error de anotación en la secuencia del gen *xylL*, definiendo con exactitud la estructura de los operones *upper* y *lower* en el plásmido TOL pWW0.**

2. ***Pseudomonas putida* mt-2 utiliza la ruta de degradación *meta* para la biodegradación de *m*-xileno o tolueno.** A pesar de que este microorganismo también puede expresar las enzimas de degradación *orto*, la transcripción de los genes *ben* no se activa en presencia de los compuestos aromáticos mencionados.

3. **Las proteínas ribosomales ocupan predominantemente una región libre de nucleoide en *Pseudomonas putida.*** La segregación de ribosomas y nucleoides es debida al efecto de exclusión de ADN cromosomal.

4. **Los ribosomas y la ARN polimerasa están espacialmente separados en *Pseudomonas putida*.** La distribución espacial de estas moléculas sugiere que la transcripción y la traducción no están acopladas en esta bacteria.

5. **Los ARNm del plásmido TOL se ubican en sitios ricos en ribosomas.** Los transcriptos se encuentran espacialmente organizados en lugar de flotar en el citoplasma, y difunden hacia zonas ricas en ribosomas.

6. **La expresión de los genes TOL está sometida al fenómeno de *transcriptional bursting*.** Los genes *xyl* no siempre se encuentran activos transcripcionalmente, y su expresión tiene lugar en pulsos de actividad. Este patrón de generación de ARNm característico da origen a expresión estocástica de los genes correspondientes.

# VII. References

References

ABRIL, M. A., MICHAN, C., TIMMIS, K. N. & RAMOS, J. L. 1989. Regulator and enzyme specificities of the TOL plasmid-encoded upper pathway for degradation of aromatic hydrocarbons and expansion of the substrate range of the pathway. *J Bacteriol,* 171**,** 6782-90.

ARANDA-OLMEDO, I., RAMOS, J. L. & MARQUÉS, S. 2005. Integration of signals through Crc and PtsN in catabolite repression of *Pseudomonas putida* TOL plasmid pWW0. *Appl Environ Microbiol,* 71**,** 4191-4198.

ASSINDER, S. J. & WILLIAMS, P. A. 1990. The TOL plasmids: determinants of the catabolism of toluene and the xylenes. *Adv Microb Physiol,* 31**,** 1-69.

AUSMEES, N., KUHN, J. R. & JACOBS-WAGNER, C. 2003. The bacterial cytoskeleton: an intermediate filament-like function in cell shape. *Cell,* 115**,** 705-13.

AZAM, T. A., HIRAGA, S. & ISHIHAMA, A. 2000. Two types of localization of the DNA-binding proteins within the *Escherichia coli* nucleoid. *Genes Cells,* 5**,** 613-26.

BAKSHI, S., SIRYAPORN, A., GOULIAN, M. & WEISSHAAR, J. C. 2012. Superresolution imaging of ribosomes and RNA polymerase in live *Escherichia coli* cells. *Mol Microbiol,* 85**,** 21-38.

BERTONI, G., MARQUES, S. & DE LORENZO, V. 1998. Activation of the toluene-responsive regulator XylR causes a transcriptional switch between $\sigma^{54}$ and $\sigma^{70}$ promoters at the divergent *Pr/Ps* region of the TOL plasmid. *Mol Microbiol,* 27**,** 651-9.

BOLSTAD, B. M., IRIZARRY, R. A., ASTRAND, M. & SPEED, T. P. 2003. A comparison of normalization methods for high density oligonucleotide array data based on variance and bias. *Bioinformatics,* 19**,** 185-93.

BORGNIA, M. J., SUBRAMANIAM, S. & MILNE, J. L. 2008. Three-dimensional imaging of the highly bent architecture of Bdellovibrio bacteriovorus by using cryo-electron tomography. *J Bacteriol,* 190**,** 2588-96.

BORONIN, A. M. 1992. Diversity of *Pseudomonas* plasmids: to what extent? *FEMS Microbiol Lett,* 79**,** 461-7.

BRIEGEL, A., DIAS, D. P., LI, Z., JENSEN, R. B., FRANGAKIS, A. S. & JENSEN, G. J. 2006. Multiple large filament bundles observed in *Caulobacter crescentus* by electron cryotomography. *Mol Microbiol,* 62**,** 5-14.

BROUDE, N. E. 2011. Analysis of RNA localization and metabolism in single live bacterial cells: achievements and challenges. *Mol Microbiol,* 80**,** 1137-47.

BURMANN, B. M., SCHWEIMER, K., LUO, X., WAHL, M. C., STITT, B. L., GOTTESMAN, M. E. & ROSCH, P. 2010. A NusE:NusG complex links transcription and translation. *Science,* 328**,** 501-4.

CABEZON, E., LANKA, E. & DE LA CRUZ, F. 1994. Requirements for mobilization of plasmids RSF1010 and ColE1 by the IncW plasmid R388: *trwB* and RP4 *traG* are interchangeable. *J Bacteriol,* 176**,** 4455-8.

CAMPOS, M. & JACOBS-WAGNER, C. 2013. Cellular organization of the transfer of genetic information. *Curr Opin Microbiol,* 16**,** 171-6.

CASES, I., PÉREZ-MARTÍN, J. & DE LORENZO, V. C. 1999. The IIANtr (PtsN) protein of *Pseudomonas putida* mediates the C source inhibition of the $\sigma^{54}$-dependent *Pu* promoter of the TOL plasmid. *J Biol Chem,* 274**,** 15562-15568.

CHENG, B. Y., ZHI, J., SANTANA, A., KHAN, S., SALINAS, E., FORREST, J. C., ZHENG, Y., JAGGI, S., LEATHERWOOD, J. & KRUG, L. T. 2012. Tiled microarray identification of novel viral transcript structures and distinct transcriptional profiles during two modes of productive murine gammaherpesvirus 68 infection. *J Virol,* 86**,** 4340-57.

CHIU, S. W., CHEN, S. Y. & WONG, H. C. 2008. Dynamic localization of MreB in *Vibrio parahaemolyticus* and in the ectopic host bacterium *Escherichia coli*. *Appl Environ Microbiol,* 74**,** 6739-45.

CHOI, K. H., KUMAR, A. & SCHWEIZER, H. P. 2006. A 10-min method for preparation of highly electrocompetent *Pseudomonas aeruginosa* cells: application for DNA fragment transfer between chromosomes and plasmid transformation. *J Microbiol Methods,* 64**,** 391-7.

CHOMCZYNSKI, P. 1992. One-hour downward alkaline capillary transfer for blotting of DNA and RNA. *Anal Biochem,* 201**,** 134-9.

CHUGANI, S. A., PARSEK, M. R. & CHAKRABARTY, A. M. 1998. Transcriptional repression mediated by LysR-type regulator CatR bound at multiple binding sites. *J Bacteriol,* 180**,** 2367-72.

COWLES, C. E., NICHOLS, N. N. & HARWOOD, C. S. 2000a. BenR, a XylS homologue, regulates three different pathways of aromatic acid degradation in *Pseudomonas putida*. *J Bacteriol,* 182**,** 6339-46.

COWLES, C. E., NICHOLS, N. N. & HARWOOD, C. S. 2000b. BenR, a XylS homologue, regulates three different pathways of aromatic acid degradation in *Pseudomonas putida*. *J Bacteriol,* 182**,** 6339-6346.

DAVID, L., HUBER, W., GRANOVSKAIA, M., TOEDLING, J., PALM, C. J., BOFKIN, L., JONES, T., DAVIS, R. W. & STEINMETZ, L. M. 2006. A high-resolution map of transcription in the yeast genome. *Proc Natl Acad Sci USA,* 103**,** 5320-5.

DE LORENZO, V. & TIMMIS, K. N. 1994. Analysis and construction of stable phenotypes in gram-negative bacteria with Tn5- and Tn10-derived minitransposons. *Methods Enzymol,* 235**,** 386-405.

DENNIS, J. J. & ZYLSTRA, G. J. 2004. Complete sequence and genetic organization of pDTG1, the 83 kilobase naphthalene degradation plasmid from *Pseudomonas putida* strain NCIB 9816-4. *J Mol Biol,* 341**,** 753-68.

DOMINGUEZ-CUEVAS, P., GONZALEZ-PASTOR, J. E., MARQUES, S., RAMOS, J. L. & DE LORENZO, V. 2006. Transcriptional tradeoff between metabolic and stress-response programs in *Pseudomonas putida* KT2440 cells exposed to toluene. *J Biol Chem,* 281**,** 11981-91.

DOMINGUEZ-CUEVAS, P., MARIN, P., MARQUES, S. & RAMOS, J. L. 2008. XylS-*Pm* promoter interactions through two helix-turn-helix motifs: identifying XylS residues important for DNA binding and activation. *J Mol Biol,* 375**,** 59-69.

DOMINGUEZ-CUEVAS, P., RAMOS, J. L. & MARQUES, S. 2010. Sequential XylS-CTD binding to the *Pm* promoter induces DNA bending prior to activation. *J Bacteriol,* 192**,** 2682-90.

DWORSKY, P. & SCHAECHTER, M. 1973. Effect of rifampin on the structure and membrane attachment of the nucleoid of *Escherichia coli*. *J Bacteriol,* 116**,** 1364-74.

ERDMANN, N., PETROFF, T. & FUNNELL, B. E. 1999. Intracellular localization of P1 ParB protein depends on ParA and *parS*. *Proc Natl Acad Sci USA,* 96**,** 14905-10.

ESUE, O., RUPPRECHT, L., SUN, S. X. & WIRTZ, D. 2010. Dynamics of the bacterial intermediate filament crescentin *in vitro* and *in vivo*. *PLoS One,* 5**,** e8855.

FERNANDEZ, M., CONDE, S., DE LA TORRE, J., MOLINA-SANTIAGO, C., RAMOS, J. L. & DUQUE, E. 2012. Mechanisms of resistance to chloramphenicol in *Pseudomonas putida* KT2440. *Antimicrob Agents Chemother,* 56**,** 1001-9.

FROST, L. S., LEPLAE, R., SUMMERS, A. O. & TOUSSAINT, A. 2005. Mobile genetic elements: the agents of open source evolution. *Nat Rev Microbiol,* 3**,** 722-32.

FUCHINO, K., BAGCHI, S., CANTLAY, S., SANDBLAD, L., WU, D., BERGMAN, J., KAMALI-MOGHADDAM, M., FLARDH, K. & AUSMEES, N. 2013. Dynamic gradients of an intermediate filament-like cytoskeleton are recruited by a polarity landmark during apical growth. *Proc Natl Acad Sci USA,* 110**,** E1889-97.

GALLEGOS, M. T., MARQUES, S. & RAMOS, J. L. 1996. Expression of the TOL plasmid xylS gene in *Pseudomonas putida* occurs from a $\sigma^{70}$-dependent promoter or from $\sigma^{70}$-and $\sigma^{54}$-dependent tandem promoter according to the compound used for growth. *J Bacteriol,* 178**,** 2356-2361.

GIBSON, D. G., YOUNG, L., CHUANG, R. Y., VENTER, J. C., HUTCHISON, C. A., 3RD & SMITH, H. O. 2009. Enzymatic assembly of DNA molecules up to several hundred kilobases. *Nat Methods,* 6**,** 343-5.

GOLDING, I. & COX, E. C. 2004. RNA dynamics in live *Escherichia coli* cells. *Proc Natl Acad Sci USA,* 101**,** 11310-5.

GOLDING, I., PAULSSON, J., ZAWILSKI, S. M. & COX, E. C. 2005. Real-time kinetics of gene activity in individual bacteria. *Cell,* 123**,** 1025-36.

GONZALEZ-PEREZ, M. M., RAMOS, J. L. & MARQUES, S. 2004. Cellular XylS levels are a function of transcription of *xylS* from two independent promoters and the differential efficiency of translation of the two mRNAs. *J Bacteriol,* 186**,** 1898-901.

GORDON, G. S., SITNIKOV, D., WEBB, C. D., TELEMAN, A., STRAIGHT, A., LOSICK, R., MURRAY, A. W. & WRIGHT, A. 1997. Chromosome and low copy plasmid segregation in *E. coli*: visual evidence for distinct mechanisms. *Cell,* 90**,** 1113-21.

GRAF, S., NIELSEN, F. G., KURTZ, S., HUYNEN, M. A., BIRNEY, E., STUNNENBERG, H. & FLICEK, P. 2007. Optimized design and assessment of whole genome tiling arrays. *Bioinformatics,* 23**,** i195-204.

GREATED, A., LAMBERTSEN, L., WILLIAMS, P. A. & THOMAS, C. M. 2002. Complete sequence of the IncP-9 TOL plasmid pWW0 from *Pseudomonas putida*. *Environ Microbiol,* 4**,** 856-71.

GREATED, A., TITOK, M., KRASOWIAK, R., FAIRCLOUGH, R. J. & THOMAS, C. M. 2000. The replication and stable-inheritance functions of IncP-9 plasmid pM3. *Microbiology,* 146 ( Pt 9)**,** 2249-58.

GUELL, M., VAN NOORT, V., YUS, E., CHEN, W. H., LEIGH-BELL, J., MICHALODIMITRAKIS, K., YAMADA, T., ARUMUGAM, M., DOERKS, T., KUHNER, S., RODE, M., SUYAMA, M., SCHMIDT, S., GAVIN, A. C., BORK, P. & SERRANO, L. 2009. Transcriptome complexity in a genome-reduced bacterium. *Science,* 326**,** 1268-71.

GUO, Z. & HOUGHTON, J. E. 1999. PcaR-mediated activation and repression of *pca* genes from *Pseudomonas putida* are propagated by its binding to both the -35 and the -10 promoter elements. *Mol Microbiol,* 32**,** 253-63.

GUTIERREZ, P. S., MONTEOLIVA, D. & DIAMBRA, L. 2012. Cooperative binding of transcription factors promotes bimodal gene expression response. *PLoS One,* 7**,** e44812.

HARAYAMA, S. & REKIK, M. 1993. Comparison of the nucleotide sequences of the meta-cleavage pathway genes of TOL plasmid pWW0 from *Pseudomonas putida* with other meta-cleavage genes suggests that both single and multiple nucleotide substitutions contribute to enzyme evolution. *Mol Gen Genet,* 239**,** 81-9.

HARWOOD, C. S. & PARALES, R. E. 1996. The beta-ketoadipate pathway and the biology of self-identity. *Annu Rev Microbiol,* 50**,** 553-90.

HOLT, C. E. & BULLOCK, S. L. 2009. Subcellular mRNA localization in animal cells and why it matters. *Science,* 326**,** 1212-6.

HOLTEL, A., MARQUES, S., MOHLER, I., JAKUBZIK, U. & TIMMIS, K. N. 1994. Carbon source-dependent inhibition of xyl operon expression of the *Pseudomonas putida* TOL plasmid. *J Bacteriol,* 176**,** 1773-6.

HOVIK, H., YU, W. H., OLSEN, I. & CHEN, T. 2012. Comprehensive transcriptome analysis of the periodontopathogenic bacterium *Porphyromonas gingivalis* W83. *J Bacteriol,* 194**,** 100-14.

HUGHES, E. J., SHAPIRO, M. K., HOUGHTON, J. E. & ORNSTON, L. N. 1988. Cloning and expression of *pca* genes from *Pseudomonas putida* in *Escherichia coli*. *J Gen Microbiol,* 134**,** 2877-87.

HUGOUVIEUX-COTTE-PATTAT, N., KOHLER, T., REKIK, M. & HARAYAMA, S. 1990. Growth-phase-dependent expression of the *Pseudomonas putida* TOL plasmid pWW0 catabolic genes. *J Bacteriol,* 172**,** 6651-60.

JENSEN, R. B. & GERDES, K. 1999. Mechanism of DNA segregation in prokaryotes: ParM partitioning protein of plasmid R1 co-localizes with its replicon during the cell cycle. *EMBO J,* 18**,** 4076-84.

JIMENEZ, J. I., MINAMBRES, B., GARCIA, J. L. & DIAZ, E. 2002. Genomic analysis of the aromatic catabolic pathways from *Pseudomonas putida* KT2440. *Environ Microbiol,* 4**,** 824-41.

JUN, S. & WRIGHT, A. 2010. Entropy as the driver of chromosome segregation. *Nat Rev Microbiol,* 8**,** 600-7.

JUNEAU, K., PALM, C., MIRANDA, M. & DAVIS, R. W. 2007. High-density yeast-tiling array reveals previously undiscovered introns and extensive regulation of meiotic splicing. *Proc Natl Acad Sci USA,* 104**,** 1522-7.

KAHNG, L. S. & SHAPIRO, L. 2003. Polar localization of replicon origins in the multipartite genomes of *Agrobacterium tumefaciens* and *Sinorhizobium meliloti*. *J Bacteriol,* 185**,** 3384-91.

KIM, J., OLIVEROS, J. C., NIKEL, P. I., DE LORENZO, V. & SILVA-ROCHA, R. 2013. Transcriptomic fingerprinting of *Pseudomonas putida* under alternative physiological regimes. *Environ Microbiol Rep,* 5**,** 883-891.

KOUTINAS, M., LAM, M. C., KIPARISSIDES, A., SILVA-ROCHA, R., GODINHO, M., LIVINGSTON, A. G., PISTIKOPOULOS, E. N., DE LORENZO, V., DOS SANTOS, V. A. & MANTALARIS, A. 2010. The regulatory logic of *m*-xylene biodegradation by *Pseudomonas putida* mt-2 exposed by dynamic modelling of the principal node *Ps/Pr* of the TOL plasmid. *Environ Microbiol,* 12**,** 1705-18.

KUDEROVA, A., NANAK, E., TRUKSA, M. & BRZOBOHATY, B. 1999. Use of rifampicin in T7 RNA polymerase-driven expression of a plant enzyme: rifampicin improves yield and assembly. *Protein Expr Purif,* 16**,** 405-9.

KUHNER, S., VAN NOORT, V., BETTS, M. J., LEO-MACIAS, A., BATISSE, C., RODE, M., YAMADA, T., MAIER, T., BADER, S., BELTRAN-ALVAREZ, P., CASTANO-DIEZ, D., CHEN, W. H., DEVOS, D., GUELL, M., NORAMBUENA, T., RACKE, I., RYBIN, V., SCHMIDT, A., YUS, E., AEBERSOLD, R., HERRMANN, R., BOTTCHER, B., FRANGAKIS, A. S., RUSSELL, R. B., SERRANO, L., BORK, P. & GAVIN, A. C. 2009. Proteome organization in a genome-reduced bacterium. *Science,* 326**,** 1235-40.

LAMBERTSEN, L. M., MOLIN, S., KROER, N. & THOMAS, C. M. 2004. Transcriptional regulation of pWW0 transfer genes in *Pseudomonas putida* KT2440. *Plasmid,* 52**,** 169-81.

LAU, I. F., FILIPE, S. R., SOBALLE, B., OKSTAD, O. A., BARRE, F. X. & SHERRATT, D. J. 2003. Spatial and temporal organization of replicating *Escherichia coli* chromosomes. *Mol Microbiol,* 49**,** 731-43.

LAWLEY, T. D. & TAYLOR, D. E. 2003. Characterization of the double-partitioning modules of R27: correlating plasmid stability with plasmid localization. *J Bacteriol,* 185**,** 3060-7.

LEWIS, P. J. 2004. Bacterial subcellular architecture: recent advances and future prospects. *Mol Microbiol,* 54**,** 1135-50.

LEWIS, P. J., THAKER, S. D. & ERRINGTON, J. 2000. Compartmentalization of transcription and translation in Bacillus subtilis. *EMBO J,* 19**,** 710-8.

LI, H. & DURBIN, R. 2009. Fast and accurate short read alignment with Burrows-Wheeler transform. *Bioinformatics,* 25**,** 1754-60.

LLOSA, M., GRANDOSO, G., HERNANDO, M. A. & DE LA CRUZ, F. 1996. Functional domains in protein TrwC of plasmid R388: dissected DNA

strand transferase and DNA helicase activities reconstitute protein function. *J Mol Biol,* 264**,** 56-67.

MADER, U., NICOLAS, P., RICHARD, H., BESSIERES, P. & AYMERICH, S. 2011. Comprehensive identification and quantification of microbial transcriptomes by genome-wide unbiased methods. *Curr Opin Biotechnol,* 22**,** 32-41.

MANDAL, M., BOESE, B., BARRICK, J. E., WINKLER, W. C. & BREAKER, R. R. 2003. Riboswitches control fundamental biochemical pathways in *Bacillus subtilis* and other bacteria. *Cell,* 113**,** 577-86.

MAO, F., DAM, P., CHOU, J., OLMAN, V. & XU, Y. 2009. DOOR: a database for prokaryotic operons. *Nucleic Acids Res,* 37**,** D459-63.

MARQUÉS, S., GALLEGOS, M.-T., MANZANERA, M., HOLTEL, A., TIMMIS, K. N. & RAMOS, J. L. 1998. Activation and repression of transcription at the double tandem divergent promoters for the *xylR* and *xylS* genes of the TOL plasmid of *Pseudomonas putida*. *J Bacteriol,* 180**,** 2889-2894.

MARQUES, S., HOLTEL, A., TIMMIS, K. N. & RAMOS, J. L. 1994. Transcriptional induction kinetics from the promoters of the catabolic pathways of TOL plasmid pWW0 of *Pseudomonas putida* for metabolism of aromatics. *J Bacteriol,* 176**,** 2517-24.

MARQUES, S., MANZANERA, M., GONZALEZ-PEREZ, M. M., GALLEGOS, M. T. & RAMOS, J. L. 1999. The XylS-dependent *Pm* promoter is transcribed *in vivo* by RNA polymerase with $\sigma^{32}$ or $\sigma^{38}$ depending on the growth phase. *Mol Microbiol,* 31**,** 1105-13.

MARQUES, S., RAMOS, J. L. & TIMMIS, K. N. 1993. Analysis of the mRNA structure of the *Pseudomonas putida* TOL meta fission pathway operon around the transcription initiation point, the *xylTE* and the *xylFJ* regions. *Biochim Biophys Acta,* 1216**,** 227-36.

MARSTON, A. L., THOMAIDES, H. B., EDWARDS, D. H., SHARPE, M. E. & ERRINGTON, J. 1998. Polar localization of the MinD protein of *Bacillus*

*subtilis* and its role in selection of the mid-cell division site. *Genes Dev,* 12**,** 3419-30.

MARTINEZ-GARCIA, E., CALLES, B., AREVALO-RODRIGUEZ, M. & DE LORENZO, V. 2011. pBAM1: an all-synthetic genetic tool for analysis and construction of complex bacterial phenotypes. *BMC Microbiol,* 11**,** 38.

MARTINEZ-GARCIA, E. & DE LORENZO, V. 2011. Engineering multiple genomic deletions in Gram-negative bacteria: analysis of the multi-resistant antibiotic profile of *Pseudomonas putida* KT2440. *Environ Microbiol,* 13**,** 2702-16.

MCGRATH, P. T., LEE, H., ZHANG, L., INIESTA, A. A., HOTTES, A. K., TAN, M. H., HILLSON, N. J., HU, P., SHAPIRO, L. & MCADAMS, H. H. 2007. High-throughput identification of transcription start sites, conserved promoter motifs and predicted regulons. *Nat Biotechnol,* 25**,** 584-92.

MONDAL, J., BRATTON, B. P., LI, Y., YETHIRAJ, A. & WEISSHAAR, J. C. 2011. Entropy-based mechanism of ribosome-nucleoid segregation in *E. coli* cells. *Biophys J,* 100**,** 2605-13.

MONTERO LLOPIS, P., JACKSON, A. F., SLIUSARENKO, O., SUROVTSEV, I., HEINRITZ, J., EMONET, T. & JACOBS-WAGNER, C. 2010. Spatial organization of the flow of genetic information in bacteria. *Nature,* 466**,** 77-81.

MORENO, R., FONSECA, P. & ROJO, F. 2010. The Crc global regulator inhibits the *Pseudomonas putida* pWW0 toluene/xylene assimilation pathway by repressing the translation of regulatory and structural genes. *J Biol Chem,* 285**,** 24412-9.

MORENO, R. & ROJO, F. 2008. The target for the *Pseudomonas putida* Crc global regulator in the benzoate degradation pathway is the BenR transcriptional regulator. *J Bacteriol,* 190**,** 1539-45.

NELSON, K. E., WEINEL, C., PAULSEN, I. T., DODSON, R. J., HILBERT, H., MARTINS DOS SANTOS, V. A., FOUTS, D. E., GILL, S. R., POP, M.,

HOLMES, M., BRINKAC, L., BEANAN, M., DEBOY, R. T., DAUGHERTY, S., KOLONAY, J., MADUPU, R., NELSON, W., WHITE, O., PETERSON, J., KHOURI, H., HANCE, I., CHRIS LEE, P., HOLTZAPPLE, E., SCANLAN, D., TRAN, K., MOAZZEZ, A., UTTERBACK, T., RIZZO, M., LEE, K., KOSACK, D., MOESTL, D., WEDLER, H., LAUBER, J., STJEPANDIC, D., HOHEISEL, J., STRAETZ, M., HEIM, S., KIEWITZ, C., EISEN, J. A., TIMMIS, K. N., DUSTERHOFT, A., TUMMLER, B. & FRASER, C. M. 2002. Complete genome sequence and comparative analysis of the metabolically versatile *Pseudomonas putida* KT2440. *Environ Microbiol,* 4**,** 799-808.

NEVO-DINUR, K., NUSSBAUM-SHOCHAT, A., BEN-YEHUDA, S. & AMSTER-CHODER, O. 2011. Translation-independent localization of mRNA in *E. coli*. *Science,* 331**,** 1081-4.

NICHOLS, N. N. & HARWOOD, C. S. 1995. Repression of 4-hydroxybenzoate transport and degradation by benzoate: a new layer of regulatory control in the *Pseudomonas putida* beta-ketoadipate pathway. *J Bacteriol,* 177**,** 7033-40.

NICOL, J. W., HELT, G. A., BLANCHARD, S. G., JR., RAJA, A. & LORAINE, A. E. 2009. The Integrated Genome Browser: free software for distribution and exploration of genome-scale datasets. *Bioinformatics,* 25**,** 2730-1.

NIKEL, P. I. & DE LORENZO, V. 2013. Engineering an anaerobic metabolic regime in *Pseudomonas putida* KT2440 for the anoxic biodegradation of 1,3-dichloroprop-1-ene. *Metab Eng,* 15**,** 98-112.

NIKEL, P. I., KIM, J. & DE LORENZO, V. 2014. Metabolic and regulatory rearrangements underlying glycerol metabolism in *Pseudomonas putida* KT2440. *Environ Microbiol,* 16**,** 239-54.

NIKI, H. & HIRAGA, S. 1997. Subcellular distribution of actively partitioning F plasmid during the cell division cycle in *E. coli*. *Cell,* 90**,** 951-7.

OCHMAN, H., LAWRENCE, J. G. & GROISMAN, E. A. 2000. Lateral gene transfer and the nature of bacterial innovation. *Nature,* 405**,** 299-304.

ORTIZ, J. O., FORSTER, F., KURNER, J., LINAROUDIS, A. A. & BAUMEISTER, W. 2006. Mapping 70S ribosomes in intact cells by cryoelectron tomography and pattern recognition. *J Struct Biol,* 156**,** 334-41.

OVERHAGE, J., PRIEFERT, H., RABENHORST, J. & STEINBUCHEL, A. 1999. Biotransformation of eugenol to vanillin by a mutant of *Pseudomonas* sp. strain HR199 constructed by disruption of the vanillin dehydrogenase (vdh) gene. *Appl Microbiol Biotechnol,* 52**,** 820-8.

PANSEGRAU, W., LANKA, E., BARTH, P. T., FIGURSKI, D. H., GUINEY, D. G., HAAS, D., HELINSKI, D. R., SCHWAB, H., STANISICH, V. A. & THOMAS, C. M. 1994. Complete nucleotide sequence of Birmingham IncP alpha plasmids. Compilation and comparative analysis. *J Mol Biol,* 239**,** 623-63.

PARALES, R. E. & HARWOOD, C. S. 1993. Regulation of the *pcaIJ* genes for aromatic acid degradation in *Pseudomonas putida*. *J Bacteriol,* 175**,** 5829-38.

PARRY, B. R., SUROVTSEV, I. V., CABEEN, M. T., O'HERN, C. S., DUFRESNE, E. R. & JACOBS-WAGNER, C. 2013. The bacterial cytoplasm has glass-like properties and is fluidized by metabolic activity. *Cell*.

PASSALACQUA, K. D., VARADARAJAN, A., ONDOV, B. D., OKOU, D. T., ZWICK, M. E. & BERGMAN, N. H. 2009. Structure and complexity of a bacterial transcriptome. *J Bacteriol,* 191**,** 3203-11.

PEREZ-MARTIN, J. & DE LORENZO, V. 1995a. Integration host factor suppresses promiscuous activation of the $\sigma^{54}$-dependent promoter *Pu* of *Pseudomonas putida. Proc Natl Acad Sci USA,* 92**,** 7277-81.

PEREZ-MARTIN, J. & DE LORENZO, V. 1995b. The $\sigma^{54}$-dependent promoter *Ps* of the TOL plasmid of *Pseudomonas putida* requires HU for transcriptional activation in vivo by XylR. *J Bacteriol,* 177**,** 3758-63.

PEREZ-MARTIN, J., TIMMIS, K. N. & DE LORENZO, V. 1994. Co-regulation by bent DNA. Functional substitutions of the integration host factor site at $\sigma^{54}$-dependent promoter *Pu* of the upper-TOL operon by intrinsically curved sequences. *J Biol Chem,* 269**,** 22657-62.

PEROCCHI, F., XU, Z., CLAUDER-MUNSTER, S. & STEINMETZ, L. M. 2007. Antisense artifacts in transcriptome microarray experiments are resolved by actinomycin D. *Nucleic Acids Res,* 35**,** e128.

PILHOFER, M., PAVLEKOVIC, M., LEE, N. M., LUDWIG, W. & SCHLEIFER, K. H. 2009. Fluorescence *in situ* hybridization for intracellular localization of *nifH* mRNA. *Syst Appl Microbiol,* 32**,** 186-92.

PRIEFERT, H., RABENHORST, J. & STEINBUCHEL, A. 2001. Biotechnological production of vanillin. *Appl Microbiol Biotechnol,* 56**,** 296-314.

PROSHKIN, S., RAHMOUNI, A. R., MIRONOV, A. & NUDLER, E. 2010. Cooperation between translating ribosomes and RNA polymerase in transcription elongation. *Science,* 328**,** 504-8.

RAJ, A., PESKIN, C. S., TRANCHINA, D., VARGAS, D. Y. & TYAGI, S. 2006. Stochastic mRNA synthesis in mammalian cells. *PLoS Biol,* 4**,** e309.

RAMOS, J. L., MARQUES, S. & TIMMIS, K. N. 1997. Transcriptional control of the *Pseudomonas* TOL plasmid catabolic operons is achieved through an interplay of host factors and plasmid-encoded regulators. *Annu Rev Microbiol,* 51**,** 341-73.

RAUHUT, R. & KLUG, G. 1999. mRNA degradation in bacteria. *FEMS Microbiol Rev,* 23**,** 353-70.

RESCALLI, E., SAINI, S., BARTOCCI, C., RYCHLEWSKI, L., DE LORENZO, V. & BERTONI, G. 2004. Novel physiological modulation of the *Pu* promoter of TOL plasmid: negative regulatory role of the TurA protein of

*Pseudomonas putida* in the response to suboptimal growth temperatures. *J Biol Chem,* 279**,** 7777-84.

REVA, O. N., WEINEL, C., WEINEL, M., BOHM, K., STJEPANDIC, D., HOHEISEL, J. D. & TUMMLER, B. 2006. Functional genomics of stress response in *Pseudomonas putida* KT2440. *J Bacteriol,* 188**,** 4079-92.

REYES-LAMOTHE, R., TRAN, T., MEAS, D., LEE, L., LI, A. M., SHERRATT, D. J. & TOLMASKY, M. E. 2013. High-copy bacterial plasmids diffuse in the nucleoid-free space, replicate stochastically and are randomly partitioned at cell division. *Nucleic Acids Res*.

RICO, A. I., GARCIA-OVALLE, M., MINGORANCE, J. & VICENTE, M. 2004. Role of two essential domains of *Escherichia coli* FtsA in localization and progression of the division ring. *Mol Microbiol,* 53**,** 1359-71.

ROBINSON, M. D. & OSHLACK, A. 2010. A scaling normalization method for differential expression analysis of RNA-seq data. *Genome Biol,* 11**,** R25.

ROBINSON, M. D. & SMYTH, G. K. 2008. Small-sample estimation of negative binomial dispersion, with applications to SAGE data. *Biostatistics,* 9**,** 321-32.

ROMERO-STEINER, S., PARALES, R. E., HARWOOD, C. S. & HOUGHTON, J. E. 1994. Characterization of the *pcaR* regulatory gene from *Pseudomonas putida*, which is required for the complete degradation of *p*-hydroxybenzoate. *J Bacteriol,* 176**,** 5771-9.

ROTHMEL, R. K., SHINABARGER, D. L., PARSEK, M. R., ALDRICH, T. L. & CHAKRABARTY, A. M. 1991. Functional analysis of the *Pseudomonas putida* regulatory protein CatR: transcriptional studies and determination of the CatR DNA-binding site by hydroxyl-radical footprinting. *J Bacteriol,* 173**,** 4717-24.

RUSSELL, J. H. & KEILER, K. C. 2009. Subcellular localization of a bacterial regulatory RNA. *Proc Natl Acad Sci USA,* 106**,** 16405-9.

RUSSELL, J. H. & KEILER, K. C. 2012. RNA visualization in bacteria by fluorescence in situ hybridization. *Methods Mol Biol,* 905**,** 87-95.

SAMBROOK, J. & RUSSELL, D. 2001. *Molecular Cloning: A Laboratory Manual*, Cold Spring Harbor Laboratory Press.

SCHELL, M. A. 1993. Molecular biology of the LysR family of transcriptional regulators. *Annu Rev Microbiol,* 47**,** 597-626.

SELINGER, D. W., CHEUNG, K. J., MEI, R., JOHANSSON, E. M., RICHMOND, C. S., BLATTNER, F. R., LOCKHART, D. J. & CHURCH, G. M. 2000. RNA expression analysis using a 30 base pair resolution *Escherichia coli* genome array. *Nat Biotechnol,* 18**,** 1262-8.

SETO, S., LAYH-SCHMITT, G., KENRI, T. & MIYATA, M. 2001. Visualization of the attachment organelle and cytadherence proteins of *Mycoplasma pneumoniae* by immunofluorescence microscopy. *J Bacteriol,* 183**,** 1621-30.

SEVASTSYANOVICH, Y. R., KRASOWIAK, R., BINGLE, L. E., HAINES, A. S., SOKOLOV, S. L., KOSHELEVA, I. A., LEUCHUK, A. A., TITOK, M. A., SMALLA, K. & THOMAS, C. M. 2008. Diversity of IncP-9 plasmids of *Pseudomonas*. *Microbiology,* 154**,** 2929-41.

SHINGLER, V., FRANKLIN, F. C., TSUDA, M., HOLROYD, D. & BAGDASARIAN, M. 1989. Molecular analysis of a plasmid-encoded phenol hydroxylase from *Pseudomonas* CF600. *J Gen Microbiol,* 135**,** 1083-92.

SHINTANI, M., TAKAHASHI, Y., YAMANE, H. & NOJIRI, H. 2010. The behavior and significance of degradative plasmids belonging to Inc groups in *Pseudomonas* within natural environments and microcosms. *Microbes Environ,* 25**,** 253-65.

SILVA-ROCHA, R., DE JONG, H., TAMAMES, J. & DE LORENZO, V. 2011a. The logic layout of the TOL network of *Pseudomonas putida* pWW0

plasmid stems from a metabolic amplifier motif (MAM) that optimizes biodegradation of *m*-xylene. *BMC Syst Biol,* 5**,** 191.

SILVA-ROCHA, R. & DE LORENZO, V. 2012a. Broadening the signal specificity of prokaryotic promoters by modifying cis-regulatory elements associated with a single transcription factor. *Mol Biosyst,* 8**,** 1950-7.

SILVA-ROCHA, R. & DE LORENZO, V. 2012b. A GFP-lacZ bicistronic reporter system for promoter analysis in environmental gram-negative bacteria. *PloS one,* 7**,** e34675.

SILVA-ROCHA, R. & DE LORENZO, V. 2012c. Stochasticity of TOL plasmid catabolic promoters sets a bimodal expression regime in *Pseudomonas putida* mt-2 exposed to *m*-xylene. *Mol Microbiol,* 86**,** 199-211.

SILVA-ROCHA, R., TAMAMES, J., DOS SANTOS, V. M. & DE LORENZO, V. 2011b. The logicome of environmental bacteria: merging catabolic and regulatory events with Boolean formalisms. *Environ Microbiol,* 13**,** 2389-402.

SKINNER, S. O., SEPULVEDA, L. A., XU, H. & GOLDING, I. 2013. Measuring mRNA copy number in individual *Escherichia coli* cells using single-molecule fluorescent in situ hybridization. *Nat Protoc,* 8**,** 1100-13.

SMETS, B. F. & BARKAY, T. 2005. Horizontal gene transfer: perspectives at a crossroads of scientific disciplines. *Nat Rev Microbiol,* 3**,** 675-8.

SMYTH, G. K. 2004. Linear models and empirical bayes methods for assessing differential expression in microarray experiments. *Stat Appl Genet Mol Biol,* 3**,** Article3.

SMYTH, G. K. & SPEED, T. 2003. Normalization of cDNA microarray data. *Methods,* 31**,** 265-73.

SO, L. H., GHOSH, A., ZONG, C., SEPULVEDA, L. A., SEGEV, R. & GOLDING, I. 2011. General properties of transcriptional time series in *Escherichia coli*. *Nat Genet,* 43**,** 554-60.

SOREK, R. & COSSART, P. 2010. Prokaryotic transcriptomics: a new view on regulation, physiology and pathogenicity. *Nat Rev Genet,* 11**,** 9-16.

SOTA, M., YANO, H., ONO, A., MIYAZAKI, R., ISHII, H., GENKA, H., TOP, E. M. & TSUDA, M. 2006. Genomic and functional analysis of the IncP-9 naphthalene-catabolic plasmid NAH7 and its transposon Tn4655 suggests catabolic gene spread by a tyrosine recombinase. *J Bacteriol,* 188**,** 4057-67.

SPECHT, M., DEMPWOLFF, F., SCHATZLE, S., THOMANN, R. & WAIDNER, B. 2013. Localization of FtsZ in *Helicobacter pylori* and consequences for cell division. *J Bacteriol,* 195**,** 1411-20.

ST JOHNSTON, D. 2005. Moving messages: the intracellular localization of mRNAs. *Nat Rev Mol Cell Biol,* 6**,** 363-75.

TAKAHASHI, Y., SHINTANI, M., YAMANE, H. & NOJIRI, H. 2009. The complete nucleotide sequence of pCAR2: pCAR2 and pCAR1 were structurally identical IncP-7 carbazole degradative plasmids. *Biosci Biotechnol Biochem,* 73**,** 744-6.

THERDEVELOPMENTCORETEAM 2011. R*:* A Language and Environment for Statistical Computing, Vienna, Austria, R Foundation for Statistical Computing.

THOMASON, M. K. & STORZ, G. 2010. Bacterial antisense RNAs: how many are there, and what are they doing? *Annu Rev Genet,* 44**,** 167-88.

THORVALDSDOTTIR, H., ROBINSON, J. T. & MESIROV, J. P. 2012. Integrative Genomics Viewer (IGV): high-performance genomics data visualization and exploration. *Brief Bioinform*.

TOLEDO-ARANA, A., DUSSURGET, O., NIKITAS, G., SESTO, N., GUET-REVILLET, H., BALESTRINO, D., LOH, E., GRIPENLAND, J., TIENSUU, T., VAITKEVICIUS, K., BARTHELEMY, M., VERGASSOLA, M., NAHORI, M. A., SOUBIGOU, G., REGNAULT, B., COPPEE, J. Y., LECUIT, M., JOHANSSON, J. & COSSART, P. 2009. The

*Listeria* transcriptional landscape from saprophytism to virulence. *Nature,* 459**,** 950-6.

TORO, E. & SHAPIRO, L. 2010. Bacterial chromosome organization and segregation. *Cold Spring Harb Perspect Biol,* 2**,** a000349.

TREVORS, J. T. 2012. Physical and biochemical nature of the bacterial cytoplasm: movement and localization of mRNA and the 30S subunits of ribosomes. *Prog Biophys Mol Biol,* 109**,** 1-5.

TROESCHEL, S. C., THIES, S., LINK, O., REAL, C. I., KNOPS, K., WILHELM, S., ROSENAU, F. & JAEGER, K. E. 2012. Novel broad host range shuttle vectors for expression in *Escherichia coli*, *Bacillus subtilis* and *Pseudomonas putida*. *J Biotechnol,* 161**,** 71-9.

TSUDA, M. & GENKA, H. 2001. Identification and characterization of Tn4656, a novel class II transposon carrying a set of toluene-degrading genes from TOL plasmid pWW53. *J Bacteriol,* 183**,** 6215-24.

TSUDA, M. & IINO, T. 1987. Genetic analysis of a transposon carrying toluene degrading genes on a TOL plasmid pWW0. *Mol Gen Genet,* 210**,** 270-6.

TURNER, S. L., BAILEY, M. J., LILLEY, A. K. & THOMAS, C. M. 2002. Ecological and molecular maintenance strategies of mobile genetic elements. *FEMS Microbiol Ecol,* 42**,** 177-85.

VALENCIA-BURTON, M., MCCULLOUGH, R. M., CANTOR, C. R. & BROUDE, N. E. 2007. RNA visualization in live bacterial cells using fluorescent protein complementation. *Nat Methods,* 4**,** 421-7.

VAN DUUREN, J. B., WIJTE, D., LEPRINCE, A., KARGE, B., PUCHALKA, J., WERY, J., DOS SANTOS, V. A., EGGINK, G. & MARS, A. E. 2011. Generation of a *catR* deficient mutant of *P. putida* KT2440 that produces *cis, cis*-muconate from benzoate at high rate and yield. *J Biotechnol,* 156**,** 163-72.

VELAZQUEZ, F., DI BARTOLO, I. & DE LORENZO, V. 2004. Genetic evidence that catabolites of the Entner-Doudoroff pathway signal C source repression of the $\sigma^{54}$ *Pu* promoter of *Pseudomonas putida*. *J Bacteriol,* 186**,** 8267-75.

VELAZQUEZ, F., PARRO, V. & DE LORENZO, V. 2005. Inferring the genetic network of *m*-xylene metabolism through expression profiling of the *xyl* genes of *Pseudomonas putida* mt-2. *Mol Microbiol,* 57**,** 1557-69.

VITALE, E., MILANI, A., RENZI, F., GALLI, E., RESCALLI, E., DE LORENZO, V. & BERTONI, G. 2008. Transcriptional wiring of the TOL plasmid regulatory network to its host involves the submission of the $\sigma^{54}$-promoter *Pu* to the response regulator PprA. *Mol Microbiol,* 69**,** 698-713.

WONG, S. M. & MEKALANOS, J. J. 2000. Genetic footprinting with mariner-based transposition in Pseudomonas aeruginosa. *Proc Natl Acad Sci USA,* 97**,** 10191-6.

WORSEY, M. J. & WILLIAMS, P. A. 1975. Metabolism of toluene and xylenes by *Pseudomonas putida* (arvilla) mt-2: evidence for a new function of the TOL plasmid. *J Bacteriol,* 124**,** 7-13.

YAMAMOTO, T., SHIMIZU, Y., UEDA, T. & SHIRO, Y. 2010. Mg2+ dependence of 70 S ribosomal protein flexibility revealed by hydrogen/deuterium exchange and mass spectrometry. *J Biol Chem,* 285**,** 5646-52.

YODER-HIMES, D. R., CHAIN, P. S., ZHU, Y., WURTZEL, O., RUBIN, E. M., TIEDJE, J. M. & SOREK, R. 2009. Mapping the *Burkholderia cenocepacia* niche response *via* high-throughput sequencing. *Proc Natl Acad Sci USA,* 106**,** 3976-81.

YUNGER, S., ROSENFELD, L., GARINI, Y. & SHAV-TAL, Y. 2010. Single-allele analysis of transcription kinetics in living mammalian cells. *Nat Methods,* 7**,** 631-3.

ZENKLUSEN, D., LARSON, D. R. & SINGER, R. H. 2008. Single-RNA counting reveals alternative modes of gene expression in yeast. *Nat Struct Mol Biol,* 15**,** 1263-71.

ZIEGELIN, G., PANSEGRAU, W., LURZ, R. & LANKA, E. 1992. TraK protein of conjugative plasmid RP4 forms a specialized nucleoprotein complex with the transfer origin. *J Biol Chem,* 267**,** 17279-86.

# VIII. Annexes

**Table S1.** Transcriptional activity on pWW0 backbone genes by RNA-seq

| Functional group | Genes | Normalized value in reference condition | Normalized value in *m*-xylene treated condition | Fold change ($Log_2$ ratio) |
|---|---|---|---|---|
| **Replication and maintenance functional genes** | *parA* | 1,056 | 2,007 | 0.93 |
| | *parB* | 1,415 | 2,288 | 0.69 |
| | *parC* | 716 | 1,444 | 1.01 |
| | *res* | 2,172 | 579 | -1.91 |
| | *rep* | 751 | 1,473 | 0.97 |
| | *korA* | 370 | 649 | 0.81 |
| **Transfer genes** | *traA* | 1,383 | 748 | -0.89 |
| | *traB* | 5,266 | 3,727 | -0.5 |
| | *traC* | 5,185 | 3,211 | -0.69 |
| | *traD* | 5,824 | 1,599 | -1.86 |
| | *mpfR* | 2,548 | 15,245 | 2.58 |
| | *mpfA* | 2,499 | 28,110 | 3.49 |
| | *mpfB* | 800 | 9,733 | 3.6 |
| | *mpfC* | 6,303 | 50,097 | 2.99 |
| | *mpfD* | 1,976 | 14,413 | 2.87 |
| | *mpfE* | 1,647 | 11,586 | 2.81 |
| | *mpfF* | 958 | 7,511 | 2.97 |
| | *mpfG* | 702 | 5,573 | 2.99 |
| | *mpfH* | 1,149 | 6,394 | 2.48 |
| | *mpfI* | 1,059 | 5,004 | 2.24 |
| | *mpfJ* | 1,034 | 4,988 | 2.27 |

Continued on the following page

| | | | | |
|---|---|---|---|---|
| **Phenotypic functional genes** | *ruvA* | 825 | 225 | -1.87 |
| | *ruvB* | 1,140 | 520 | -1.13 |
| | *merB* | 1,100 | 722 | -0.61 |
| | *merR* | 4,812 | 3,573 | -0.43 |
| **Catabolic proteins-coding genes** | *xylU* | 2,137 | 14,636 | 2.78 |
| | *xylW* | 1,355 | 22,714 | 4.07 |
| | *xylC* | 1,255 | 56,265 | 5.49 |
| | *xylM* | 1,543 | 64,603 | 5.39 |
| | *xylA* | 256 | 30,240 | 6.89 |
| | *xylB* | 289 | 33,595 | 6.86 |
| | *xylN* | 250 | 16,623 | 6.05 |
| | *xylX* | 1,505 | 317,230 | 7.72 |
| | *xylY* | 1,015 | 132,317 | 7.03 |
| | *xylZ* | 670 | 127,404 | 7.57 |
| | *xylL* | 555 | 50,036 | 6.49 |
| | *xylT* | 563 | 59,908 | 6.73 |
| | *xylE* | 1,560 | 227,998 | 7.19 |
| | *xylG* | 1,775 | 179,272 | 6.66 |
| | *xylF* | 1,385 | 123,811 | 6.48 |
| | *xylJ* | 961 | 73,689 | 6.26 |
| | *xylQ* | 2,079 | 78,754 | 5.24 |
| | *xylK* | 2,678 | 74,026 | 4.79 |
| | *xylI* | 1,764 | 58,312 | 5.05 |
| | *xylH* | 185 | 6,963 | 5.23 |
| | *xylR* | 26,406 | 7,717 | -1.77 |
| | *xylS* | 5,318 | 30,508 | 2.52 |

Continued on the following page

| | | | | |
|---|---|---|---|---|
| | *orf4* | 980 | 2,274 | 1.21 |
| | *orf5* | 1,568 | 2,362 | 0.59 |
| | *orf6* | 1,962 | 2,719 | 0.47 |
| | *orf7* | 1,323 | 1,244 | -0.09 |
| | *orf12* | 460 | 74 | -2.64 |
| | *orf13* | 21,409 | 151,835 | 2.83 |
| | *orf14* | 305 | 223 | -0.45 |
| | *orf 15* | 3,495 | 1,671 | -1.06 |
| | *orf 16* | 3,552 | 1,211 | -1.55 |
| | *orf 18* | 3,979 | 1,145 | -1.8 |
| | *orf 19* | 4,891 | 1,200 | -2.03 |
| **Conserved hypothetical proteins-coding genes** | *orf 20* | 2,362 | 337 | -2.81 |
| | *orf 21* | 836 | 170 | -2.3 |
| | *orf 22* | 313 | 74 | -2.08 |
| | *orf 23* | 264 | 48 | -2.46 |
| | *orf 24* | 953 | 323 | -1.56 |
| | *orf 26* | 588 | 113 | -2.38 |
| | *orf 27* | 640 | 312 | -1.04 |
| | *orf 29* | 147 | 138 | -0.09 |
| | *orf 30* | 280 | 528 | 0.91 |
| | *orf 31* | 773 | 3,689 | 2.25 |
| | *orf 32* | 675 | 1,008 | 0.58 |
| | *recX* | 2,850 | 854 | -1.74 |
| | *ssb* | 3,242 | 2,438 | -0.41 |
| | *orf 35* | 2,335 | 504 | -2.21 |
| | *orf 37* | 588 | 425 | -0.47 |
| | *KorA2* | 3,203 | 1,892 | -0.76 |
| | *orf 40* | 122 | 42 | -1.54 |
| | *orf 41* | 2,077 | 1,265 | -0.72 |

Continued on the following page

| | | | | |
|---|---|---|---|---|
| | *orf 43* | 1,527 | 707 | -1.11 |
| | *orf 44* | 1,731 | 2,350 | 0.44 |
| | *orf 45* | 2,104 | 1,565 | -0.43 |
| | *orf 46* | 11,839 | 16,143 | 0.45 |
| | *orf 55* | 35,747 | 34,522 | -0.05 |
| | *orf 56* | 2,283 | 2,964 | 0.38 |
| | *orf 57* | 724 | 460 | -0.65 |
| | *orf 58* | 3,318 | 1,280 | -1.37 |
| | *orf 59* | 1,712 | 1,119 | -0.61 |
| | *orf 61* | 400 | 472 | 0.24 |
| | *orf 63* | 5,865 | 1,211 | -2.28 |
| | *orf 65* | 171 | 52 | -1.72 |
| **Conserved hypothetical proteins-coding genes** | *orf 66* | 256 | 128 | -1 |
| | *orf 69* | 634 | 141 | -2.17 |
| | *orf 70* | 471 | 273 | -0.79 |
| | *orf 74* | 509 | 181 | -1.49 |
| | *orf 76* | 599 | 153 | -1.97 |
| | *orf 82* | 321 | 103 | -1.64 |
| | *orf 86* | 343 | 426 | 0.31 |
| | *orf 87* | 1,102 | 620 | -0.83 |
| | *orf 105* | 177 | 91 | -0.96 |
| | *orf 106* | 163 | 69 | -1.24 |
| | *orf 109* | 161 | 112 | -0.52 |
| | *orf 112* | 63 | 38 | -0.72 |
| | *orf 113* | 63 | 10 | -2.65 |
| | *orf 116* | 8 | 13 | 0.67 |
| | *orf 117* | 14 | 10 | -0.44 |
| | *orf 118* | 33 | 16 | -1.03 |

Continued on the following page

| | | | | |
|---|---|---|---|---|
| **Conserved hypothetical proteins-coding genes** | *orf 122* | 174 | 114 | -0.61 |
| | *orf 124* | 171 | 609 | 1.83 |
| | *orf 125* | 150 | 570 | 1.93 |
| | *orf 126* | 253 | 1,666 | 2.72 |
| | *orf 145* | 893 | 527 | -0.76 |
| | *orf 149* | 408 | 173 | -1.24 |
| | *orf 150* | 612 | 443 | -0.47 |
| | *orf 154* | 563 | 254 | -1.15 |
| | *orf 155* | 710 | 354 | -1 |
| | *orf 156* | 640 | 592 | -0.11 |
| | *orf 163* | 3,535 | 1,789 | -0.98 |
| | *orf 164* | 2,207 | 888 | -1.31 |
| | *orf 171* | 1,110 | 379 | -1.55 |
| | *orf 173* | 817 | 435 | -0.91 |
| | *orf 175* | 1,715 | 1,177 | -0.54 |
| | *orf 176* | 5,359 | 1,435 | -1.9 |
| | *orf 177* | 13,355 | 5,292 | -1.34 |
| | *orf 188* | 1,369 | 12,633 | 3.21 |
| | *orf 189* | 2,390 | 7,955 | 1.74 |
| | *orf 191* | 909 | 5,169 | 2.51 |
| | *orf 199* | 1,315 | 8,265 | 2.65 |
| | *orf 200* | 808 | 5,087 | 2.65 |

**Table S2.** Complementary oligonucleotides for mRNA FISH assay

| **Sequence** | |
|---|---|
| ***xylUW* probe set** | ***xylX* probe set** |
| AGCAACCAATCTGAACAGAG | AGGTGCATTGTCATGGTCAT |
| CCCGCTTTGAGGATATACAT | ACTATCTATATAGTCGAGCC |
| TCACAGACTCCAGGCGTAAC | TAGATGCCCTCGTTCTCATC |
| CTCAGAAAGCACTAGGCCAG | GAACATCTCGCGCTTGCAGC |
| CTCACCAAAATTGGTGGTCG | AATCGAACAGCCGAGGGTCG |
| ATAACTGCGACGAAAATGGT | TCAAAGATGTGTTTCATCTC |
| CCTATCACGAGAGATGAAGC | GGCGAGATAAATCCAGTTGC |
| CGTTGGACTGGCATCTATAA | GTTCTTCTCGGGAATCTGGC |
| ATTGAAGATTGATGCAGCCG | CCATCTGCGTGGTGTAATAG |
| CTGGGCATATAGTCGGTTGA | TGTGATGAATATCGGCTGCC |
| CAGGCTGGATATATCGTTGC | TCAGCTCACCATCTTTGTTG |
| GGTAGATGACTAAGGCTCGA | GACTGCAGGCATTGACGAAG |
| TAGTAATGTCGCTGCAGCTG | CACTCCTAAAGCGACAGAGC |
| TTCCGAGATCGACACGACTA | CCGAATTGCTGAAGGTCCAG |
| AAGTTCTCGGCAACAACACG | TCTTTGACCTTGAGCAGCTT |
| ACTTAATGCATCACATGCAG | AGTCGAAGCTGTCCGGATAG |
| TTATAGGTAGCAAGGACGGC | TTCTTCAGGTCGTGCGAGCC |
| GCGAGCATTGAATCACCTAT | GTAGGAAGCAAAGCGCGCAA |
| GCCCTGCTTTAGTTTTCCTT | CAGGCTGCCGAATAGAAATC |
| CACATCATCGACAGATAGCC | GACTCGCCGAGGAACTCTTC |
| AGTACTGTGGGCCTCTTTAG | GACCATGTCGATGACCTTCC |
| AGTCAGTACCACAGATACCG | AGCACTTCCAGACCTTCGGG |
| TCATTCTTTTGGCGAACTCG | AAACATAGGTACTGGAACCG |
| CGCTAACTTCATGACCCAAG | TGCACTTTCCAGTTGCCTTC |
| GATCCGACCTGTTCAATCAC | TACTGACGTGGTAGCCGTCG |
| CAGGCCTTAGACCTTTAACG | GCGGCGTAGTTCCAGTGAAC |
| AGATGACTCTCCAGACTGAC | TCTCTCAGCTTGCGCTGCTG |
| CGTGTAGCACGTTCCACAAG | GTCATGGCGCGAATATCATC |
| CGTCTTAGGACAAACATGCG | TTCAAAGGAGTAGAAACCGC |

| | |
|---|---|
| GAAGCCTCCATCAAAGTCGA | GTGCCCAGACCATCTGGTGG |
| TTTCCGGAACCACAACGAAA | GGCGGTTTTTCGGGTCACCC |
| CGCAACCAGAAACAAGAACA | CGATCTCGCTCGGCGAACAG |
| TGCAATGTTCATAAGTCCGA | TTCACCAAACTCGCTGGCTA |
| GATGAATGTCCGGTGCAATG | GAGACGCCGATCATCCAGTC |
| ATTTTGGCTGCTGCAGTGAG | GAACTGGTCCATCAGGTAGA |
| GCATTAATGCATTCATCCGC | GACGGGTGATACGCAACTGC |
| CGCACAGTCTTATAAACGCT | GATTTCGGTTCTATCCACCG |
| GCTTGCCCAGAATAGTCAAT | CTCGGCGTTTCGCCTTTGGG |
| AATAAGCTCCTTTAACGCCG | GTCCTCGTACTGACGGACAC |
| AAATATCATGTGACGGGACG | CCATGCCGCTGACATTGAAG |
| CCACGTACAATAAGGCCTTT | GGAATTCCTCCAGGTCGTCC |
| ATCTTTCATACAGACGCCTG | CACGGGACATGTCGTTCATC |
| CCAATAAGCTAGTTGAACGC | CCCTCGATCCAGTGTTTGGC |